Study on Biomolecular Motor based Micro-Robot Programmed by DNA Processor

DNA プロセッサーによりプログラムされる生体分子モーターを基盤としたマイクロロボットの研究

A dissertation for the degree of

Doctor of Science

Jakia Jannat Keya

Material Chemistry Laboratory
Graduate School of Chemical Sciences and Engineering,
Hokkaido University, Japan

September 2017

CONTENTS

Chapter 1: General Introduction

Chapter 2: DNA Programmed Control of Swarming in a Biomolecular Motor System

Chapter 3: Controlling Swarming of Biomolecular Motor System through DNA Logic Gates and Photoirradiation

Chapter 4: High-Resolution Imaging of Gliding Microtubules and Protofilament of Tubulins by HS-AFM

CHAPTER 1

General Introduction

1.1 Purpose

Swarming is a collective behavior exhibited by living organisms in nature[1]. Through swarming they obtain advantages which are unachievable by single entity[2-7]. Being motivated by the attractive features of natural swarming, researchers have been trying to understand and demonstrate the swarming of self-propelled objects in the artificial world, as a result of which, a new field named 'swarm robotics' has emerged. Considerable amount of experimental works, which made use of various kinds of self-propelled mechanical robots, have been undertaken to mimic the swarming of living organisms alongside the theoretical and simulation based studies[8-13]. The limitation of mechanical robots, however, lies on their large size and low efficiency that restricted their application for demonstration of swarming. In contrast, supramolecular chemistry are directing on synthetic micromotors for demonstrating swarming driven by local forces and externally applied field[14-16] which is yet to be developed by overcoming the low speed of motors and controlling over their dynamic self-assembly. On the other hand, chemists and biologists have independently employed self-propelled biomolecular motor system, the smallest natural machine that has been promising for demonstrating swarming. Their small size and high efficiency of energy conversion[17-19] offers controllability over a large number of swarm units. Self-organization of these natural molecular building blocks such as microtubule (MT)-kinesin, actin-myosin by energy dissipation opens a new era to realize swarming of a natural system in artificial setting which becomes possible by latest technological advancements in chemistry and biotechnology. A number of collective studies have been found in the literature on demonstrating swarming by manipulation of interaction among the MTs filaments applying different interacting agents both under the thermal diffusion and self-propelled condition[20-22]. However, still the key challenge has been modulation of the interactions among the neighbor units which can control the swarms in a programmable way. Adaptability of extent of swarming corresponding to external signals and control over their reversibility is yet to be achieved for developing sensitivity and responsiveness which is prohibited due to lack of computer based programming like in mechanical robots. In this way

supramolecular building block, DNA, the most attractive molecular computer remarkable so far could be employed to design and control biomolecular swarming by selective and specific interaction in a highly programmable fashion[23-30]. Therefore in this dissertation, I focus to control swarming of a biomolecular motor system using cytoskeletal filamentous protein MTs driven by molecular motor kinesin *in vitro* through DNA programming. Emergence of different swarm patterns by bottom up approach and controlling their mode of motion was studied systematically by employing DNA interaction. Sensitivity and responsiveness was further introduced by controlling the swarming using unique features of DNA such as logic gate operation and DNA induced photoirradiation[31, 32]. This work would help us to develop the knowledge of constructing molecular robot by programming the swarming of self-propelled MTs through DNA in a synthetic system. Moreover, while considering the progressive development of such biomolecular motor protein system based swarming, study of the mechanical activity of MTs during their motility is a great concern. Study of gliding behavior of MTs at the molecular level is still a big challenge using conventional fluorescence techniques due to lower resolution of images. Therefore, in this dissertation I also attempted to study the different phenomena that occur during gliding of MTs by high resolution images using high speed atomic force microscopy (HS-AFM)[33-35]. This work would also provide us information to understand the dynamics of MTs at molecular level, demanding for future micro-robot design.

1.2 Swarming in nature and development of artificial swarm robots

Swarming is a collective behavior exhibited by similar individual agents particularly from animals to micro-organisms often observed in nature like ant colonies, fish schools, bird flocks, etc (**Figure 1.1**). It is the self-organization or self-assembly of thousands to millions or trillions of individual agents which can give rise to some unpredictable or emergent functions like parallelism, flexibility, robustness and scalability that is not achieved when they are in single state[2-7]. Swarming pattern moving in a particular direction is generally formed by local interaction among the nearest neighbors in a decentralized way. Instead of having a sophisticated controller for a whole swarm system, mutual interactions among many unsophisticated single entities play the key role in swarming of the living organisms. The dynamic coordination of the single units into large pattern and again dispersion into single

entities retaining their individuality makes the whole system unique to work in a more sophisticated way[2]. Through this swarming behavior the living entities can get some advantages like protection from predators, forage of foods, migration from one place to another, etc.

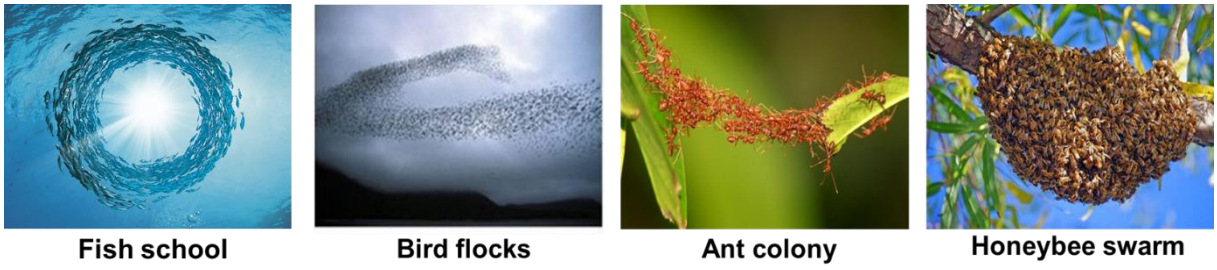

Figure 1.1 Swarming of living beings in nature[36-49].

Inspired by this natural swarming, a research field in robotics has been emerged named as swarm robotics. Swarm robotics is a new approach to the coordination of multi-robot systems which consist of large numbers of mostly simple physical robots. To complete a sophisticated task, swarm robots can work together through inter-group cooperation and takes the advantage of reusability of the simple agents and the low cost of construction and maintenance compared to single conventional robot. The criteria of swarm robotics would be many such as parallel, scalable, stable, economical and energy efficient to mimic natural swarm. Developing of single swarm robots has been growing interest day by day to demonstrate swarming by local interaction[40]and optimize the artificial intelligence (**Figure 1.2a**). The swarm robotics can be applied to sophisticated problems involving large amount of time, space or targets, and a certain danger that may exist in the environment.

Supramolecular chemistry in contrast, provides the means to create large numbers of functional building blocks and program their interactions, potentially enabling "swarming" at the molecular scale. There are already many examples of particle assembly driven by local forces or externally applied fields. Externally applied light, magnetic, electric, and acoustic fields can drive symmetric particles into ordered arrays[14-16]. Autonomously moving nano- and micromotors[41] exhibit rich collective behavior including swarming and schooling[42], predator–prey interactions[43], attraction and repulsion between rotors[44], spatiotemporal oscillations[43], and dynamic self-assembly[45]. Electrocatalytic decomposition of bimetallic rods and hydrophobic surface can also drive the assembly of micromotors[46, 47] (**Figure 1.2b, 1.2c**). But still the key

challenge is to create molecular robots which are motile and interact with each other in a programmable way. Designing the size, power, physical interaction, sensing, signaling and capability is highly challenging task which are prerequisite for further application in different area at molecular scale like in medical applications or nanotechnology.

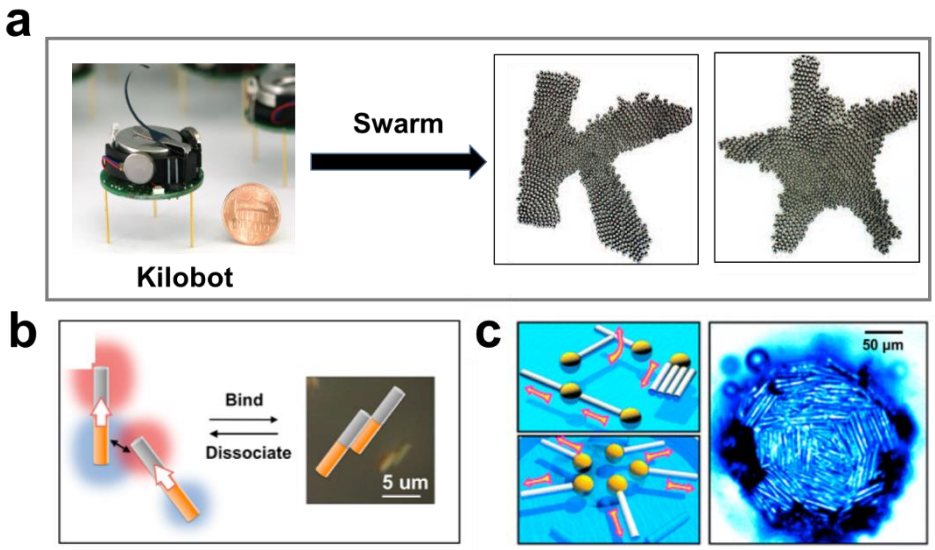

Figure 1.2 Swarm robots (kilobots) and their swarming by local interaction into different swarming pattern[33] (a), The reversible binding and dissociation of pairs of bimetallic rods propelled by the electrocatalytic decomposition of H_2O_2[46] (b) and assembly induced by capillary forces between bubble-propelled microtubes[47](c).

Therefore to design swarming at the molecular level, molecular devices with essential functionalities is required which is yet to be studied. However, natural molecular units such as in biomolecular motor system, MTs act as robotic arms grasping chromosomes or waving cilia and the study of these systems generates valuable insights into molecular robotics for demonstration of swarming[48].

1.3 Biomolecular motor system

Biomolecular motors, also known as motor proteins, are unique stimulus-responsive polymers which are known as the active workhorses of cells[49]. These particular amino acid polymers will undergo dramatic conformational changes as they bind and hydrolyze ATP and release the products in a cyclic process. Linear motors, such as myosin and kinesin, operate in conjunction with cytoskeletal filaments – actin filaments and MTs, respectively. These two are known as the classical motor protein systems that have been widely studied which are found to work in relatively larger living organisms and organs of animals. In this study we used MT-kinesin system as the model system for development of micro-robots.

MT, known as cytoskeletal 'track' are hollow cylinders polymerized of α, β-tubulin heterodimers[50]. During polymerization, tubulin dimers bind head-to-tail to form linear protofilament (PF) with an 8 nm repeat distance and a variable number (10-18, often 13) of PFs assemble into a cylindrical structure with an outer diameter of about 25 nm and a length of many micrometers[51-55] (**Figure 1.3**). Since the PFs bind to each other in the same orientation, the MT also develops structural polarity. The end exposing α-tubulin is slow-growing and called the minus end, and the fast-growing end exposing β-tubulin is named the plus end. The lateral inter-PF contacts are mostly electrostatic, but the intra-PF interactions (-αβ- αβ-) are basically hydrophobic[52, 55]. The structural properties of MTs are critical to their cellular functions as well as their nanotechnological applications. MTs serve as scaffolds for a wide variety of MT-associated molecular motors or 'trucks' (i.e. kinesins and dyneins families) in cell[56].

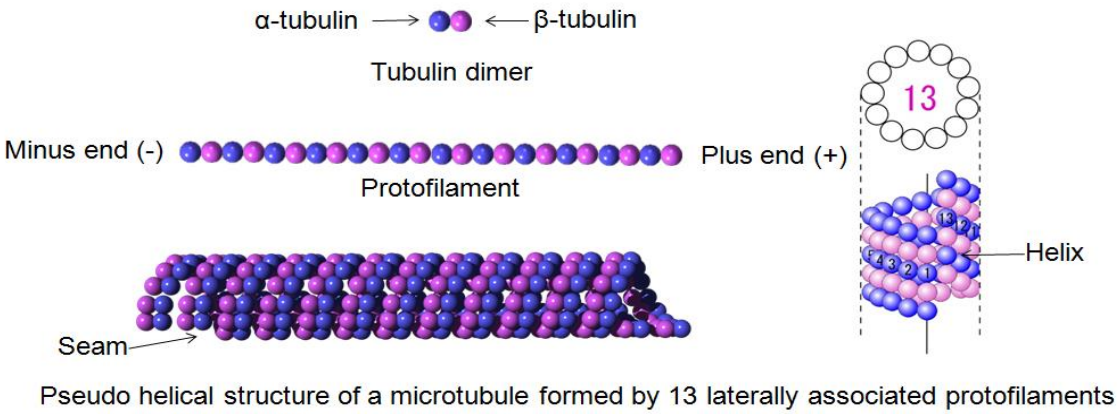

Figure 1.3 Schematic image of structure of MT

These motors can utilize chemical energy to generate mechanical motion. Between these trucks the molecular motor kinesin is a homodimer containing two heads-globular domains each of which has an ATP- and a MT-binding site. It is a tetramer of two identical "heavy chains", and two associated light chains. The heavy chains fold into two globular heads at one end, a stalk with a hinge in the middle, and a tail domain at the other end[57] (**Figure 1.4a**). The heads step on the binding sites along the MT PFs. These sites are spaced 8 nm apart. Thus moving the entire molecule 8 nm in each step in a hand-over-hand mechanism[58]. For every step, kinesin consumes one ATP molecule[59] (**Figure 1.4b**). Kinesin-1 motors are primarily involved in intracellular transport of vesicles and organelles[60], cell division[61], and the organization of cilia and flagella[62]. The kinesin-1 (conventional kinesin) is of particular utility in nanotechnology, because their primary function is the exertion of force. Micromechanical recordings from single kinesin molecules indicate that one motor can exert a force as great as 5 pN. The efficiency of kinesin is in the order of 50%, considering the free energy available from ATP hydrolysis. Because of its high degree of processivity, even a single kinesin molecule is capable of propelling MTs along a surface[63]. The small size and high efficiency of MT-kinesin system makes it fascinating to apply it as molecular devices for a wide range of purposes which become possible in synthetic environment such as motility assay system.

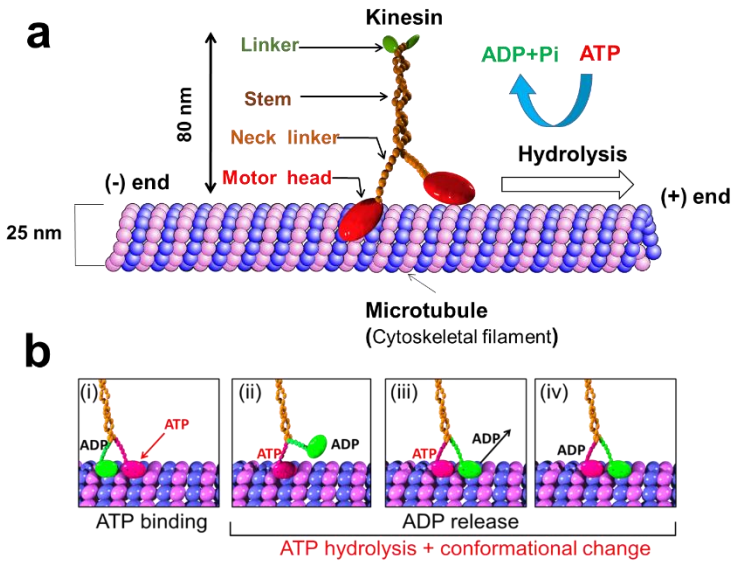

Figure 1.4 Schematic image of structure of kinesin on MT track (a) and its movement on MT hydrolyzed by ATP (b).

1.3.1 *In vitro* motility assay of biomolecular motor system

The *in vitro* motility assay is the most promising setup for nanotechnological usage of biomolecular motor system (**Figure 1.5**). To investigate the property of biomolecular motor systems *in vitro*, motor proteins and their associated cytoskeletal filaments were fabricated successfully by latest technological advancements. In this way at first, movement of myosin coated fluorescent beads were successfully observed on F-actin fixed substrate by Sheetz and Spudich[64]. Vale and his colleagues discovered uni-directional gliding motion of MTs in the cell extract from squid axon on a substrate driven by biomolecular motor (kinesin and dynein)[65]. They named this method "*in vitro* motility assay" as gliding of filaments was observed which helps to investigate property of biomolecular motor systems. Later, Spudich has also developed a similar *in vitro* motility assay where motility of F-actin on a glass surface coated with myosin was demonstrated[66]. These works have opened the door for understanding how biomolcular motors transport cargo molecules involved in numerous cellular processes, including cell polarity, cell division, cellular movement and signal transduction.

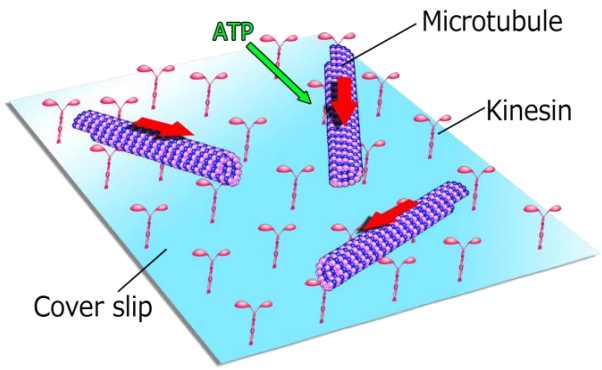

Figure 1.5 Schematic image of *in vitro* gliding assay of MTs on kinesin coated surface.

With recent progress in the nanotechnology, *in vitro* gliding assay has been attracting interest for serving the smallest autonomous moving objects[67]. They provide transport of various nano- or micro-sized cargo molecules. This function is applicable for development of various kinds of micro devices which sort, separate, concentrate, probe, analyze and assembled materials[68-73]. For example, Hess *et al.* used *in vitro* motility assay as piconewton forcemeter[74]. By considering one MT as a molecular cantilever they calculated the force from bending of the cantilever when moving MTs collided with cantilever (**Figure 1.6a**). Furthermore, Hess *et al*

introduced *in vitro* motility assay into a new method of surface imaging[75] (**Figure 1.6b**). Further exploration with this system have been made with considerable efforts to achieve directed motility, control of moving direction by employing either chemical patterning[76-78] of biomolecular motors or fabricated topographic patterns by using photolithography technique[79, 80]. The direction of the moving filaments has been also controlled by employing electric field[81, 82] or magnetic field[83]. The directional motion of filaments can be applied to sense mechanical deformation of surface which is advancement for soft surface induced nanotechnological applications reported by Inoue *et. al*[84].

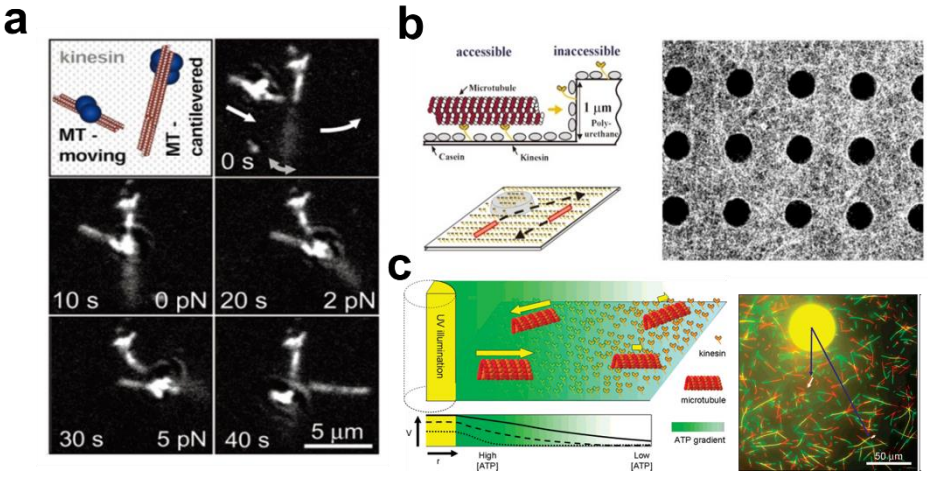

Figure 1.6 Piconewton forcemeter[74] (a), surface measurement[75] (b), light activation and control of molecular shuttles[85] (c).

Alongside with many applicable features of self-propelled MTs, this molecular shuttle was also applied to demonstrate swarm in a discrete level controlled by external stimuli or guiding direction. For example, investigation on the control over molecular shuttles by sequestration of enzyme activities was studied by Hess *et al* using gliding assay of MTs. Localized release and enzymatic sequestration of the substrate ATP creates a spatially and temporally well-defined concentration profile, which in turn leads to controlled activation (**Figure 1.6c**) of a small number of molecular shuttles suggesting that these nanosystems are most efficiently addressed as a swarm rather than as individuals[85]. Hess and Nitta also reported the mechanisms responsible for the dispersion of a swarm of "molecular shuttles", consisting of functionalized MTs propelled by surface-adhered kinesin motor proteins. It was revealed that, overall the

dispersion of such molecular shuttles is comparable to the dispersion of a sample plug transported by electroosmotic flow[86]. Besides this, an extensive study on swarming or collective behavior of biomolecular motor systems has been found in the literature which is based on energy dissipative self-organization process.

1.3.2 Self-organization of biomolecular motor systems *in vitro*

Nanotechnological applications of biomolecular motor systems have been possible to further amplify by integrating them using active self-organization (ACSO). The self-organization is accomplished through introducing attractive interaction between the cytoskeletal filaments driven by biomolecular motors using chemical energy of ATP hydrolysis allowing the creation of non-equilibrium structures. Energy dissipative self-organization of these natural building blocks is significantly important in consideration of force integration by biomolecular motors and construction of diverse assembled patterns that autonomously change their structure with time[87, 88].

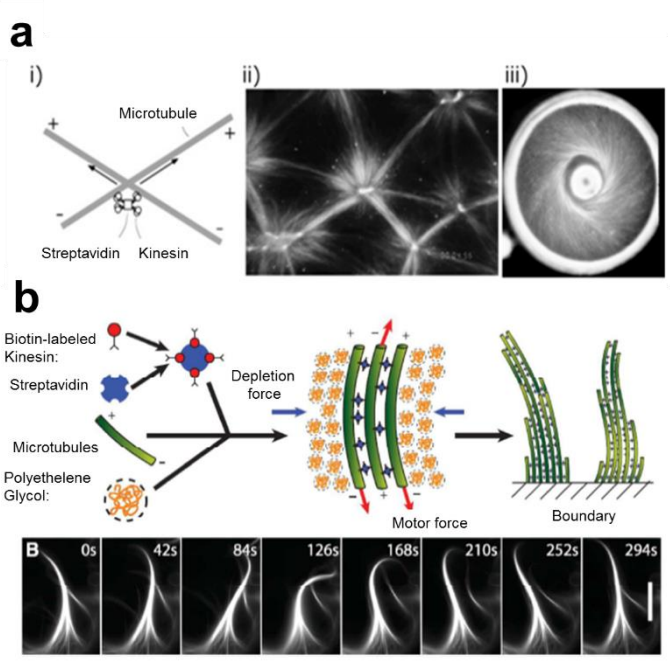

Figure 1.7 Active self-organization of MTs crosslinked by kinesin multi cluster[89] (**a**) (i) Schematic diagram of MTs with kinesin multi cluster, (ii) aster and (iii) vortex pattern emerging from MTs. Cilia like bundle of MTs[90] (b).

For example, aster and vortex pattern from MTs conjugating with kinesin multi cluster by self-organization was reconstructed similar to meiotic and mitotic spindles in vivo[89] (**Figure 1.7a**). Depending on the concentration of the MTs and kinesin used dynamic vortices can be formed instead of asters which help us to understand the dynamic processes that take place in the cell. Recently, this method also contributes to reproduce cilia like beating bundles and active nematic network of MTs like cytoplasmic streaming observed *in vivo*[90, 91] (**Figure 1.7b**).

Furthermore, collective behavior into hierarchical structures by self-organization of the biomolecular motor systems was demonstrated using high dense system. Bausch *et al.* reported *in vitro* motility assay of highly concentrated F-actins propelled by immobilized myosin on a surface[92]. F-actin can exhibit collective motion due to excluded volume effect and fascinating wave-like or a vortex patterns emerged from collective motion of large population of F-actin. Oiwa group reported the emergence of streaming like pattern and lattice of vortices pattern from highly concentrated MTs moving on a dynein coated surface[93]. Regulating MTs movements driven by motor protein kinesin by applying depleting agents was reported by Inoue *et al*. where self-propelled filaments show collective motion depending on the depletion force acting on them[94].

Considerable number of studies were carried out that demonstrated assembly formation by the biomolecular motor systems under thermal diffusion and swarming of motor propelled cytoskeletal proteins, by controlling their mutual interactions making use of electrostatic effects[95, 96], associated proteins[97-99] or ligand-receptor based crosslinking[100-110]. To understand the inherent activity of cytoskeleton dynamic properties of filaments, wide range of self-organization of actin was explored by Bausch *et al*. (**Figure 1.8a**) using different crosslinking proteins[92]. They showed that wide range of active patterns from large-scale polar structures to contract networks can be controlled by using high density motility assay which depends on the interplay of only three components –molecular motor, filamentous actin and crosslinking proteins. Self-assembly of moving MTs has been developed and vastly studied based on the *in vitro* motility assay by using strong non-covalent interaction e.g., streptavidin (St)-biotin (Bt) interaction or by using some kinds of cytoskeletal filament related proteins[100-110]. By using this method a wide variety of assembled structures was obtained e.g. bundle, network, and ring-shaped structures that differ in size or shape[103, 110]. It was found that stiffer MTs with high

bending rigidity favored the production of linear bundles while larger and longer bundles require more building blocks i.e; higher initial density of MTs. On the other hand, MT spools assembled from longer and flexible one is an example of such non-equilibrium structures, capable of storing bending energies on the order of 10^5 kT[109].

Kakugo *et al.* have thoroughly investigated and determined phase diagram of ordered structures by changing the experimental conditions such as density of MTs and the strength of interaction of streptavidin/biotin (**Figure 1.8b**)[110].

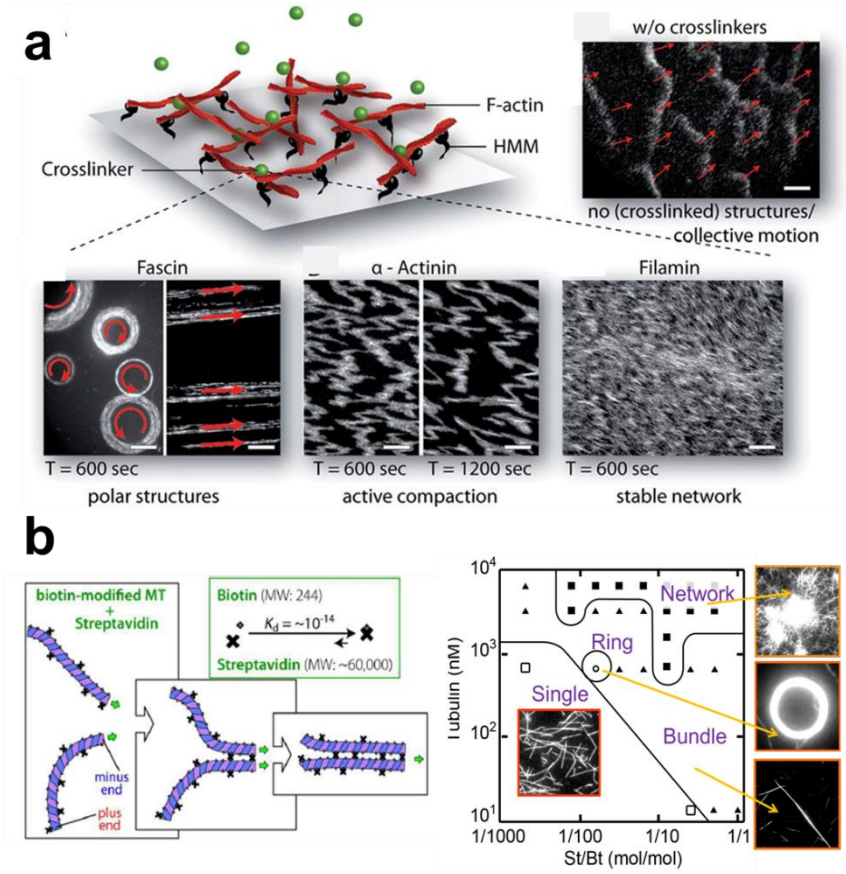

Figure 1.8 Crosslinking proteins control the structure formation in active systems. Schematic representation of the motility assay setup for actin filaments. In the absence of crosslinkers, density waves of coherently moving actin filaments evolve. Fascin leads to polar structures, rings and elongated fibres. While a-actinin/actin networks disintegrate to form contractile patches, filamin/actin networks remain stable[92] (a). Phase diagram of active self-assembly based on *in vitro* motility assay using streptavidin/biotin interaction[110] (b).

Despite of extensive studies of collective behavior of biomolecular motor system which was effective for understanding their cell behavior and nanotechnological applications still it is lacking far behind for engineering robotic applications. Control over their collective behavior through a programmable processor is required to open a considerable scope for demonstrating tunable swarming with computing properties.

1.4. DNA- a smart crosslinker and processor

DNA nanotechnology opens a new door that aims to create molecular structures and devices through the exclusive use of DNA as an engineering material[111]. It is the purist's approach to biomolecular engineering which depends on the programmability of Watson-Crick base pairing combining with a decrease in the cost of synthesis. Structural simplicity and controllable binding interactions of DNA by four base units (A (adenine), C (cytosine), G (guanine), T (thymine)) results in a simpler structure and predictable behavior. Other than this structural features there are two important and exclusive properties that make DNA suitable for molecular level constructions such as molecular recognition and self-assembly. The pioneering efforts of Seeman[112-114] in DNA nanotechnology and the revolutionizing work of Rothemond[115] on DNA origami paved the way to enable rational design of DNA nanostructures. Adleman[116] demonstrated the use of DNA to perform logical operations by solving a complex mathematical problem using only DNA oligonucleotides. The self-assembly behavior of DNA was further computed to design different logical operations for engineering complex structures and exploit their functions[117-126]. This attractive phenomenon of programming of DNA was further used for engineering the self-assembly of different building blocks to enhance their functionalities with higher ordered structures. DNA programming was also successfully applied in DNA template self-assembly of other functional materials like nanoparticles and proteins. Higher-order structures that originate from the specific and reversible DNA-directed self-assembly of microscopic building blocks hold great promise for future technologies[127-131]. Applications of these self-assembly strategies span from photonics and plasmonics[132], to biosensing[133] and gene therapy[134]. Moreover, the same self-assembly strategy has been applied to compliant Brownian units, including emulsion droplets[135, 136], lipid vesicles[137-142], time dependent assembly of functional clusters that results in a rationally designed mesoscopic structures[143].

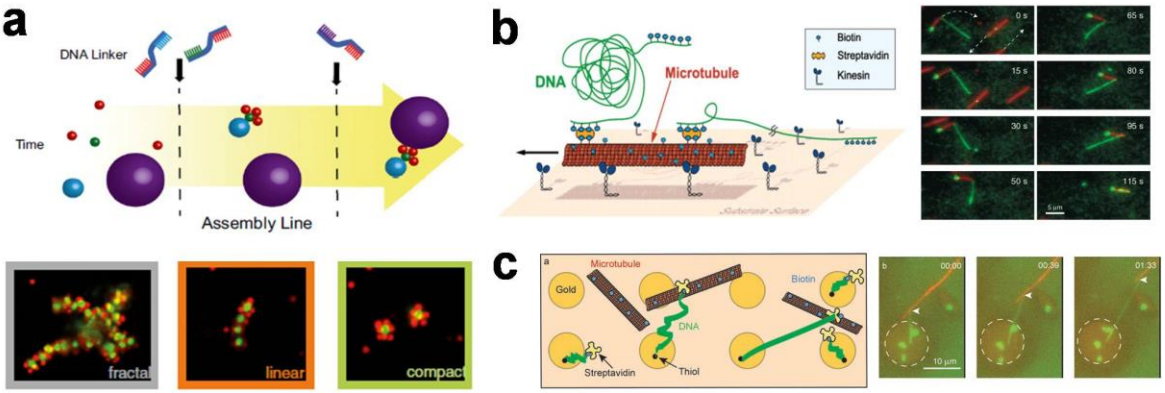

Figure 1.9 Mesoscopic structures with a defined complex geometry[143] (a), DNA transportation[134] (b) and stretching of DNA by kinesin-driven MTs[135] (c).

Although DNA programming is successfully applied with different building blocks there have been a few excellent studies utilizing DNA in combination with cytoskeleton–motor protein systems[144-156]. Most of them, however, use DNA as intelligent glue to assemble multiple motor proteins to prepare multimers[144, 145] or to attach them onto DNA origami scaffolds to construct more sophisticated complexes. Conjugation of DNA to MTs has been done only to load them as a cargo itself by using strong cross linking interaction [148, 149] or for the purpose of cargo loading/unloading[150-156]. No direct control of MT assembly or swarming by DNA had been reported, except for the MT aster formation using DNA-motor protein complexes instead[145]. Thus In this study DNA was applied to program swarming of bimolecular motor system to develop swarm robot at molecular level which would provide a new concept to understand and apply swarming phenomenon that is observed in nature.

1.5 HS-AFM a tool for studying the molecular events of dynamic system

In quest of the knowledge of mechanism and function of protein, various key techniques and instruments have been developed to scrutinize a certain protein from various angles. However, tracing a protein in action, at high spatial and temporal resolutions no technology is available to link these different aspects of a protein along a time axis. Atomic force microscopy (AFM)[157] made it possible for the first time to view a nanometer-scale world in an aqueous environment[158-161]. To directly visualize the dynamic processes that occur in biopolymers,

biosupramolecules, organelles, and cells, rapidly acquire successive high-resolution images of individual biomolecules at work is required. This is solely because this type of imaging is impossible using other techniques. However, the imaging rate of conventional AFM is too slow to observe dynamic behavior of active biomolecules. Recent progress of AFM in biological research has resulted in remarkable improvements in both the imaging rate and the tip force acting on the sample named as HS-AFM (**Figure 1.10a**). Alongside with improving the instrumental techniques, designing of substrate surfaces is also particularly important for successful imaging. Depending on the surface property the desired protein is attached on the surface by specific adsorption without impeding their dynamic behavior [33, 162-165] (**Figure 1.10b**). These improvements have enabled the direct visualization of dynamic structural changes and dynamic interactions occurring in individual biomolecules. HS-AFM opens up a new opportunity to directly visualize dynamic events of proteins[162-168], DNA-protein complexes[169, 170] and other molecular systems[171, 172].

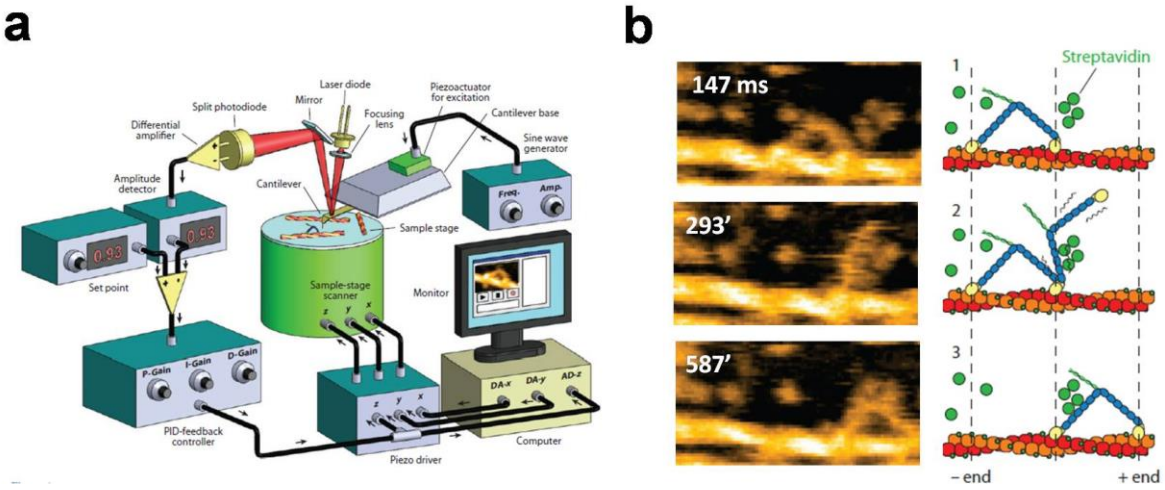

Figure 1.10 Schematic for general configuration of a tapping-mode HS-AFM system (a), Walking tail-truncated myosin V (M5-HMM) and unfolding of coiled-coil tail captured by HS-AFM[33] (b).

Despite of these successful results there is still no report on the dynamic behavior of MTs yet. Therefore using the advantage of HS-AFM, gliding behavior of MTs and PFs was investigated to know about the molecular events of MTs in action with motor protein.

1.6 Dissertation outline

In this dissertation, study on development of micro-robots by controlling swarm of a self-propelled biomolecular motor system with DNA programming and also HS-AFM study of self-propelled system have been summarized in 5 chapters including general introduction and concluding remarks.

In **chapter 1**, the purpose of this dissertation and background of this study has been described.

In **chapter 2**, construction of swarm units by conjugation of MTs with DNA and demonstration of swarming of them by dynamic self-assembly process have been discussed. Control of swarming pattern and their mode of motion were also studied by varying the physical property of swarm units through assembly and disassembly using DNA interaction. The effects of different relevant parameters on swarming were also investigated systematically to control the swarm behavior.

In **chapter 3**, swarming has been programmed using different DNA logic gate operations. Coexistence behavior of different patterns with distinct mode of motion using molecular recognition of DNA was also demonstrated which is presented in this chapter. Finally, applying external physical stimuli the reversible control of swarming was successfully demonstrated by photoregulation.

In **chapter 4**, different features of MTs and PFs during their gliding motion was monitored using high speed AFM to understand the gliding behavior of them. The splitting of single PFs from MTs and the cause of change of their direction of motion was investigated by high resolution images using HS-AFM.

In **chapter 5**, all the important results and future prospects of this research work have been summarized in the concluding remarks.

1.7 References

1. Bonabeau, E.; Dorigo, M.; Theraulaz, G. *Swarm Intelligence: From Natural to Artificial Systems*, Oxford University Press, Oxford, New York, **1999**.
2. Blum, C.; Merkle, D. Eds., *Swarm Intelligence: Introduction and Applications*, Springer, Natural Computing series, **2008**.
3. Niven, J. E. *Science* **2011**, *335*, 43-44.
4. Vittori, K.; Talbot, G.; Gautrais, J.; Fourcassié, V.; Araújo, A. F. R.; Theraulaz, G. *J. Theor. Biol.* **2006**, *239*, 507-515.
5. Beshers, S. N.; Fewell, J. H. *Annu Rev Entomol* **2001**, *46*, 413-440.
6. Thorup, K.; Alerstam, T.; Hake, M.; Kjelle´n, N. *Proc Biol Sci*, **2003**, *270*, 8-11.
7. Menzel, R.; Giurfa, M. *Trends Cogn Sci*. **2001**, *5*, 62-71.
8. Wei, H. X.; Chen, Y. D.; Tan, J. D.; Wang, T. M. *IEEE/ASME Trans Mechatron* **2011**, *16*, 745-757.
9. Seyfried, J.; Szymanski, M.; Bender, N.; Estana, R.; Thiel, M.; Wörn, H. *LNCS* **2005**, *3342*, 70-83.
10. Sahin, E. *LNCS* **2005**, *3342*, 10-20.
11. McLurkin, J.; Smith, J. *In: Distributed autonomous robotic systems 6. Japan: Springer* **2007**, 399-408.
12. Turgut, A. E.; Celikkanat, H.; Gökçe, F.; Sahin, E. *Swarm Intell.* **2008**, *2*, 97-120.
13. Arvin, F; Murray, J. C.; Shi, L.; Zhang, C.; Yue, S. *Mechatronics and Automation (ICMA), 2014 IEEE International Conference on*, **2014**, 635-640.
14. Velev, O. D.; Gangwal, S.; Petsev, D. N.; *Annu Rep Prog Chem* C **2009**, *105*, 213-245.
15. Klajn, R.; Bishop, K. J. M.; Grzybowski, B. A. *Proc, Natl. Acad. Sci. USA* **2007**, 104, 10305-10309.
16. Juárez, J. J.; Mathai, P. P.; Liddle, J. A.; Bevan, M. A. *Lab Chip* **2012**, *12*, 4063-4070.
17. Knoblauch, M.; Peters, W. S. *Cell. Mol. Life Sci.* **2004**, *61*, 2497-2509.
18. Mahadevan, L.; Matsudaira, P *Science* **2000**, *288*, 95-99.
19. Hess, H.; Vogel, V. *Rev. Mol. Biotechnol.* **2001**, *82*, 67-85.
20. Hess, H. *Soft Matter* **2006**, *2*, 669-677.
21. Koenderink G. H.; Dogic, Z.; Nakamura, F.; Bendix, P. M.; MacKintosh, F. C.; Hartwig, J. H.; Stossel, T. P.and Weitz, D. A. *Proc, Natl. Acad. Sci. USA* **2009**, *106*, 15192-15197.

22. Idan, O.; Lam, A.; Kamcev, J.; John, G.; Agarwal, A.; Hess, H. *Nano Lett.* **2012**, *12*, 240-245.
23. Qian, L. & Winfree, E. *Science* **2011**, *332*, 1196-1201.
24. Rogers, W. B.; Manoharan, V. N. *Science* **2015**, *347*, 639-642.
25. Zhang, D. Y.; Hariadi, R. F.; Choi, H. M. T.; Winfree, E. *Nat. Commun.* **2013**, *4*:1965.
26. Winfree, E.; Liu, F.; Wenzler, L. A; Seeman, N. C. *Nature* **1998**, *394*, 539-544.
27. Gu, H.; Chao, J.; Xiao, S. J.; Seeman, N. C. *Nature* **2010**, *465*, 202-205.
28. Douglas, S. M.; Dietz, H.; Liedl, T.; Högberg, B.; Graf, F.; Shih, W. *Nature* **2009**, *459*, 414-418.
29. Bonnet, J.; Yin, P.; Ortiz, M. E.; Subsoontorn, P.; Endy, D. *Science* **2013**, *340*, 599-603.
30. Goodman, R. P.; Heilemann, M.; Doose, S.; Erben, C. M.; Kapanidis A. N.; Turberfield, A. R. *Nat. Nanotechnol.* **2008**, *3*, 93-96.
31. Zadegan R. M.; Jepsen, M. D. E.; Hildebrandt, L. L.; Birkedal, V.; Kjems, J. *Small* **2015**, *11*, 1811-1817.
32. Kuzyk, A.; Yang, Y.; Duan, X.; Stoll, S.; Govorov, A. O.; Sugiyama, H.; Endo, M.; Liu, N. *Nat. Commun.* **2016**, *7*:10591.
33. Kodera, N.; Yamamoto, D.; Ishikawa, R.; Ando, T. *Nature* **2010**, *468*, 72-76.
34. Ando, T.; Kodera, N.; Takai, E.; Maruyama, D.; Saito, K.; Toda, A. *Proc, Natl. Acad. Sci. USA* **2001**, *98*, 12468-12472.
35. Ando, T.; Uchihashi, T.; Kodera, N.; Miyagi, A.; Nakakita, R.; Yamashita, Hayato.; Sakashita, M. *Japanese journal of applied physics* **2006**, *45*, 1897-1903.
36. http://www.simontuckett.com/_Portfolio/PortPages_Hi/Il_FishSchool.html.
37. http://www.wikiwand.com/en/Flock (birds).
38. https://www.nextnature.net/2013/07/what-ant-colony-networks-can-tell-us-about-what%E2%80%99s-next-for-digital-networks.
39. http://www.explorenature.org/latest-blog/honey-bee-swarms.
40. Rubenstein, M.; Cornejo, A.; Nagpal, R. *Science* **2014**, *345*, 795-799.
41. Hong, Y.; Velegol, D.; Chaturvedi, N.; Sen, A. *Phys. Chem. Chem. Phys.* **2010**, *12*, 1423-1435.
42. Palacci, J.; Sacanna, S.; Steinberg, A. P.; Pine, D. J.; Chaikin, P. M. *Science* **2013**, *339*,

936-940.

43. Ibele, M.; Mallouk, T. E.; Sen, A. *Angew. Chem. Int. Ed.* **2009**, *48*, 3308-3312.
44. Gibbs, J. G.; Zhao, Y. *Small* **2010**, *6*, 1656-1662.
45. Ebbens, S.; Jones, R. A. L.; Ryan, A. J.; Golestanian, R.; Howse, J. R. *Phys Rev E Stat Nonlin Soft Matter Phys* **2010**, *82*, 015304.
46. Wang, W.; Duan, W.; Sen, A.; Mallouk, T. E. *Proc, Natl. Acad. Sci. USA* **2013**, *110*, 17744-17749.
47. Solovev, A. A.; Sanchez, S.; Schmidt, O. G. *Nanoscale* **2013**, *5*, 1284-1293.
48. Hess, H.; Ross, J. L. *Chem. Soc. Rev.* **2017**, DOI: 10.1039/C7CS00030H.
49. Diez, S.; Howard, J. *Physics in Canada* **2009**, *65*, 7-12.
50. Nogales, E.; Wolf, S. G.; Downing, K. H. *Nature* **1998**, *391*, 199-203.
51. Chretien, D.; Metoz, F.; Verde, F.; Karsenti, E.; Wade, R. H. *J Cell Biol*. **1992**, *117*, 1031-1040.
52. Wang, H. W.; Nogales, E. *Nature* **2005**, *435*, 911-915.
53. Vanburen, V.; Odde, D. J.; Cassimeris, L. *Proc, Natl. Acad. Sci. USA* **2002**, *99*, 6035-6040.
54. Drabik, P.; Gusarov, S.; Kovalenko, A. *Biophys. J.* **2007**, *92*, 394-403.
55. Nogales, E.; Whittaker, M.; Milligan, R. A.; Downing, K. H. *Cell* **1999**, *96*, 79-88.
56. Schliwa, M.; Woehlke, G. *Nature* **2003**, *422*, 759-765.
57. Hirokawa, N.; Pfister, K. K.; Yorifuji, H.; Wagner, M. C.; Brady, S. T.; Bloom, G. S. *Cell* **1989**, *56*, 867-878.
58. Asbury, C. L. *Curr Opin Cell Biol* **2005**, *17*, 89-97.
59. Coy, D. L.; Wagenbach, M.; Howard. J. *J Biol Chem* **1999**, *274*, 3667-3671.
60. Hirokawa, N.; Takemura, R. *Exp. Cell Res.* **2004**, *301*, 50-59.
61. Sharp, D. J.; Rogers, G. C.; Scholey, J. M. *Nature* **2000**, *407*, 41-47.
62. Insinna, C.; Besharse, J. C. *Dev. Dynam.* **2008**, *237*, 1982-1992.
63. Howard, J.; Hudspeth, A. J.; Vale, R. D. *Nature* **1989**, *342*, 154-158.
64. Sheetz, M. P.; Spudich, J. A. *Nature* **1983**, *303*, 31-35.
65. Schnapp, B. J.; Vale, R. D.; Sheetz, M. P.; Reese, T. S. *Cell* **1985**, *40*, 455-462.
66. Kron, S. J.; Spudich, J. A. *Proc, Natl. Acad. Sci. USA* **1986**, *83*, 6272-6276.
67. Hess, H.; Vogel, V. *Rev. Mol. Biotech.* **2001**, *82*, 67-85.

68. Hess, H.; Bachand, G. D.; Vogel, V. *Chem. Eur. J*. **2004**, 10, 2110-2116.
69. Agarwal, A.; Katira, P.; Hess, H. *Nano Lett.* **2009**, *9*, 1170-1175.
70. Bachand, G. D.; Rivera, S. B.; Boal, A. K.; Gaudioso, J.; Liu, J.; Bunker, B. C. *Nano Lett*. **2004**, *4*, 817-821.
71. Böhm, K. J.; Stracke, R.; Muhlig, P.; Unger, E. *Nanotechnology*. **2001**, *12*, 238-244.
72. Hiyama, S.; Gojo, R.; Shima, T.; Takeuchi, S.; Sutoh, K. *Nano Lett*. **2009**, *9*, 2407-2413.
73. Schmidt, C.; Vogel, V. *Lab Chip* **2010**, *10*, 2195-2198.
74. Hess, H.; Howard, J.; Vogel, V. A. *Nano Lett*. **2002**, *2*, 1113-1115.
75. Hess, H.; Clemmens, J.; Howard, J.; Vogel, V. *Nano Lett*. **2002**, *2*, 113-116.
76. Jaber, J. A.; Chase, P. B.; Schlenoff, J. B. *Nano Lett.* **2003**, *3*, 1505-1509.
77. Ionov, L.; Stamm, M.; Diez, S. *Nano Lett.* **2005**, *5*, 1910-1914.
78. Reuther, C.; Hajdo, L.; Tucker, R.; Kasprzak, A. A.; Diez, S. *Nano Lett.* **2006**, *6*, 2177-2183.
79. Suzuki, H.; Yamada, A.; Oiwa, K.; Nakayama, H.; Mashiko, S. *Biophys. J.* **1997**, *72*, 1997-2001.
80. Hiratsuka, Y.; Tada, T.; Oiwa, K.; Kanayama, T.; Uyeda, T. Q. P. *Biophys. J.* **2001**, *81*, 1555-1561.
81. Van den Heuvel, M. G. L.; De Graaff, M. P.; Dekker, C. *Science* **2006**, *312*, 910-914.
82. Kim, T.; Kao, M.-T.; Hasselbrink, E. F.; Meyhofer, E. *Nano Lett.* **2007**, *7*, 211−217.
83. Platt, M.; Hancock, W. O.; Muthukrishnan, G.; Williams, M. E. *J. Am. Chem. Soc*. **2005**, *127*, 15686-15687.
84. Inoue, D.; Nitta, T.; Kabir, A. M. R.; Sada, K.; Gong, J. P.; Konagaya, A.; Kakugo, A. *Nat. Commun.* **2016**, *7*, 12557.
85. Tucker, R.; Katira, P.; Hess, H. *Nanoletters* **2008**, *8*, 221-226.
86. Nitta, T.; Hess, H. *Nanoletters* **2005**, *5*, 1337-1342.
87. Alberts, B.; Lewis, J.; Raff, M.; Walter, P.; Roberts, K.; Johnson, A.; Nakamura, K. Molecular Biology of the Cell 5E, Garland Science, pp. 965-1052 (**2010**).
88. Cross, R. A.; McAinsh, A. *Nat. Rev. Mol. Cell Biol.* **2014**, *15*, 257-271.
89. Nédélec, F. J.; Surrey, T.; Maggs, A. C.; Leible, S. *Nature* **1997**, *389*, 305-308.
90. Sanchez, T.; Welch, D.; Nicastro, D.; Dogic, Z.; *Science* **2011**, *333*, 456-459.
91. Sanchez, T.; Chen, D. T. N.; DeCamp, S. J.; Heymann1, M.; Dogic, Z. *Nature* **2012**,

431, 491-435.

92. Schaller, V.; Weber, C. A.; Semmrich, C.; Frey, E.; Bausch, A. R. *Nature* **2010**, *467*, 73-77.
93. Sumino, Y.; H. Nagai, K.; Shitaka, Y.; Tanaka, D.; Yoshikawa, K.; Chate H.; Oiwa, K. *Nature* **2012**, *483*, 448-452.
94. Inoue, D.; Mahmot, B.; Kabir, A. M. R.; Farhana, T. I.; Tokuraku, K.; Sada, K.; Konagaya, A.; Kakugo, A. *Nanoscale* **2015**, *7*, 18054-18061.
95. Kakugo, A.; Shikinaka, K.; Takekawa, N.; Sugimoto, S.; Osada, Y.; Gong, J. P. *Biomacromolecules* **2005**, *6*, 845-849.
96. Bachand, M.; Bouxsein, N. F.; Cheng, S.; von Hoyningen-Huene, S. J.; Stevensc, M. J; Bachand, G. D. *RSC Adv.* **2014**, *4*, 54641-54649.
97. Lansky, Z.; Braun, M.; Lüdecke, A.; Schlierf, M.; ten Wolde, P. R.; Janson, M E.; Diez, S. *Cell* **2015**, *160*, 1159-1168.
98. Schallera, V.; Weberb, C. A.; Hammericha, B.; Freyb, E.; Bausch, A. R. Frozen steady states in active systems. *Proc, Natl. Acad. Sci. USA* **2011**, *108*, 19183-19188.
99. Schaller, V.; Schmoller, K. M.; Karaköse, E.; Hammerich, B.; Maier, M.; Bausch A. R *Soft Matter* **2013**, *9*, 7229-7233.
100. Hess, H.; Clemmens, J.; Brunner, C.; Doot, R.; Luna, S.; Ernst, K. H.; Vogel, V. *Nano Lett*. **2005**, *5*, 629-633.
101. Ito, M.; Kabir, A. M. R.; Inoue, D.; Torisawa, T.; Toyoshima, Y.; Sada, K.; Kakugo, A. *Polym. J*. **2014**, *46*, 220-225.
102. Kakugo, A.; Shikinaka, K.; Matsumoto, K.; Gong, J. P.; Osada, Y. *Bioconjugate Chem*. **2003**, *14*, 1185-1190.
103. Kawamura, R.; Kakugo, A.; Osada, Y.; Gong, J. P. *Langmuir* **2010**, *26*, 533-537.
104. Kawamura, R.; Kakugo, A., Shikinaka, K.; Osada Y.; Gong, J. P. *Biomacromolecules* **2008**, *9*, 2277-2282.
105. Liu, H.; Spoerke, E. D.; Bachand, M.; Koch, S. J.; Bunker, B. C.; Bachand, G. D. *Adv. Mater*. **2008**, *20*, 4476-4481.
106. Liu, H.; Bachand, G. D. *Cell Mol. Bioeng.* **2012**, *6*, 98-108.
107. Luria, I.; Crenshaw, J.; Downs, M.; Agarwal, A.; Seshadri, S. B.; Gonzales, J.; Idan, O.; Kamcev, J.; Katira, P.; Pandey, S.; Nitta, T.; Phillpota, S. R.; Hess, H. *Soft Matter* **2011**,

7, 3108-3115.

108. Kawamura, R.; Kakugo, A.; Osada, Y.; Gong, J. P. *Nanotechnology*. **2010**, *21*, 145603-145614.
109. Lam, A. T.; Curschellas, C.; Krovvidi, D.; Hess, H. *Soft Matter* **2014**, *10*, 8731-8736.
110. Tamura, Y.; Kawamura, R.; Shikinaka, K.; Kakugo, A.; Osada, Y.; Gong, J. P.; Mayama, H. *Soft Matter* **2011**, *7*, 5654-5659.
111. Pinheiro, A. V.; Han, D. Shih, W. M.; Yan, H. *Nat. Nanotechnol.* **2011**, *6*, 763-772.
112. Seeman, N.C. *Annu. Rev. Biochem.* **2010**, *79*, 65-87.
113. Seeman, N.C. *J. Theor. Biol.* **1982**, *99*, 237-247.
114. Seeman, N.C. *Cell Biol.* **1991**, *10*, 475-486.
115. Rothemund, P.W. *Nature* **2006**, *440*, 297-302.
116. Adleman, L. M. *Science* **1994**, 266, 1021-1024.
117. Goodman, R.P.; Berry, R.M.; Turberfield, A. J. *Chem. Commun.* **2004**, *12*, 1372-1373.
118. Wang, Z. G.; Elbaz, J.; Willner, I. *Nano Lett.* **2010**, *11*, 304-309.
119. Shin, J. S.; Pierce, N. A. *J. Am. Chem. Soc.* **2004**, *126*, 10834-10835.
120. Bath, J.; Green, S. J.; Turberfield, A. J. *Angew. Chem. Int. Ed.* **2005**, *44*, 4358-4361.
121. Omabegho, T.; Sha, R.; Seeman, N. C. *Science* **2009**, *324*, 67-71.
122. Sherman, W. B.; Seeman, N. C. *Nano Lett.* **2004**, *4*, 1203-1207.
123. Tian, Y.; He, Y.; Chen, Y.; Yin, P.; Mao, C. *Angew. Chem. Int. Ed.* **2005**, *44*, 4355-4358.
124. Douglas, S. M.; Dietz, H.; Liedl, T.; Hogberg, B.; Graf, F.; Shih, W.M. *Nature* **2009**, *459*, 414-418.
125. Douglas, S. M.; Bachelet, I.; Church, G. M. *Science* **2012**, *335*, 831-834.
126. Kuzuya, A.; Komiyama, M. *Chem.Commun.* **2009**, *28*, 4182-4184.
127. Mirkin, C. A.; Letsinger, R. L.; Mucic, R. C.; Storhoff, J. J. *Nature* **1996**, *382*, 607-609.
128. Maye, M. M.; Kumara, M. T.; Nykypanchuk, D.; Sherman W. B.; Gang, O. *Nat. Nanotechnol.* **2010**, *5*, 116–120.
129. Nykypanchuk, D.; Maye, M. M.; van der Lelie, D.; Gang, O. *Nature* **2008**, *451*, 549-552.
130. Cigler, P.; Lytton-Jean, A. K. R.; Anderson, D. G.; Finn M. G.; Park, S. Y. *Nat. Mater.* **2010**, *9*, 918–922.

131. Michele, L. D.; Varrato, F.; Kotar, J.; Nathan, S. H.; Foffi, G.; Eiser, E. *Nat. Commun.* **2013**, *4*:2007.
132. Michele, L. D.; Fiocco, D.; Varrato, F.; Sastry, S.; Eiser, E.; Foffi, G. *Soft Matter* **2014**, *10*, 3633-3648.
133. Young, K. L.; Ross, M. B.; Blaber, M. G.; Rycenga, M.; Jones, M. R.; Zhang, C.; Senesi, A. J.; Lee, B.; Schatz, G. C.; Mirkin, C. A. *Adv. Mater.* **2014**, *26*, 653-659.
134. Wu, X. A.; Choi, C. H. J.; Zhang, C.; Hao, L.; Mirkin, C. A. *J. Am. Chem. Soc.* **2014**, *136*, 7726-7733.
135. Leunissen, M. E.; Frenkel, D. *J. Chem. Phys.* **2011**, *134*, 084702.
136. M. Hadorn, Boenzli, E.; Sørensen, K. T.; Hotz P. E.; Hanczyc, M. M. *Proc, Natl. Acad. Sci. USA* **2012**, *109*, 20320-20325.
137. Feng, L.; Pontani, L. L.; Dreyfus, R.; Chaikin, P.; Brujic, J. *Soft Matter* **2013**, *9*, 9816-9823.
138. Hadorn, M.; Boenzli, E.; Srensen, K. T.; Lucrezia, D.; Hanczyc M. M; Yomo, T. *Langmuir* **2013**, *29*, 15309-15319.
139. Hadorn, M.; Hotz, P. E. *PLoS One* **2010**, *5*, e9886.
140. Beales, P. A.; Vanderlick, T. K. *J. Phys. Chem. A* **2007**, *111*, 12372-12380.
141. Beales, P. A.; Nam, J. Vanderlick, T. K. *Soft Matter* **2011**, *7*, 1747-1755.
142. Beales, P. A.; Vanderlick, T. K. *Adv. Colloid Interface Sci.* **2014**, *207*, 290-305.
143. Hechta, F. M.; Bausch, A. R. *Proc, Natl. Acad. Sci. USA* **2016**, *113*, 8577-8582.
144. Rogers, A. R; Driver, J. W; Constantinou, P. E; Kenneth Jamison, D.; Diehl, M. R. *Phys. Chem. Chem. Phys.* **2009**, *11*, 4882-4889.
145. Wollman, A. J. M.; Sanchez-Cano, C.; Carstairs, H. M.; Cross, R. A.; Turberfield, A. J. *Nat. Nanotech.* **2014**, *9*, 44-47.
146. Derr, N. D.; Goodman, B. S.; Jungmann, R.; Leschziner, A. E.; Shih, W. M.; Reck-Peterson, S. L. *Science* **2012**, 338, 662-665.
147. Iwaki, M.; Wickham, S. F.; Ikezaki, K.; Yanagida, T.; Shih, W. M. *Nat. Commun.* **2016**, *7*:13715.
148. Dinu, C. Z.; Opitz, J.; Pompe, W.; Howard, J.; Mertig, M.; Diez, S. *Small* **2003**, *2*, 1090-1098.

149. Diez, S.; Reuther, C.; Dinu, C.; Seidel, R.; Mertig, M.; Pompe, W.; Howard, J. *Nano Lett.* **2003**, *3*, 1251-1254.
150. Hiyama, S.; Inoue, T.; Shima, T.; Moritani, Y.; Suda T.; Sutoh, K. *Small* **2008**, *4*, 410-415.
151. Hiyama, S.; Gojo, R.; Takeuchi, S.; Sutoh, K. *Nano Lett.* **2009**, *9*, 2407-2413.
152. Hiyama, S.; Moritani, Y.; Gojo, R.; Takeuchi, S.; Sutoh, K. *Lab Chip* **2010**, 10, 2741-2748.
153. Schmidt, C.; Vogel, V. *Lab Chip* **2010**, *10*, 2195-2198.
154. Steuerwald, D.; Früh, S. M.; Griss, R.; Lovchik, R. D.; Vogel, V. *Lab Chip* **2014**, *19*, 3729-3738.
155. Kagan, D.; Campuzano, S.; Balasubramanian, S.; Kuralay, F.; Flechsig, G.-U.; Wang, J. *Nano Lett.* **2011**, *11*, 2083-2087.
156. Orozco, J.; Campuzano, S.; Kagan, D.; Zhou, M.; Gao, W.; Wang, J. *Anal. Chem.* **2011**, *83*, 7962-7969.
157. Binnig, G.; Quate, C.F.; Gerber, Ch. *Phys. Rev. Lett.* **1986**, *56*, 930-933.
158. Marti, O.; Drake, B.; Hansma, P. K. *Appl. Phys. Lett.* **1987**, *51*, 484-486.
159. Marti, O.; Elings, V.; Haugan, M.; Bracker, C. E.; Schneir, J.; Drake, B.; Gould, S. A.; Gurley, J.; Hellemans, L.; Shaw, K.; Weisenhorn, A. L.; Zasadzinski, J.; Hansma, P. K. J. *Microsc*. **1988**, *152*, 803-809.
160. Lin, J. N.; Drake, B.; Lea, A. S.; Hansma, P. K.; Andrade, J. D. *Langmuir* **1990**, *6*, 509-511.
161. Gould, S.; Marti, O.; Drake, B.; Hellemans, L.; Bracker, C. E.; Hansma, P. K.; Keder, N. L.; Eddy, M. M.; Stucky, G.D. *Nature* **1988**, *332*, 332-334.
162. Uchihashi, T.; Iino, R.; Ando, T.; Noji, H. *Science* **2011**, 333, 755 -758.
163. Igarashi, K.; Uchihashi, T.; Koivula, A.; Wada, M.; Kimura, S.; Okamoto, T.; Penttilä, M.; Ando, T.; Samejima, M. *Science* **2011**, 333, 1279-1282.
164. Yamamoto, D.; Nagura, N.; Omote, S.; Taniguchi, M.; Ando, T. *Biophys. J.* **2009**, *97*, 2358-2367.
165. Shibata, M.; Yamashita, H.; Uchihashi, T.; Kandori, H.; Ando, T. *Angew. Chem. Int. ed.* **2011**, *50*, 4410-4413.

166. Yamashita, H.; Voïtchovsky, K.; Uchihashi, T.; Contera, S. A.; Ryan, J. F.; Ando, T. *J. Struct. Biol.* **2009**, *167*, 153-158.
167. Milhiet, P.-E.; Yamamoto , D.; Berthoumieu, O.; Dosset, P.; Grimellec, C. L.; Verdier, J.-M., Marchal, S.; Ando, T. *PLoS* ONE **2010**, *5*, e13240.
168. Casuso, I.; Sens, P.; Rico, F.; Scheuring, S. *Biophys. J.* **2010**, *99*, 47-49.
169. Miyagi, A.; Ando, T.; Lyubchenko, Y. L. *Biochemistry* **2011,** *59*, 7901-7908.
170. Sanchez, H.; Suzuki, Y.; Yokokawa, M.; Takeyasu, K.; Wyman, C. *Integr. Biol.* **2011**, *3*, 1127-1134.
171. Inoue, S.; Uchihashi, T.; Yamamoto, D.; Ando, T. *Chem. Commun.* **2011**, *47*, 4974-4976.
172. Giocondi, M. C.; Yamamoto, D.; Lesniewska, E.; Milhiet, P. E.; Ando, T.; Grimellec, Le. C. *Biochim. Biophys. Acta.-Biomembranes* **2010**, *1798*, 703-718.

CHAPTER 2

DNA Programmed Control of Swarming in a Biomolecular Motor System

Abstract

Swarming of a biomolecular motor system has been demonstrated using DNA programming. Swarm units were prepared by conjugation of cytoskeletal filamentous protein, microtubules (MTs) with DNA through copper free click reaction. Swarming of this information processed units was demonstrated by active self-assembly driven by motor protein kinesin using simple DNA interaction. Shape of swarming pattern as well as their mode of motion such as translational and rotational motion was regulated by tuning physical properties of swarm units. Swarming morphology was also regulated by tuning the relevant parameters. Finally, mode of motion was controlled by dissociation of swarm groups applying DNA strand displacement reaction. Such control of swarming pattern and mode of motion through DNA programming gives us the opportunity to understand swarming observed in nature.

2.1 Introduction

Swarming or collective behavior is the most extensively used process which enables nature to build complex forms, from multicellular organisms to complex animal structures purely by local interaction. Examples can be found across a wide range of physical scales and systems at the molecular scale with self-assembly of crystals or rotary motors of bacterial flagella[1, 2], at the cellular scale with the development of multicellular organisms[3, 4], and at the colony level with ants creating structures such as rafts, chains, and nests using only their interconnected bodies as building material[5, 6]. By emergence of different structures or patterns they get various advantages like forage of foods, protection from predators depending on different shape and size through reversible swarming which is not possible by individual entities[7]. Scientists are being interested by these features trying to understand swarming and demonstrate it using engineered system such as synthetic chemical system[8] and robotic system[9], etc. Alongside these approaches, another approach has been extensively studied using natural biomolecular motor system demonstrating swarm of tiny self-propelled units[10-12]. Their small size offers controllability over a large number of units at a time forming non-equilibrium higher order structures. When propelled by motor proteins, local interaction or cross linking among the neighbor units using modulating agents plays key role that resulted various patterns of organized structures, e.g. stream, vortex, spool, networks and bundles as reported in the literature[13-31]. The structures prevail as long as energy is dissipated in the system retaining their dynamic behavior. Therefore, biomolecular motor system is an excellent tool for demonstration of swarming. However, despite their highly self-organizing behavior, reversible control of swarming still remains challenging due to lack of proper programming of interaction among them. For this, modulation of interaction between them is required in a programmed way. Regarding this, DNA has emerged as the exceedingly precise interacting molecule for its high specificity and selective bonding nature which makes it versatile as programming molecule[32-35]. DNA can also be a potential candidate in dynamic condition due to its strand displacement property[36-39] which has been successful to control reversible aggregation of different synthetic molecules to form macroscopic assembly[40, 41]. However, only a few studies in combination of motor protein-DNA found in the literature which mainly focused on DNA self-assembly or cargo transportation by single MT-DNA conjugation[42-50] but no study on controlling swarm has been found yet. Thus, swarming of cytoskeletal filamentous protein MTs driven by motor protein kinesin was demonstrated employing unique feature of DNA to program interaction among them. The swarming units were designed by conjugating DNA to MTs containing

specific information for self-assembly in presence of their complementary linker DNA (*l*-DNA). Swarming with different pattern with their corresponding mode of motion was demonstrated by changing the inherent properties of MTs using DNA interaction. Interchange of swarming mode of motion was successfully demonstrated by dissociation of swarm using DNA strand displacement reaction which makes the system more reliable for study of natural swarming. Such control over swarming of a biomolecular motor system by DNA programmed self-assembly gives us a new concept to design swarm robots at molecular level.

2.2 Results and Discussion

2.2.1 Preparation of swarm units by conjugation of DNA to MT

For demonstration of swarming, single swarm units were prepared from natural components using synthetic chemical reaction. The swarm units were designed by conjugating MTs with single-stranded DNA through copper free click reaction[51-54], where DNA was labeled with DBCO (dibenzocyclooctyl) at the 5´ end which can react with azide functionalized MT and a fluorescence dye in 3´ end for allowing monitoring of the swarm units (**Figure 2.1a**). For constructing swarm units, MTs were prepared by polymerization of azide labeled tubulin with polymerization agent GMPCPP (guanosine-5´[(α, β)-methyleno] triphosphate). The cylindrical body size of the MT was 25-nm thick with length in a range of micrometer scale (~2 to ~10 μm). For designing DNA logic gates, two receptor DNA (*r*-DNA) sequences T_{16} and $(TTG)_5$ were chosen that are not complementary to each other (detailed sequence given in 2.4 section). From melting temperature simulation, the DNA sequences were designed by considering the base number and sequences that can only operate (*vide infra*) in presence of input signals avoiding any undesired interactions at the working temperature of the swarm units (25 ^{o}C). The DNA sequences were labeled with two different dyes to distinguish the swarm units as red (R)-swarm units and green (G) swarm units (**Figure 2.1b**).

After conjugation of *r*-DNA to MTs the labeling ratio of *r*-DNA was determined using UV-spectrophotometer. With increasing the *r*-DNA concentration for conjugation, the labeling ratio was found to increase as can be clearly observed from **Figure 2.2a**. Each spectrum at different concentration was analyzed to determine the final concentration of *r*-DNA conjugated MTs and the resulted labeling ratio (**Figure 2.2b and Table 2.2.1**).

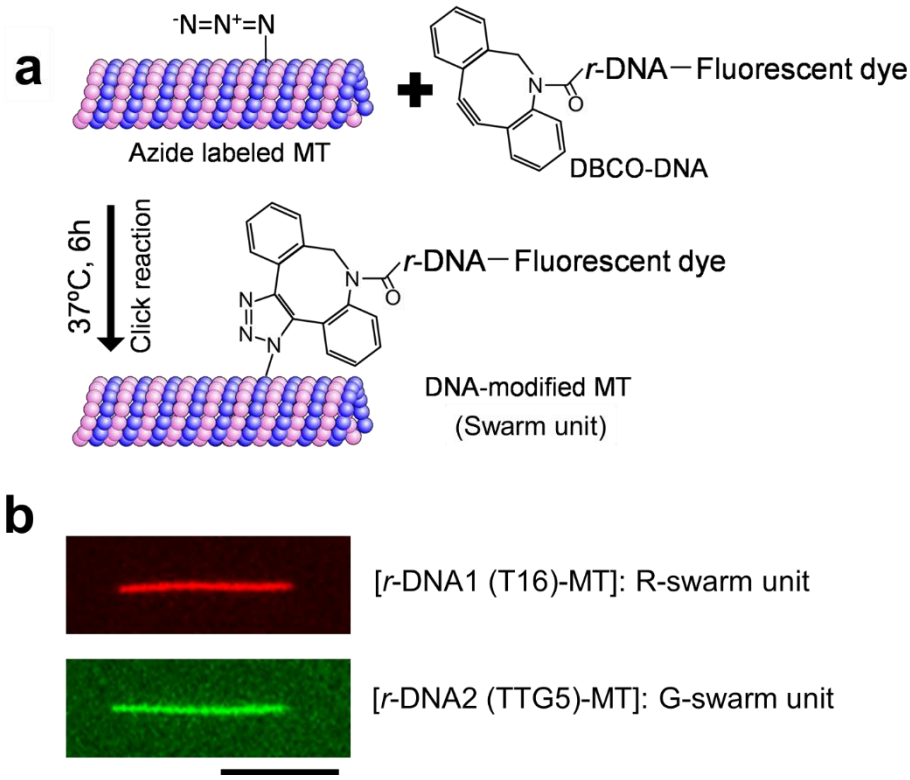

Figure 2.1 Schematic diagram of preparation of swarm unit through conjugation of MT with *r*-DNA by click reaction (a) and fluorescence image of swarm units, scale bar: 5 μm (b).

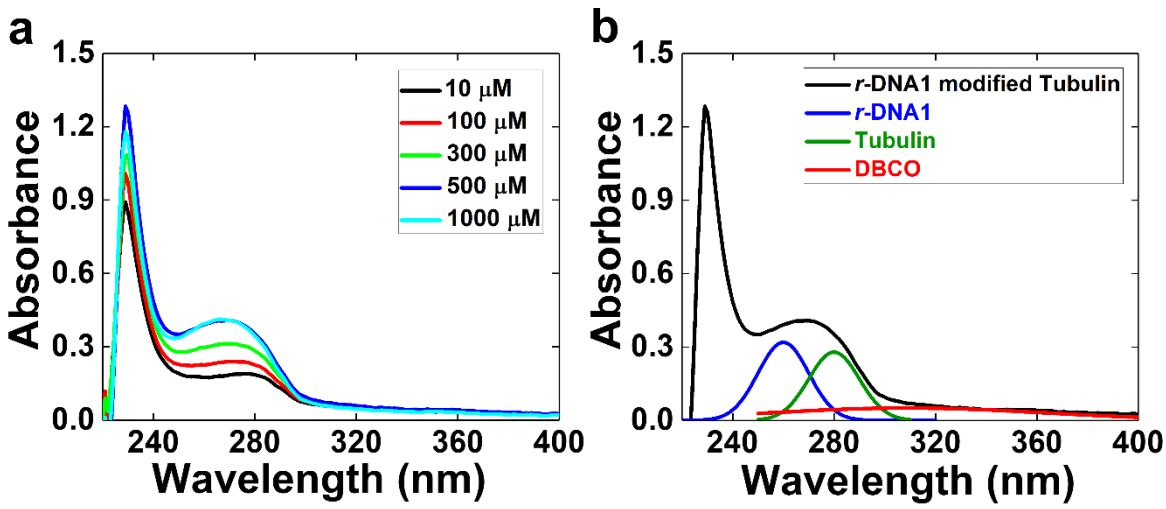

Figure 2.2 Representative plot of absorbance of *r*-DNA1 conjugated MTs at various concentrations of *r*-DNA1 as mentioned in the inset (a) and evaluation of absorbance peaks of *r*-DNA1, tubulin and DBCO by Gaussian distribution function (b).

Table 2.2.1 Labeling ratio of swarm units for various concentrations of *r*-DNA modifiers

Conc. of *r*-DNA (µM)	Final conc. of MT (µM)	Final conc. of *r*-DNA1 (µM)	Labeling ratio of *r*-DNA1-MT (%)	Final conc. of MT (µM)	Final conc. of *r*-DNA2 (µM)	Labeling ratio of *r*-DNA2-MT (%)
10	12	8	70	12	8	66
100	15	12	84	14	11	76
300	18	17	93	17	16	92
500	24	25	101	24	23	96
1000	23	25	107	19	21	106

The labeling ratio of *r*-DNA to MTs was found ~100% after 500 µM DNA concentration. Thus the surface of MT was considered as saturated with the *r*-DNA strands which in combination form swarm units.

2.2.2 Investigation of motility of swarm units in *in vitro* gliding assay and their bioactivity by changing modification ratio of *r*-DNAs

The motility of DNA conjugated swarm units were verified using *in vitro* motility assay. After preparing a flow cell, kinesins (recombinant conventional kinesin-1 consisting of 573 amino acid) were immobilised on the glass surface of the flow cell. Swarm units i.e; DNA conjugated MTs were then applied to the flow cell. Here MTs with length 5.4 ± 2.1 and 5.4 ± 3.3 µm conjugated with T_{16} and $(TTG)_5$ were used for demonstrating motility respectively. Finally, motility of swarm units was initiated by adding ATP to the flow cell. The flow cell was then placed in the inert chamber after the addition of ATP. The motility of MTs was monitored using a fluorescence microscope. Almost all of the swarm units were found to move with a mean velocity of ~0.60 ± 0.05 µm s^{-1}. Unidirectional translational motion of the swarm units confirmed that DNA conjugation to MTs does not hinder MT-kinesin interaction (**Figure 2.3**).

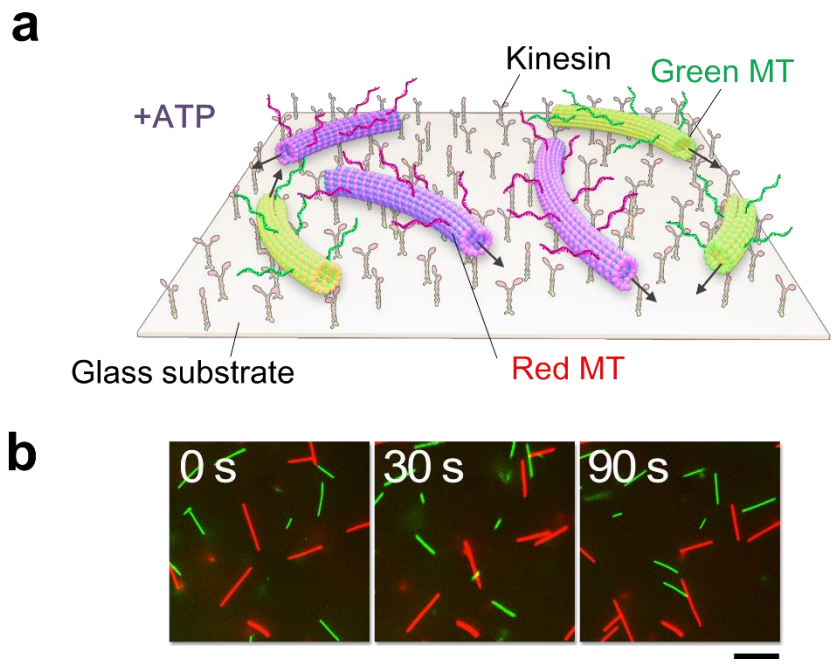

Figure 2.3 Schematic image of *in vitro* motility assay of swarm units (a) and time lapse images of motility of R and G-swarm units (b). Scale bar: 10 µm.

To understand the effect of DNA modification on the surface of MTs on their motility, *r*-DNA concentrations was varied from 50 to 1000 µM. The results shown in **Figure 2.4** are the velocities estimated for different concentration of *r*-DNA1.

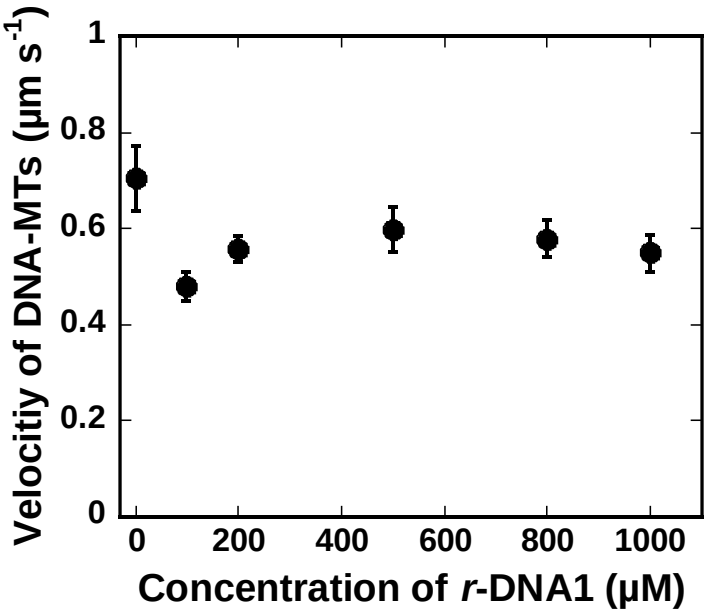

Figure 2.4 Effect of *r*-DNA for modification of swarm units on their velocity. By varying the concentration of *r*-DNA1, the labeling ratio of MT to the DNA was varied. Number of swarm unit considered was 30. Error bar: Standard Error (S. E.).

Upon varying the conjugation ratio of *r*-DNA1 to MTs it was revealed that, the velocity of swarm units fluctuated, although no clear tendency was observed. The bioactivity of swarm units was thus retained after conjugation of DNA to MTs with a moderate velocity that is prerequisite for demonstrating swarming.

2.2.3 Demonstration of swarming by active self-assembly of swarm units using input *l*-DNA signals

Swarming of the single swarm units was demonstrated using two types of individual swarm units with two designed DNA (T_{16} and $(TTG)_5$, termed as 'receptor DNA' (*r*-DNA) as mentioned in the previous sections. *l*-DNA1, partially complementary to the *r*-DNAs (CAA5A16), was designed to allow hybridization of the *r*-DNA strands in a zipping manner (**Figure 2.5**).

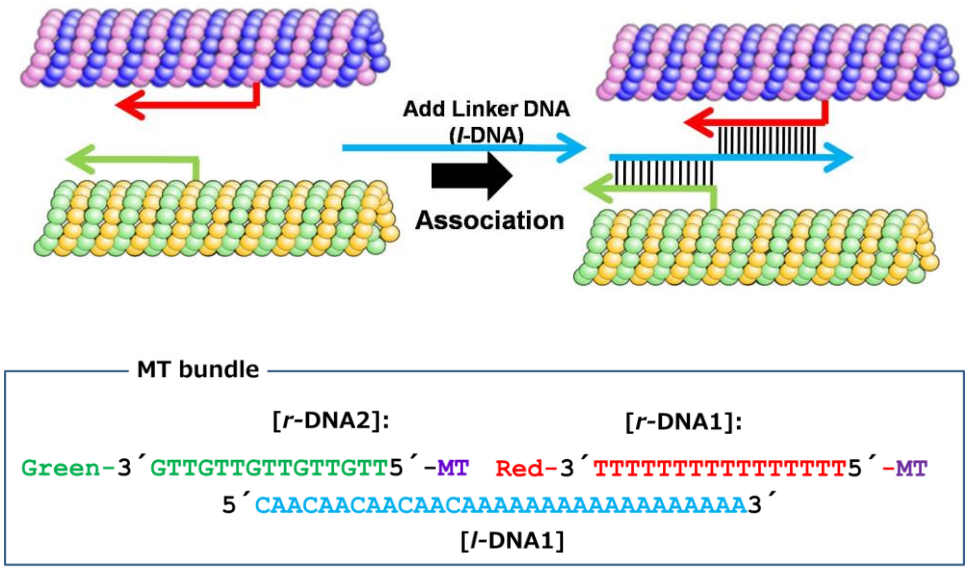

Figure 2.5 Schematic diagram of self-assembly of R and G-swarm units by input DNA signal.

Here to demonstrate swarming, individual swarm units were placed on a kinesin coated substrate at a density of ~40,000 per mm^2 area (density was measured in 0.0167 mm^2 area) with almost an equal density of the two types of swarm units. The swarming was initiated with adding *l*-DNA1 in the system which is favored by the active or dynamic self-assembly of swarm units using driving force of molecular motor kinesin powered by ATP. It is to be mentioned that, in static condition i.e; in absence of ATP or kinesin swarming behavior didn't take place or requires a longer time to reach the saturated condition where some aggregates were found to observe (**Figure 2.6**).

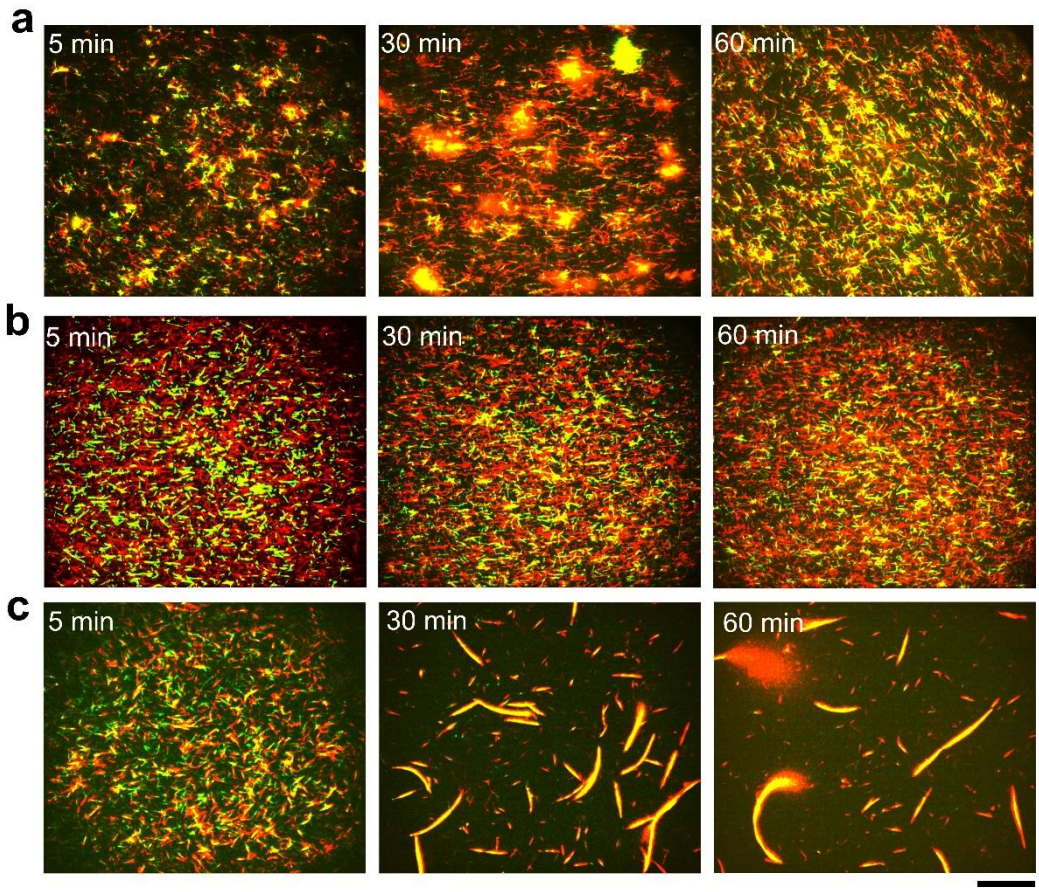

Figure 2.6 In a static system e.g. in bulk solution swarm units were found to form aggregates which were not stable with time (a). In an unfueled system, such as on a kinesin coated surface in the absence of ATP, no swarm group was formed (b). In the dynamic system, on a kinesin coated surface in the presence of ATP, swarm groups were formed with time through encountering of motile swarm units (c). Scale bar: 50 µm.

In static condition i.e; in bulk solution some aggregates were formed which were no longer stable with time (**Figure 2.6a, 2.6b**). These aggregates were mainly formed by the Brownian motion of swarm units with input *l*-DNA1 that takes place in equilibrium condition while swarm units attached on the kinesin coated surface without ATP were restricted to move by Brownian or dynamic motion which even prevents the aggregate formation. On the other hand, in presence of ATP, by self-propelling the size of the groups of swarm units increased through encountering of the groups. Despite the increase in size (length), the groups of swarm units exhibited translational motion with a velocity (0.51 ± 0.02 µm s^{-1}) close to that of single units (0.60 ± 0.05 µm s^{-1}) (**Figure 2.6c**). Swarming is preferentially formed by the unidirectional moving swarm units with similar velocity in active self-assembly process in presence of *l*-DNA1. The high motility of these swarm groups with translational motion suggested that there

could be highly ordered structures with unipolarity where the assembly took place by the sophisticated interaction of DNA.

By monitoring the change of color, the association of individual swarm units into swarm groups was characterized by using the equation 2.4.1 (Section 2.4). Upon association of individual R and G swarm units the association ratio was increased linearly with length of yellow part during association (**Figure 2.7**).

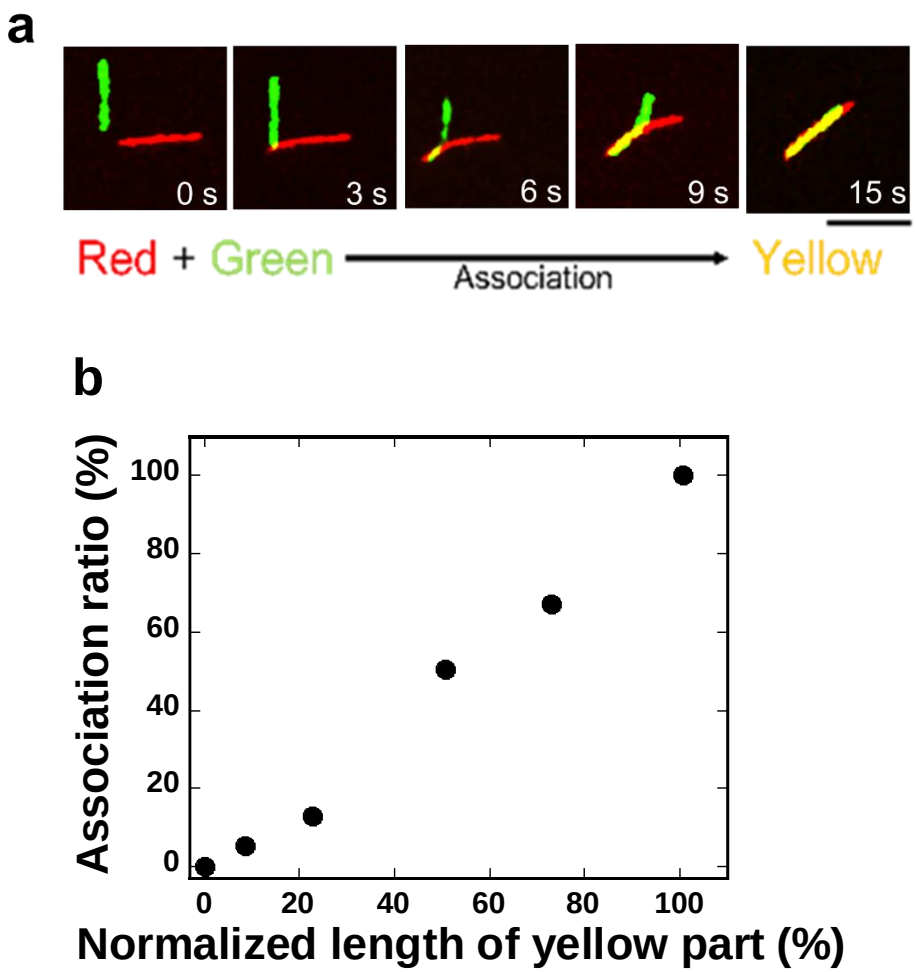

Figure 2.7 An encounter event of two individual swarm units with red and green color associated visible in yellow color, scale bar: 5 µm. (a). Estimation of association ratio from a swarming event of two swarm units (b). Here association ratio is estimated following the swarming of a red and a green swarm unit into a yellow swarm group (a).

The length of yellow part of the swarm was measured with time, which represents the association of the red and green units and normalized the length with respect to the final length of the yellow swarm group formed after complete association of the R and G swarm units. The association ratio was obtained almost 100% which indicates that, the individual swarm units

are associated fully to behave like a swarm. To support and verify the methodology for analysis of association ratio another approach was also performed based on single swarm unit (MTs) counting which is described in the **Appendix** section.

Bundles or linear shaped swarming was obtained from the above demonstration, morphology of which may depend on a number of parameters. Kinesin concentration was fixed at 300.0 nM in all cases which was optimized by varying the concentration of kinesin. To investigate the effect of different parameters association time was considered 60 min after passing ATP buffer at which the association ratio reached a saturated value (~70%) with addition of the *l*-DNA1. I also systematically studied the effects of different relevant parameters on the swarming and also on their morphology such as time, concentration of *r*-DNAs, *l*-DNA1, and length of *l*-DNA1 and density of MTs to find out the optimized condition.

2.2.3.1 Effect of motor protein kinesin on swarming

To investigate the effect of kinesin on swarming, the concentration of kinsein was varied from 1-1000 nM. At relatively low kinesin concentrations (~1, 10 nM) a small number of swarm units was found to attach on the kinesin coated surface. Concentration of *r*-DNAs was 500.0 µM and the concentration of *l*-DNA1 was kept constant at 0.06 µM. On increasing the concentration of kinesin (~100-500 nM), the density of swarm units increased, which facilitated the swarm group formation due to collision among them (**Figure 2.8**). The swarm group formation was decreased with further increase in kinesin concentration (~1000 nM). Higher driving force with increased kinesin density on the surface prevented the formation of stable swarm groups. The change in association ratio with increasing the concentration of swarm units is shown in **Figure 2.9**.

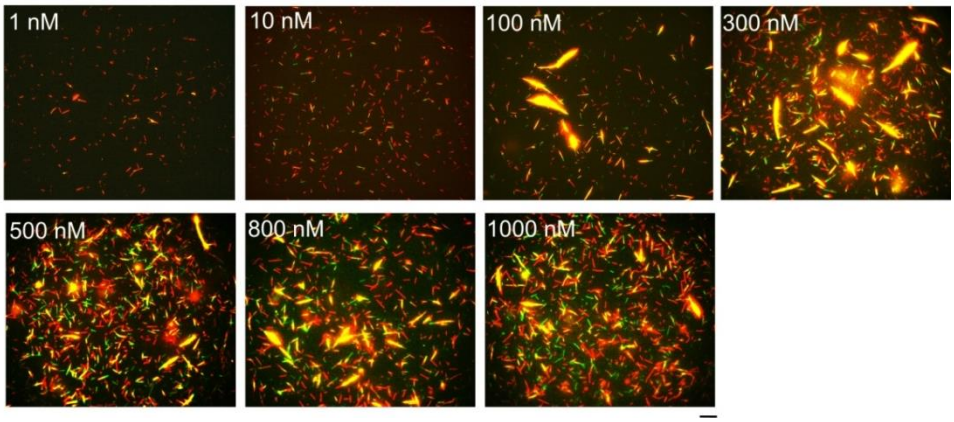

Figure 2.8 Fluorescence microscopy images showing effect of kinesin concentration in feed on the swarming of swarm units. The images were captured after 30 min of ATP addition. Scale bar: 20 µm.

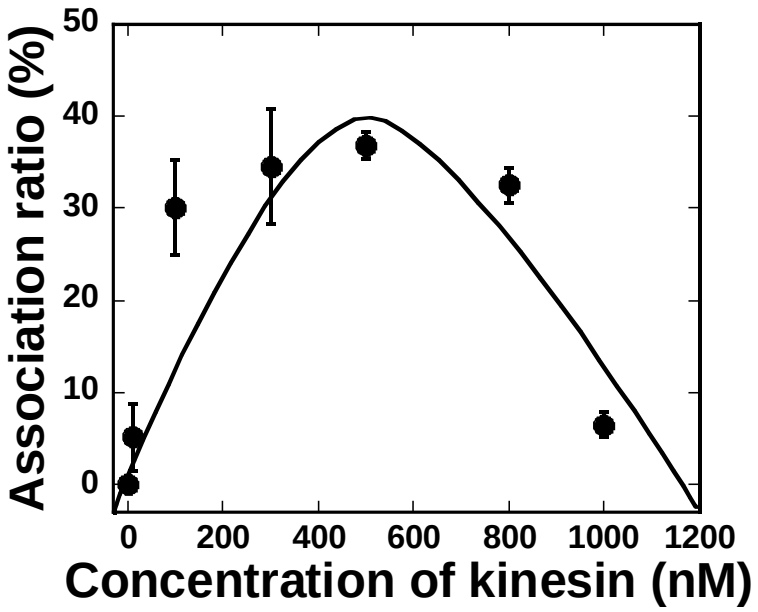

Figure 2.9 Change in association ratio of swarm units on changing the concentration of kinesin. The line was drawn to guide the eye. Error bar: S. E.

2.2.3.2 Effect of time on translational mode of swarming

To investigate time dependent swarming by active self-assembly of swarm units concentration of *r*-DNA was 500 µM while the *l*-DNA1 was kept constant at 0.6 µM. For driving the self-association in non-equilibrium system, the kinesin concentration was used 300.0 nM with density of R and G-swarm units ~40,000 per mm^2 area. The fluorescence microscopic observation was performed just after the ATP addition using inert chamber system with scavengers. **Figure 2.10** shows the time lapse images where change in size and number of swarm groups can be clearly observed.

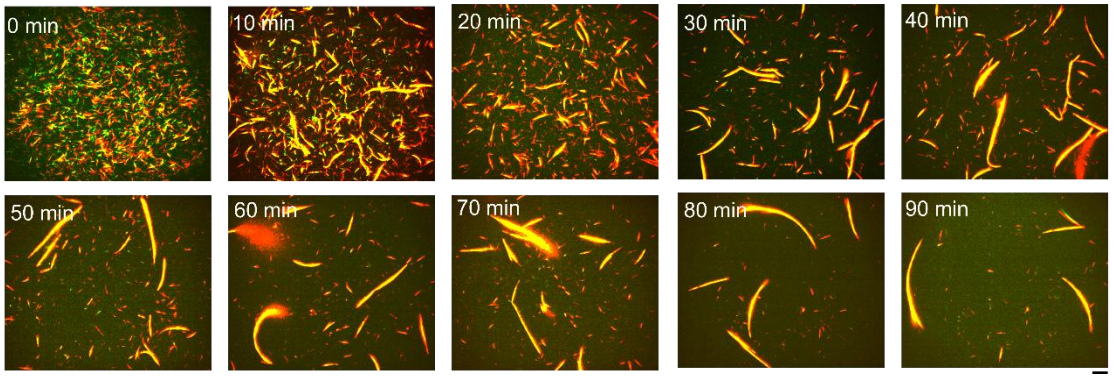

Figure 2.10 Time lapse fluorescence microscopy images showing how the size and number of swarm groups changed with time. Scale bar: 20 µm.

The association ratio increased with time and reached a saturated value (~70%) within 60 min of addition of the *l*-DNA1 (**Figure 2.11**).

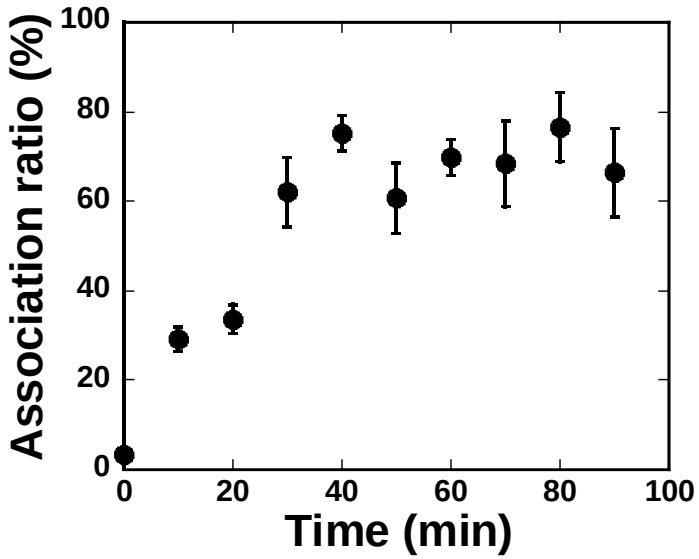

Figure 2.11 Association ratio of swarm units with time after addition of ATP in the system. Error bar. S. E.

Upon collision of the red and green swarm units, swarm groups with an average size of ~14.05±8.26 µm were produced which was larger in size than the individual swarm units (average length of ~5.31± 1.77 µm). Over time the size of the swarm groups increased as ~27.42± 12.36 µm at 60 min (**Figure 2.12**).

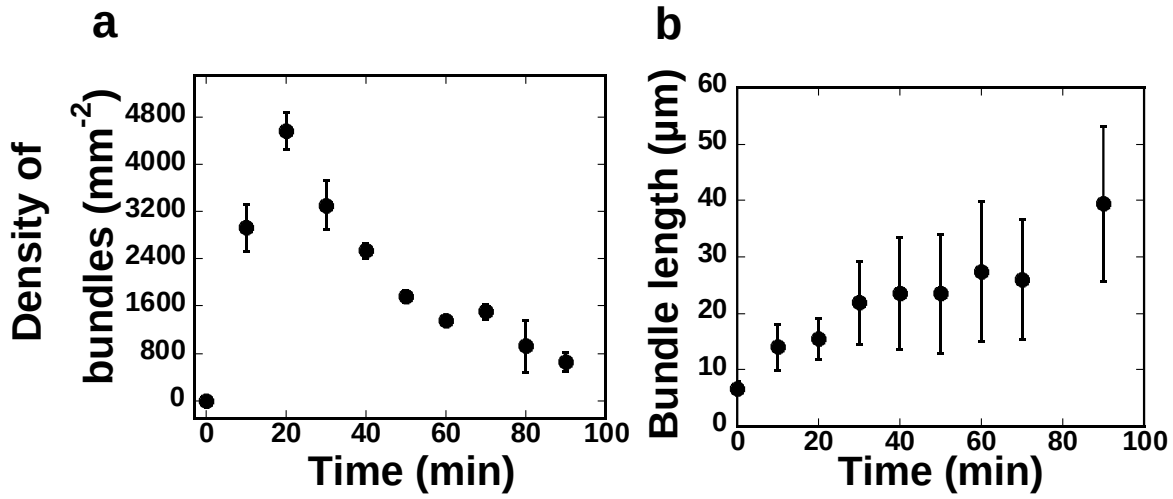

Figure 2.12 Change in number of swarm per mm^2 unit area (a) and size of swarm groups (b) with time. The number of swarm groups with translational motion increased initially just after ATP addition and then decreased with time. The association of swarm groups into larger ones

caused such decrease in number which is ascribed to the change in their bundle length with time (b). Error bar: S. E.

2.2.3.3 Effect of concentration of *r*-DNAs on swarming

The *r*-DNAs could have significant effect on the association of swarm units as the interaction of *l*-DNA1 depends on the probability of interaction with *r*-DNAs of swarm units. To investigate the effect, the concentration of *r*-DNA was varied from 50-1000 µM while the concentration of *l*-DNA1 was kept constant at 0.6 µM. For self-assembly, R and G-swarm units were applied in the motility assay followed by passing of 300.0 nM kinesin. The images of self-assembly were captured after 60 min of passing ATP buffer when the swarming of single units become saturated (**Figure 2.13**). At lower concentration the self-assembly of swarm units was not observed despite presence of *l*-DNA1 while with increasing the *r*-DNA concentration i.e; labeling ratio of DNA to MTs, the swarming increases which was confirmed from the yellow color and long bundle length of swarm groups which shows translation motion. After 500 µM concentration, the self-assembly becomes saturated as can be clearly understood from their association ratio (**Figure 2.14**). At this concentration the surface of MTs was saturated with *r*-DNAs as confirmed from their labeling ratio at which the probability of swarming was found to be increased.

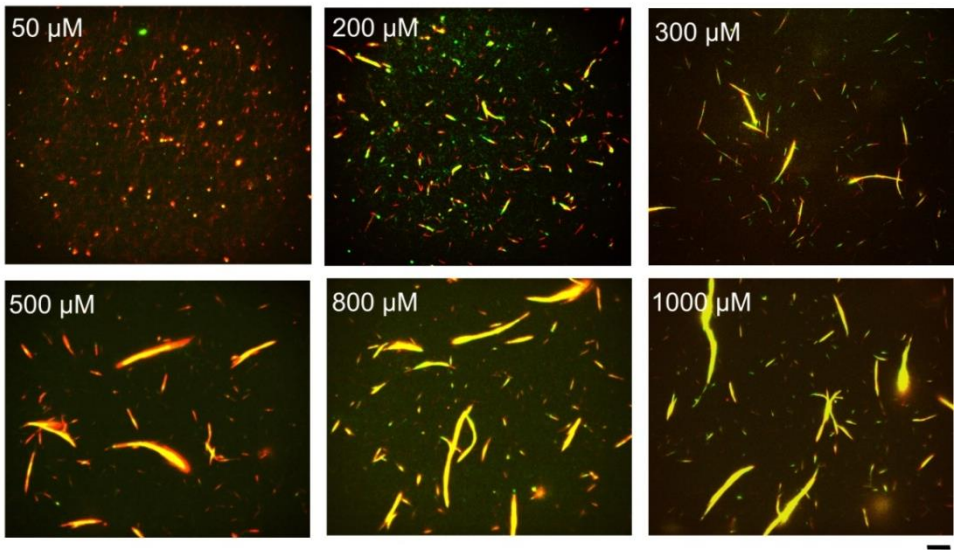

Figure 2.13 Effect of concentration of receptor DNA (*r*-DNA1 and *r*-DNA2) on the swarming. Fluorescence microscopy images showing swarm groups formed when concentration of *r*-DNA1 and *r*-DNA2 was varied as mentioned in the inset. Scale bar: 20 µm. The images were captured after 60 min of ATP addition.

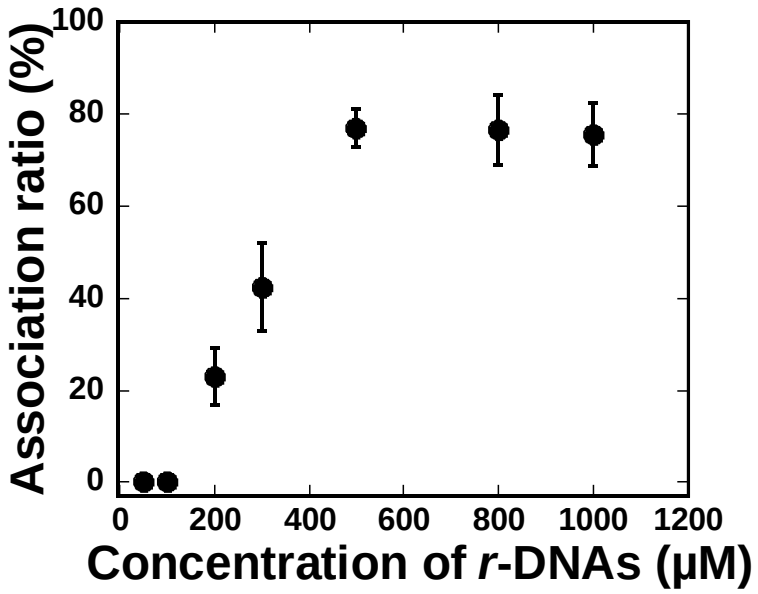

Figure 2.14 Change in association ratio of swarm units upon changing the concentration of *r*-DNA1 and *r*-DNA2. With increasing the concentration of *r*-DNAs the association ratio rapidly increased and reached a plateau at 500 μM. Error bar: standard error (S. E.).

2.2.3.4 Effect of concentration of *l*-DNA1 on swarming

For demonstrating swarming, *l*-DNA1 (CAA5A16) partially complementary to *r*-DNAs used as input chemical signals. To investigate the effect, the concentration of *l*-DNA1 was varied from 0.001-1.0 μM while the *r*-DNAs concentration was used 500 μM for modification. The images of self-assembly was captured after 60 min of passing ATP buffer when the swarming of single units become saturated (**Figure 2.15**).

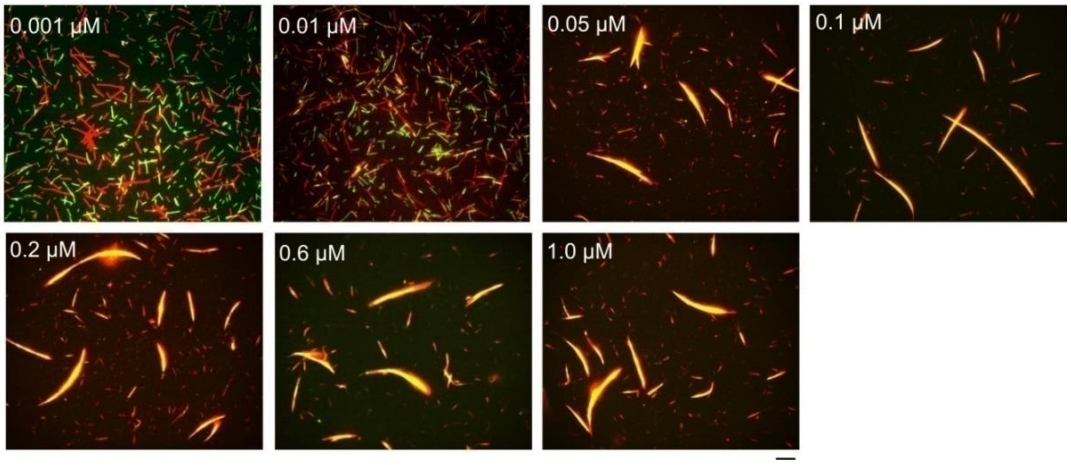

Figure 2.15 Fluorescence microscopy images of swarm groups formed for various concentration of *l*-DNA1. The images were captured after 60 min of ATP addition. Scale bar: 20 μm.

From the images it is clearly observed that the swarming started after 0.05 μM *l*-DNA1 concentration. Initially a sharp rise in association ratio with increasing the concentration of *l*-DNA1 was observed, which then decreased on increasing the concentration of *l*-DNA1 further (**Figure 2.16**). The result indicates that, a critical concentration of *l*-DNA1 (0.05 μM) is required for initiation of swarming in presence of saturated concentration of *r*-DNA.

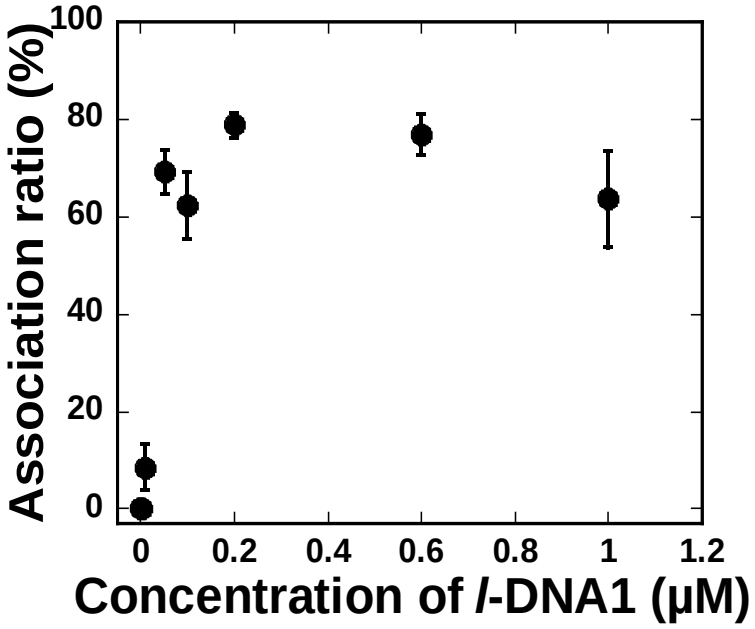

Figure 2.16 Effect of concentration of *l*-DNA1 on the association ratio of swarm units with conjugation ratio of 100.82% and 96.29% for *r*-DNA1 and *r*-DNA2 respectively. The association ration was measured after 60 min of starting association of the swarm units. Error bar: S. E.

2.2.3.5 Effect of length of *l*-DNA1 on swarming

Length of *l*-DNA1 can significantly alter the extent of swarming depending on the DNA hybridization strength at room temperature. Basically, the strength of DNA interaction depends on the number of bases and also type of bases present in the sequences in addition to experimental conditions which changes the melting temperature (T_m) of DNA hybridization. T_m is the key parameter for designing DNA sequences. I changed the length of *l*-DNA1 (CAAA16-CAA5A16) depending on which the swarming was investigated with time (**Figure 2.17**). From the T_m of DNA interaction and its corresponding free energy change also reveals that swarming become thermodynamically favorable with increasing T_m of DNA hybridization. The length of *l*-DNA was varied with increasing the length of sequence $(TTG)_x$ which contains

the GC content. The change in T_m and corresponding free energy change with increasing the base number of DNA can be understood from the following Table **2.2.2**

Table 2.2.2 T_m and free energy change for DNA interaction between *r*-DNAs with different length of *l*-DNA

	T_m of DNA interaction (°C)	ΔG Kcal/mol (TTG/CAA interaction)
a	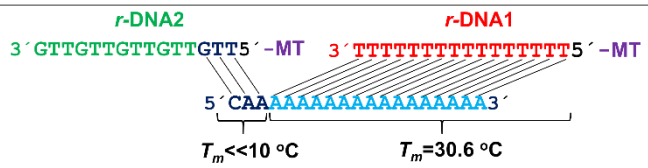	-
b	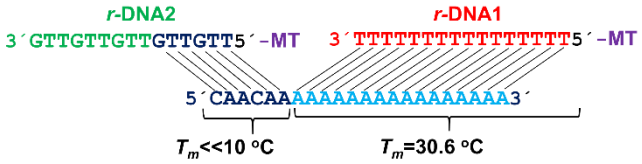	-
c	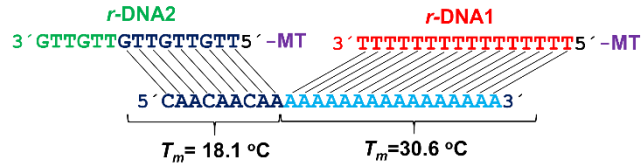	6.7
d	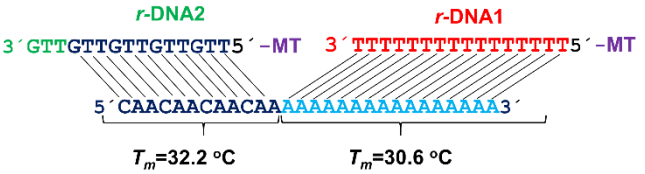	11.1
e	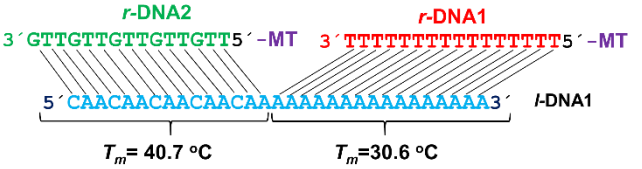	15.5

T_m calculated based on nearest neighbor effects contributed through base stacking[55-57] by OligoAnalyzer 3.1 and ΔG calculated by oligocalc calculator at the standard thermodynamic conditions: 1M NaCl at 25 °C at pH 7. For T16/A16 the change in ΔG is 13 kcal/mol.

From the T_m values we can see that, DNA interaction is not feasible when the number of $(TTG)_x$ is x=1 or 2. When the number of base sequences increases to 3 free energy for DNA hybridization becomes favorable and further increased for the longest sequence $(TTG)_5$ used. T_m of DNA duplex formation can also influence the swarming accordingly, which was investigated thoroughly for the *l*-DNA sequences as shown in **Figure 2.17**.

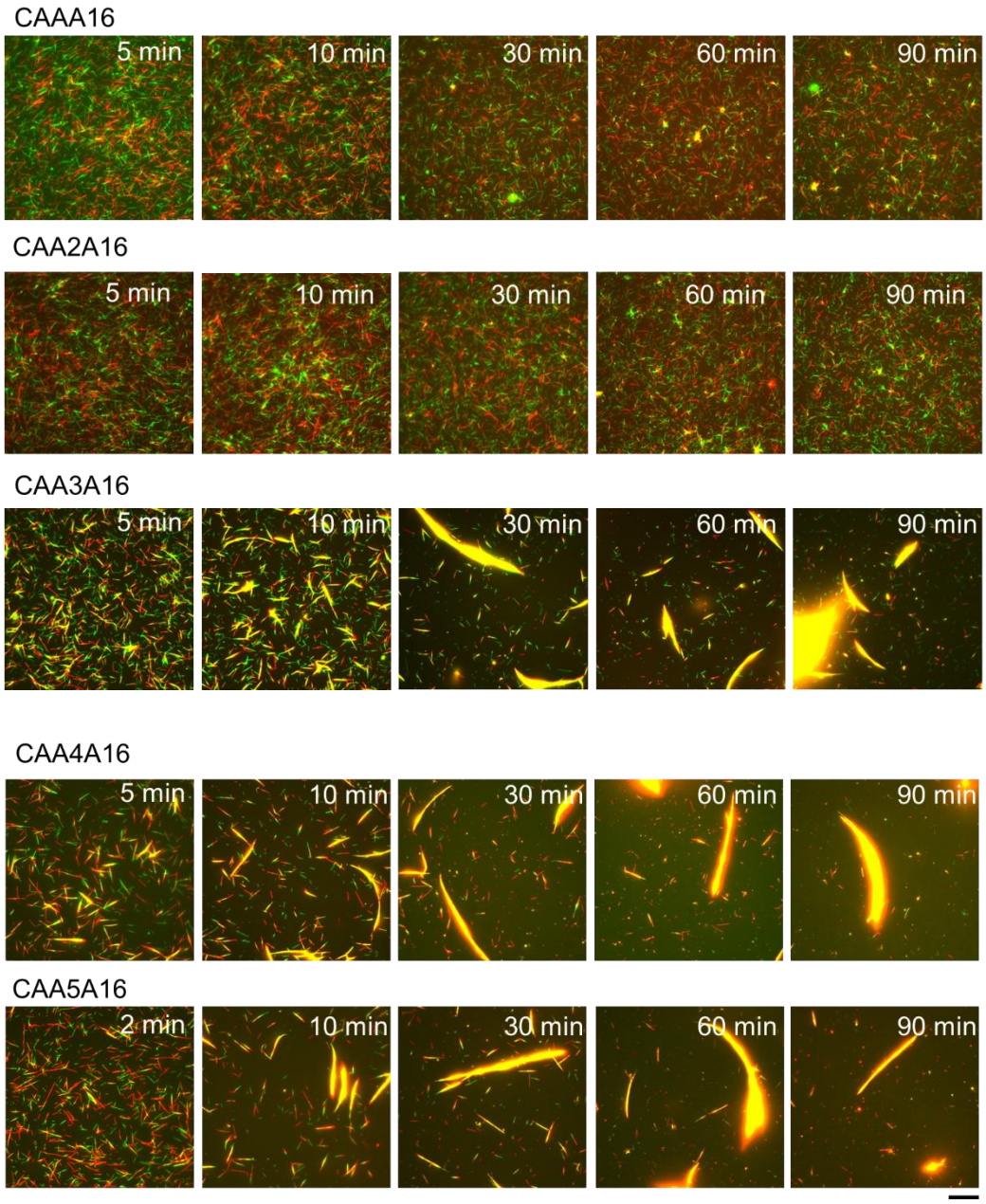

Figure 2.17 Fluorescence microscopy images of swarm groups formed in presence of different length of *l*-DNA1 with time. Scale bar: 20 µm.

From **Figure 2.17** it was observed that, swarming started to form when the length of *l*-DNA reached to 25 base sequences (CAA3A16). In case of shorter length of *l*-DNA than this no swarming was observed so far (CAAA16-CAA2A16). For demonstrating swarming I used in my system CAA5A16 (31 base sequence) which is fully complementary to the base sequences of *r*-DNAs (T_{16} and $(TTG)_5$) described in previous sections. Increase of extent of swarming with increasing the length of *l*-DNA sequence is clearly observed from their association ratio with time as shown in **Figure 2.18**. Thus kinetics of the self-assembly of swarm units can also be controlled by designing the T_m of input DNA signals.

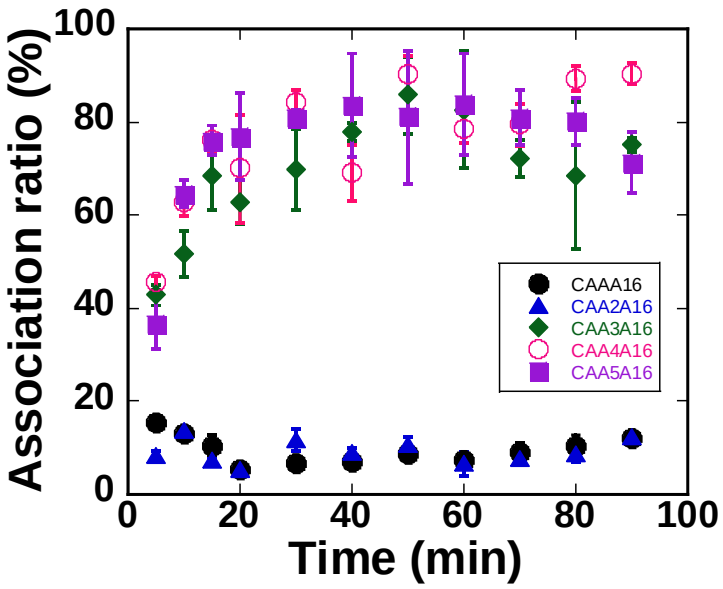

Figure 2.18 Association ratio of swarm units in presence of different length of *l*-DNA1. The base sequences were varied from CAAA16-CAA5A16. Error bar: S. E.

2.2.3.6 Effect of density of swarm units on swarming

Swarming at large scale depends not only on the concentration of *r*-DNA and *l*-DNA1 but also significantly on the density of R and G swarm units in action. I investigated the effect of density of swarm units varying the density of R-swarm units while keeping the density of G-swarm units almost constant. The density ratio of R-swarm units: G-swarm units = 0.05:1, 0.5:1, 1:1, 2:1, 7:1 was used where the density was measured in 0.066 mm^2 area. The swarming and the length of swarm groups was found to increase with increasing the density of R-swarm units and reached maximum when the ratio is 1:1. The length of swarm groups decreased again with further increasing the concentration of R-swarm units (2:1, 7:1) as shown in the fluorescence microscopic images of **Figure 2.19**. At density ratio of 7:1 it is seen that, bundles were formed but they were not stable enough after 60 min of passing ATP buffer. As the density ratio come close to 1:1, stable yellow colored long bundles were found on the surface. Again when the ratio is 0.05:1 the size of swarm group decreased which can be also revealed in **Figure 2.20a**. The *l*-DNA concentration was used 0.6 μM in all cases.

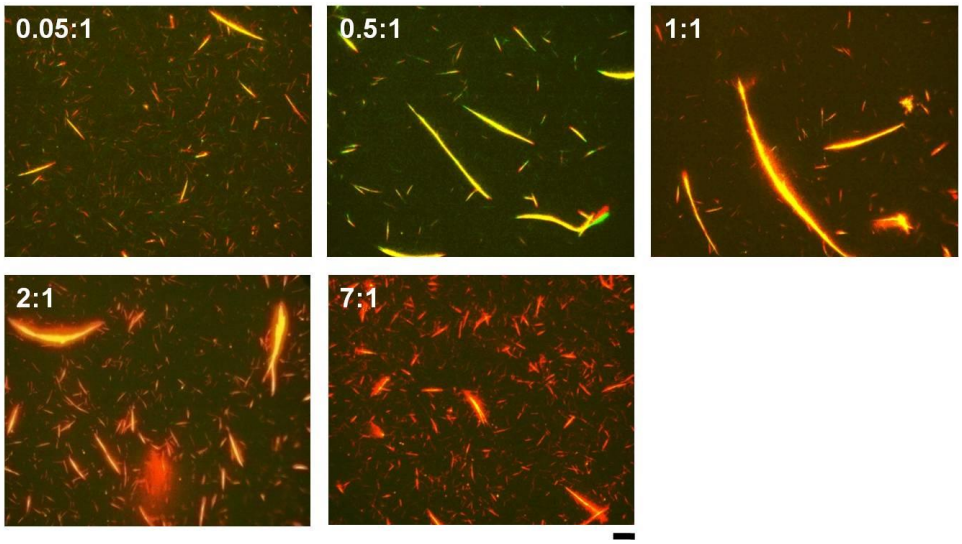

Figure 2.19 Fluorescence microscopy images showing swarm groups formed with different ratio of the two swarm units (R-swarm units: G-swarm units = 0.05:1, 0.5:1, 1:1, 2:1, 7:1). Scale bar: 20 µm.

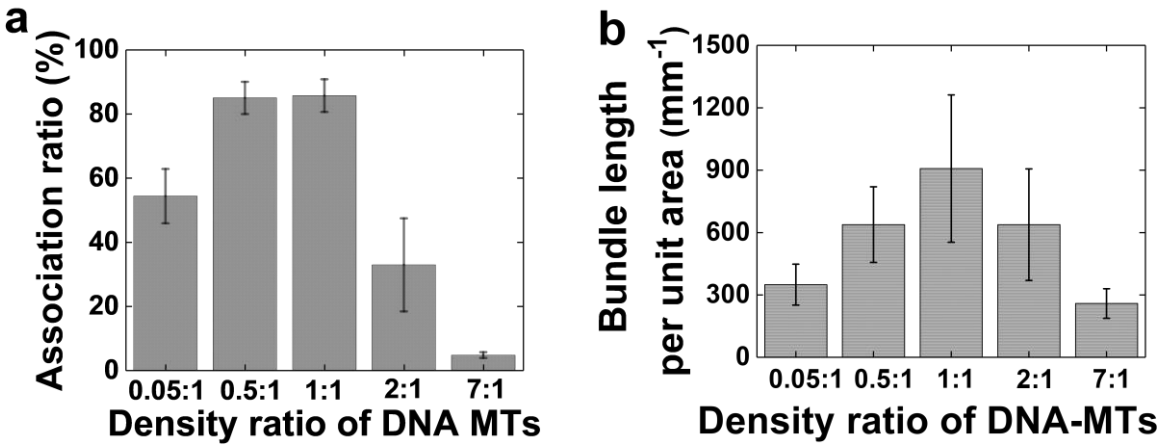

Figure 2.20 Change in association ratio depending on the density ratio of R- and G-swarm units. (a), Change of length of swarm groups with changing density ratio of two types of swarm units reveals that size of pattern was highest when the ratio was 1:1 i.e; for similar density of R-swarm units and G-swarm units (b). At higher density ratio the swarm group formation was found to decrease which can be observed from the change in association ratio and bundle length. Error bar: S. E.

To understand the effect of density of swarm units on the morphology of self-assembled structures, the length of bundles were estimated per mm^2 area. **Figure 2.20b** shows the length of bundles with density of swarm units which also shows similarity with the fluorescence microscopic images. It is to be observed that, with high density of R or G-swarm units, the size

of the swarm become shorter. This may be attributed to the increasing collision tendency of swarm units or swarms from multidirection, which hinders the longer and stable bundle formation with time.

2.2.4 Control of swarming pattern and mode through regulation of physical properties of swarm units

In natural swarms, the functional swarm pattern is determined by the type of performing task which emerges the geometrical shape and size of swarm groups[7].Therefore, it would be more interesting if we can control the swarming pattern and their mode of motion which would give rise to different functionalities. To control the swarming pattern and mode of motion I tuned the rigidity and length of MTs[58]. Flexible and long length MTs was prepared by polymerization of tubulins with GTP (guanidine-5′-triphosphate). From the trajectory of movement of the swarm units on the kinesin coated substrate, path persistence length, L_p of the swarm units i.e; MTs was measured (**Figure 2.21**).

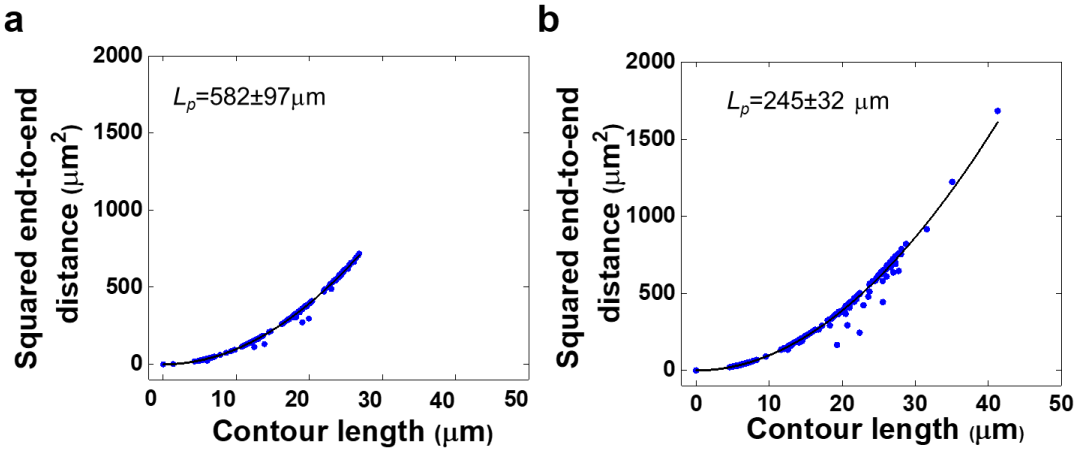

Figure 2.21 Measurement of path persistence length (L_p) from the motility of swarm units on a kinesin coated substrate. Determination of L_p of rigid (a) and flexible swarm units (b**)**. The curves were fitted according to the equation, $R^2 = 2Lp[\frac{L}{Lp} - 1 + \exp(-\frac{L}{Lp})]$ where R=end to end distance, L=contour length=L1+L2+….+Ln. *Lp* is the path persistence length.

Unlike the body length and path persistence length (L_p) of GMPCPP-MTs (5.37 ± 2.46 μm and 582 μm respectively) the body length of GTP-MTs was obtained 27 ± 8.7 μm, and path L_p of 245 μm. While gliding on kinesins the flexible swarm units exhibited enhanced randomness compared to the rigid one. Unlike the rigid swarm units, the flexible units exhibited swarming with circular motion (**Figure 2.22**).

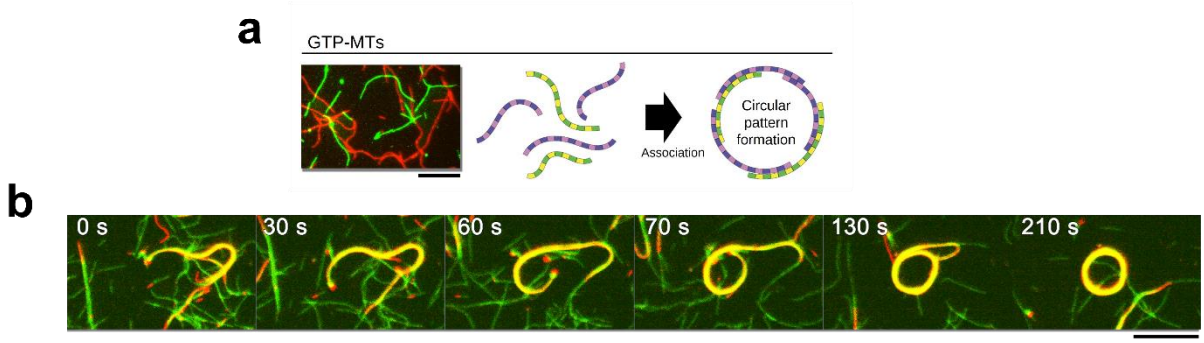

Figure 2.22 Fluorescence microscopy images of flexible swarm units and schematic illustration showing circular swarming mode by the swarm units (a). Time lapse fluorescence microscopy images showing formation of a swarm group with circular motion from flexible swarm units with body length of 27 ± 8.7 µm, and path L_p of 245 µm (b). Scale bar: 20 µm.

However, the size and number of swarm groups with circular motion were dependent not only on the rigidity of the individual units but also on their length, concentration of *r*-DNA, *l*-DNA and time similar in case of linear swarming pattern with translational motion. At 60 min after passing ATP buffer the number of ring patterns were found maximum so in all experiments the saturation time was considered as 60 min. The shape and size of circular pattern can be also controlled by tuning the length and rigidity of swarm units which is discussed in the following sections.

2.2.4.1 Effect of time on swarming with circular motion

Time dependent swarming of flexible swarm units was demonstrated using *r*-DNA concentration 500 µM while the *l*-DNA1 was kept constant at 0.6 µM. The kinesin concentration was used 300 nM as similar for rigid swarm units. The fluorescence microscopic observation was performed just after the ATP addition using inert chamber system with scavengers. **Figure 2.23** shows the time lapse images of circular swarm pattern formation (0-90 min). The number of ring pattern increased with time and reached a platue which can be clearly understood from their increasing association ratio (**Figure 2.24a**). Density of single swarm units found to decrease abruptly after 20 min of ATP addition and shows a plateau (**Figure 2.24b**) while number of ring formation increases upto 60 min (**Figure 2.24c**). This result suggests that single swarm units started to form assembly just after the ATP addition as longer and flexible bundles which form ring shaped structure further with time and reached a plateau up to 60 min.

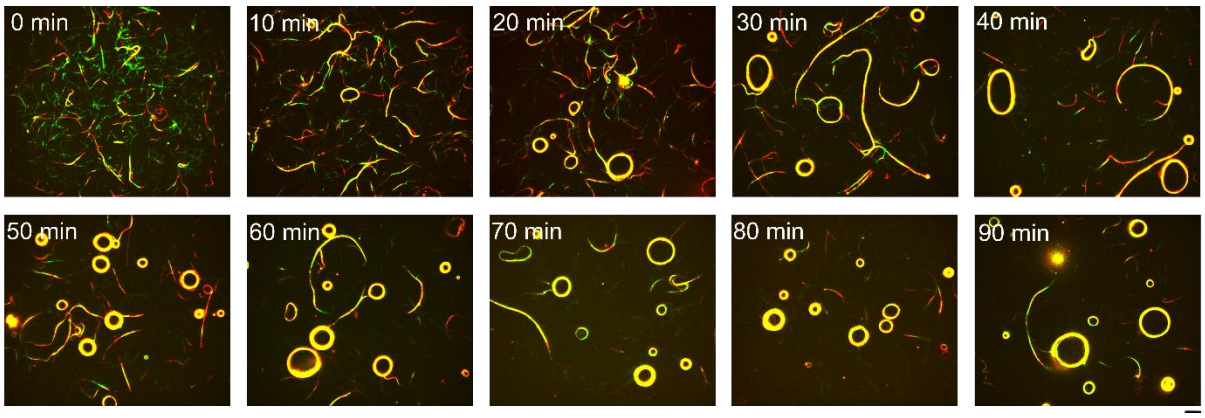

Figure 2.23 Time lapse fluorescence microscopy images showing the effect of time on the formation of swarm groups with circular motion mode. Scale bar: 20 µm.

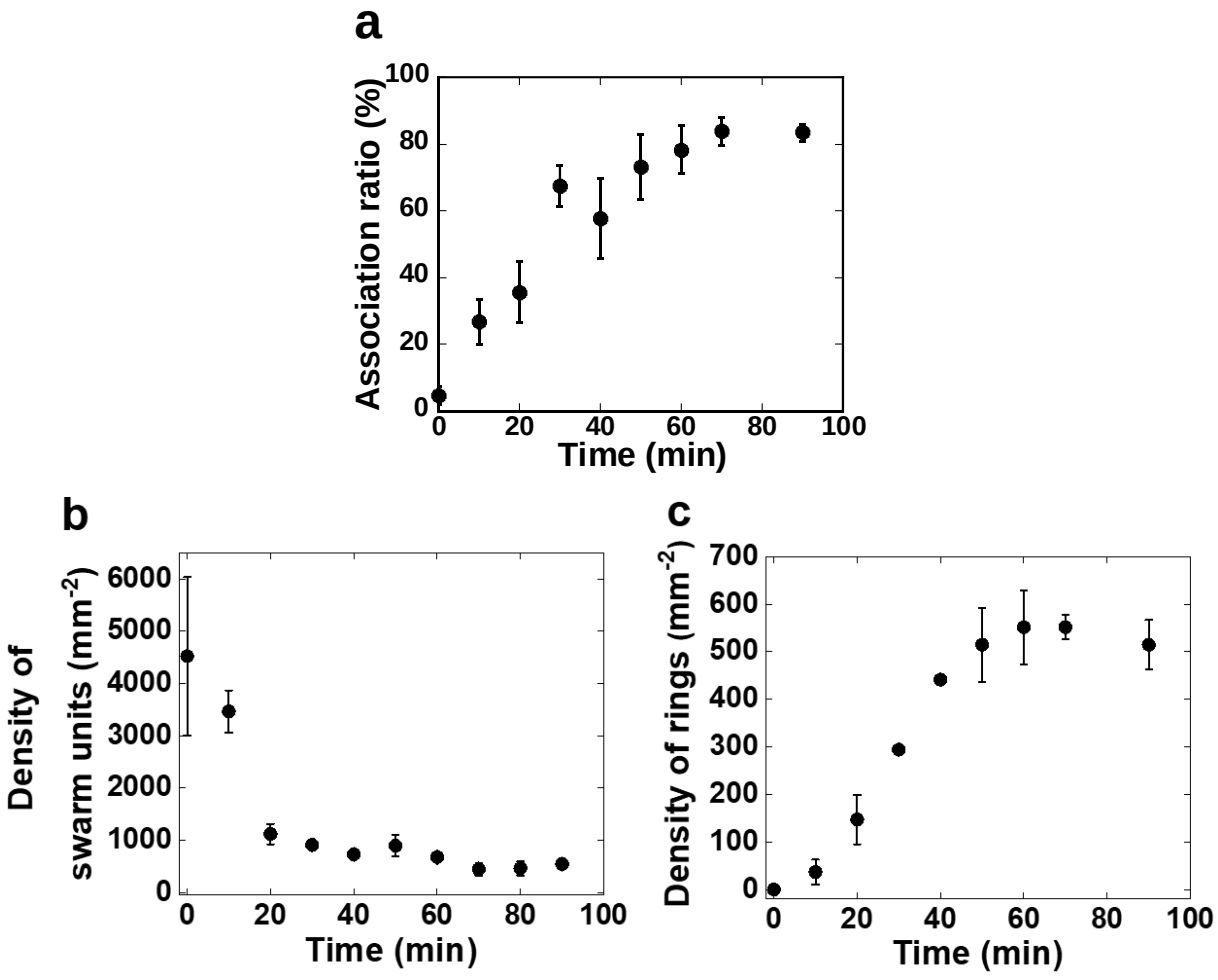

Figure 2.24 Change in association ratio (a), density of single swarm units (b) and number of ring shaped swarm groups (c) with time. By 60 min the association ratio and number of groups reached plateau which indicates that the system was saturated by that time. Error bar: S. E.

2.2.4.2 Effect of concentration of *r*-DNAs on swarming with circular motion

To investigate the effect of *r*-DNAs on the swarming mode of motion, the concentration was varied from 50-1000 µM maintaining the other conditions similar as the rigid swarm units.

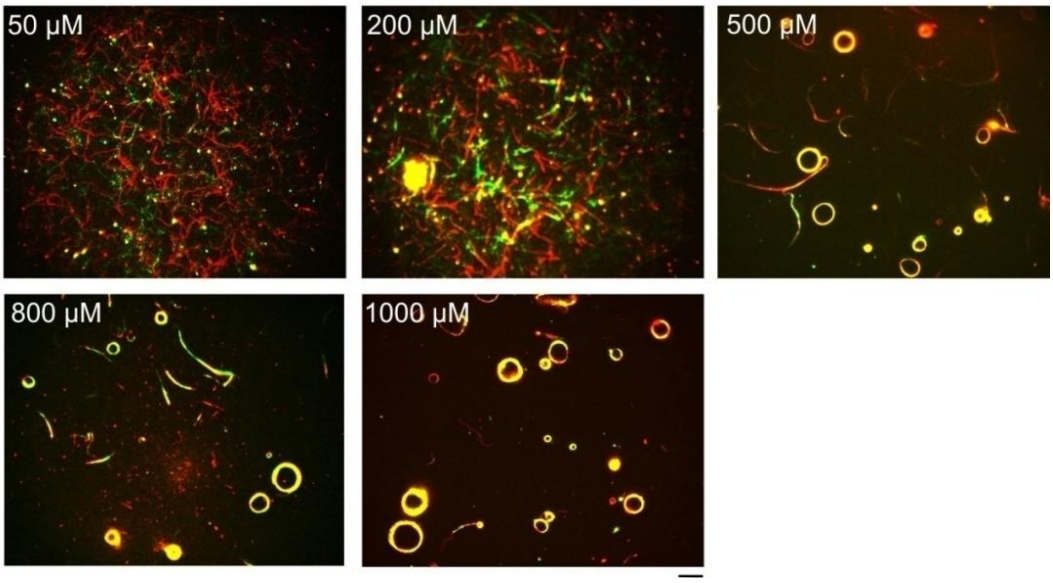

Figure 2.25 Fluorescence microscopy images of swarm groups with rotational motion formed for different concentration of *r*-DNAs. The concentration was varied from 50-1000 µM maintaining the other conditions similar as the rigid swarm units. With increasing the *r*-DNA concentration the circular pattern formation increases (500-1000 µM). The images were captured after 60 min of passing ATP buffer. Scale bar: 20 µm.

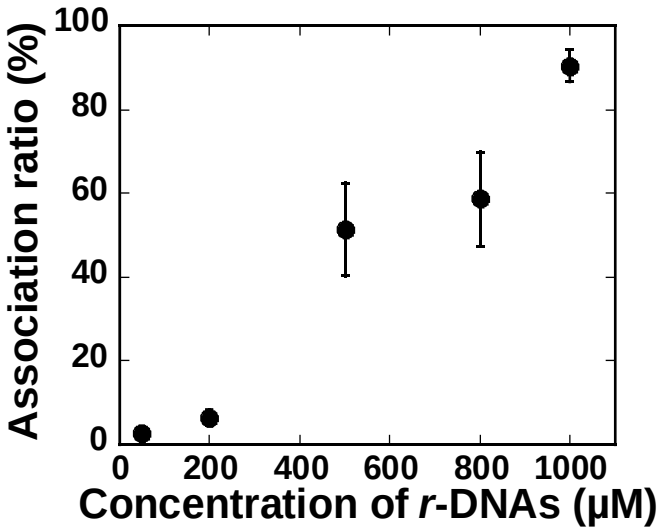

Figure 2.26 Change in association ratio on changing the concentration of *r*-DNAs. The association ratio increases with increasing the concentration of *r*-DNAs. Error bar: S. E.

With increasing the *r*-DNA concentration the circular pattern formation increases (500-1000 µM) as shown in fluorescence images in **Figure 2.25**. Also the increased association ratio with the increase of *r*-DNA concentration indicates that large number of swarm groups was formed on increasing the *r*-DNA concentration **Figure 2.26**.

2.2.4.3 Effect of concentration of *l*-DNA1 on swarming with circular motion

The effect of concentration of *l*-DNA1 was also investigated on the swarm with circular motion varying the concentration from 0.001-1 µM keeping the all conditions similar as for rigid swarm units. The fluorescence images were captured after 60 min of passing ATP buffer as shown in **Figure 2.27**.

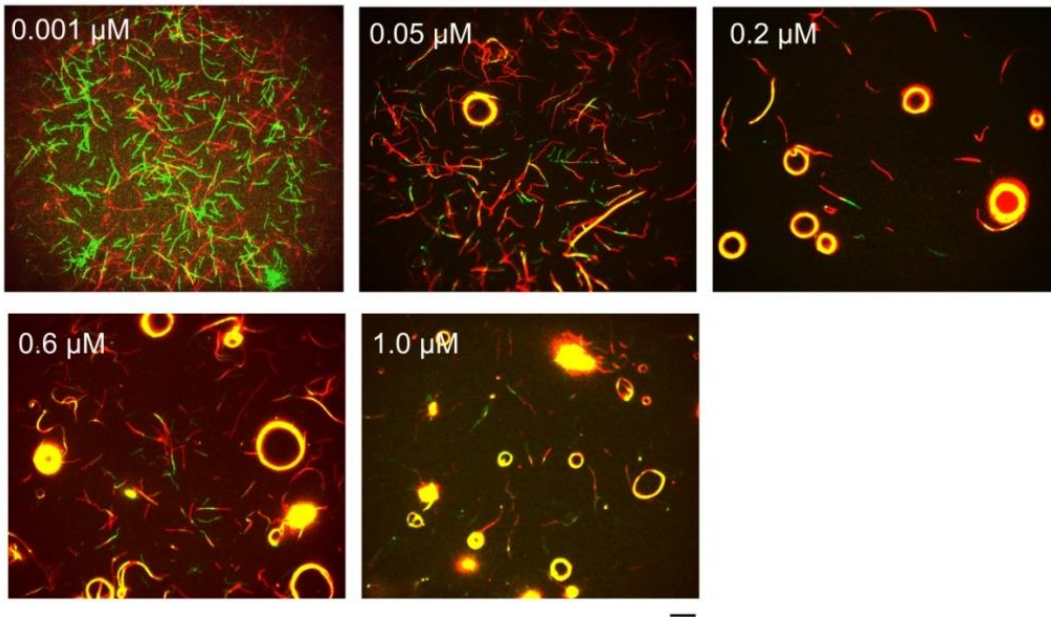

Figure 2.27 Fluorescence microscopy images showing swarm groups with rotational motion, formed at different concentration of *l*-DNA1. The images were captured after 60 min of passing ATP buffer. Scale bar: 20 µm

Figure 2.27 shows the increase in number of circular swarm groups with increasing concentration of *l*-DNA1 at 0.05 µM and become plateau on further increase of concentration which is also revealed from their association ratio (**Figure 2.28**).

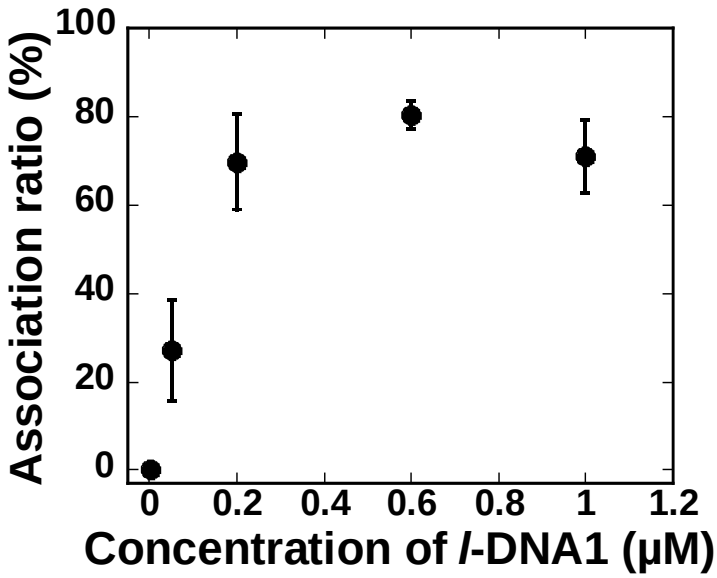

Figure 2.28 Change in association ratio with increasing the concentration of *l*-DNA1. *r*-DNAs concentration was kept constant at 500 μM. Error bar: S. E.

2.2.4.4 Effect of length of swarm units on swarming with circular motion

The circular mode of swarming of flexible swarm units are favored by the DNA interaction which mainly depends on their long body length and lower L_p value i.e; bending rigidity (**Figure 2.21** and **2.22**). So, it is important to investigate the effect of body length on the rotational mode of motion. The length of swarm units was tuned by applying stress on the flexible swarm units and by shear treatments using a micro syringe[59].

Figure 2.29 shows the length and distribution of length of flexible swarm units with the change of the number of shear treatments. The distribution of length of swarm units shifted to lower values and became narrower by shear treatments. The average length of GTP-MTs decreased from ~25±11 μm to 4±3 μm by ten times of shear treatment. Swarming mode was found to be changed from rotational to translational with changing the pattern from rings to bundles with decreasing the body length of swarm units.

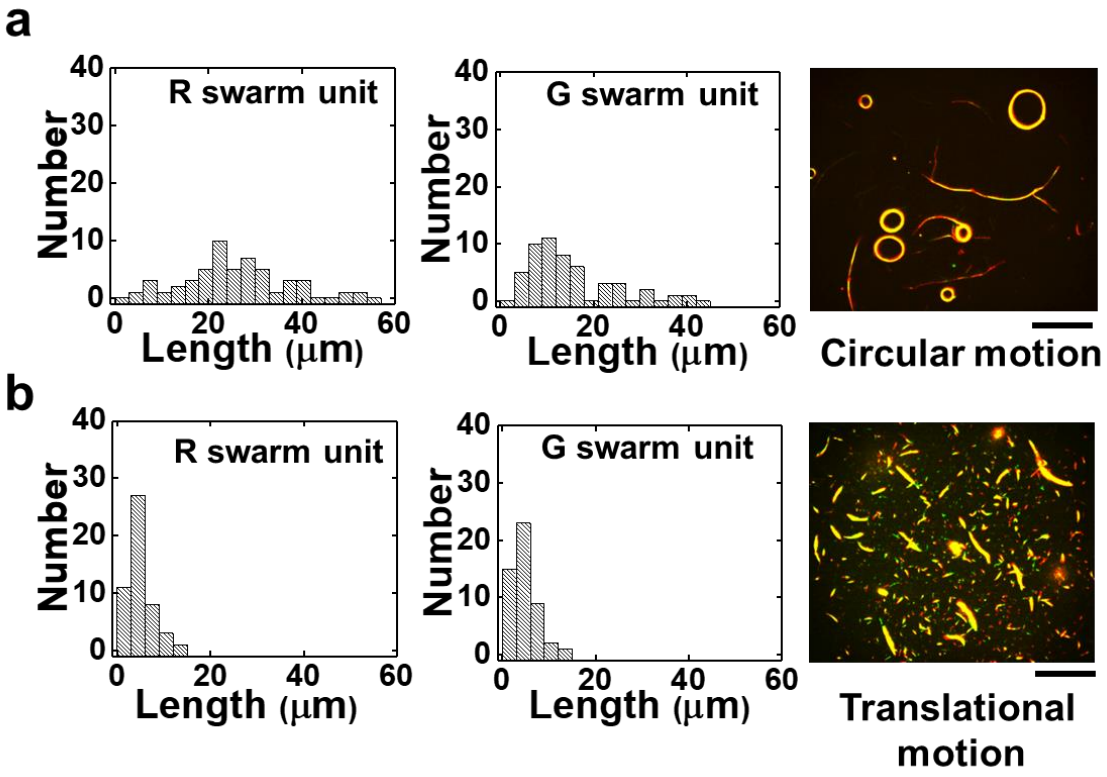

Figure 2.29 Swarm units with relatively longer body length (~22±13 μm for R swarm units and 16±9 μm for G swarm units, n=50) and L_p= 245 μm formed swarm groups that exhibited rotational motion (a). Swarm units with relatively shorter length (5±3 μm for R swarm units and 5±2 μm for G swarm units, n=50) but with same L_p= 245 μm i.e; same rigidity, produced swarm groups that exhibited translational motion (b). Scale bar: 50 μm. A critical length of swarm units is required to demonstrate swarming with rotational motion.

This result clearly suggests that ring-shaped swarming patterns are formed from longer bundles of swarm units that are initially formed by the association of single swarm units through *l*-DNA interaction. It is to be noted that, the detaching tendency of swarm units with shorter length after shear treatment become higher may be due to the change of interaction of filaments with kinesin on the surface. High density of shorter filaments is required for active swarming mode with translational motion after shear treatment than the longer filaments with circular motion.

2.2.4.5 Effect of rigidity of swarm units on the size of circular swarm pattern

To investigate the effect of rigidity on the size of the circular swarm pattern, flexible R and rigid G-swarm units were used to demonstrate swarming in presence of *l*-DNA1 (**Figure 2.30**).

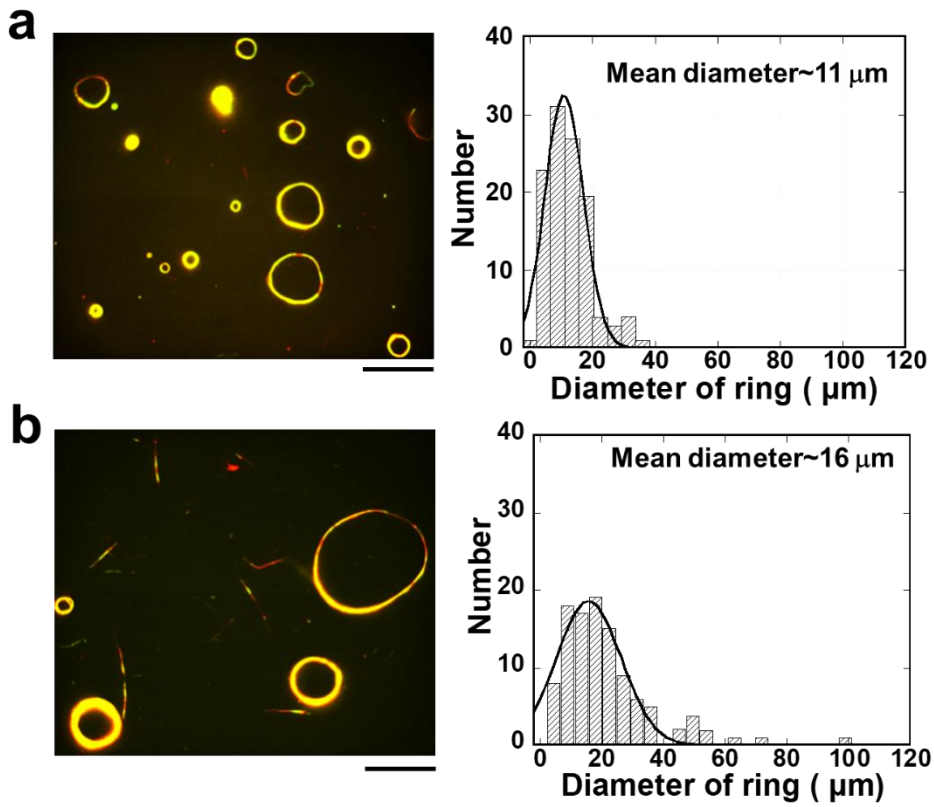

Figure 2.30 Flexible R- and G-swarm units with body length of ~25±11 μm and ~18±11 μm respectively formed swarm groups with rotational motion with an average diameter of ~11 μm (R^2= 0.93) (a). Flexible R-swarm units and rigid G-swarm units with body length ~25±11 μm and ~5±10 μm respectively formed swarm groups with an average diameter of 15.826 μm (R^2= 0.92) (b). Size of swarm groups with rotational motion can be controlled by changing properties of swarm units. The average diameter of the swarm groups was estimated from Gaussian fitting of the histograms of their size distribution. Number of swarm groups considered was 113 in each case. Scale bar: 50 μm.

In presence of different rigidity of swarm units the size of ring shaped pattern was found to increase compared to the swarm units with same rigidity. The rigid G-swarm units at first form bundles with flexible R-swarm units which increase the bending rigidity of the bundles as a result longer bundle was formed which favors ring pattern with larger diameter.

2.2.5 Dissociation of swarm groups into single motile swarm units by DNA strand displacement reaction

To control swarming and their mode of motion in group and discrete level, I employed DNA strand displacement reaction by using complementary sequence of *l*-DNA1. *d*-DNA was applied with ATP in the system which helps to withdraw the *l*-DNA1 from the swarm pattern and dissociate the swarming into individual swarm units which retain motility with their initial mode of motion i.e; translational motion.

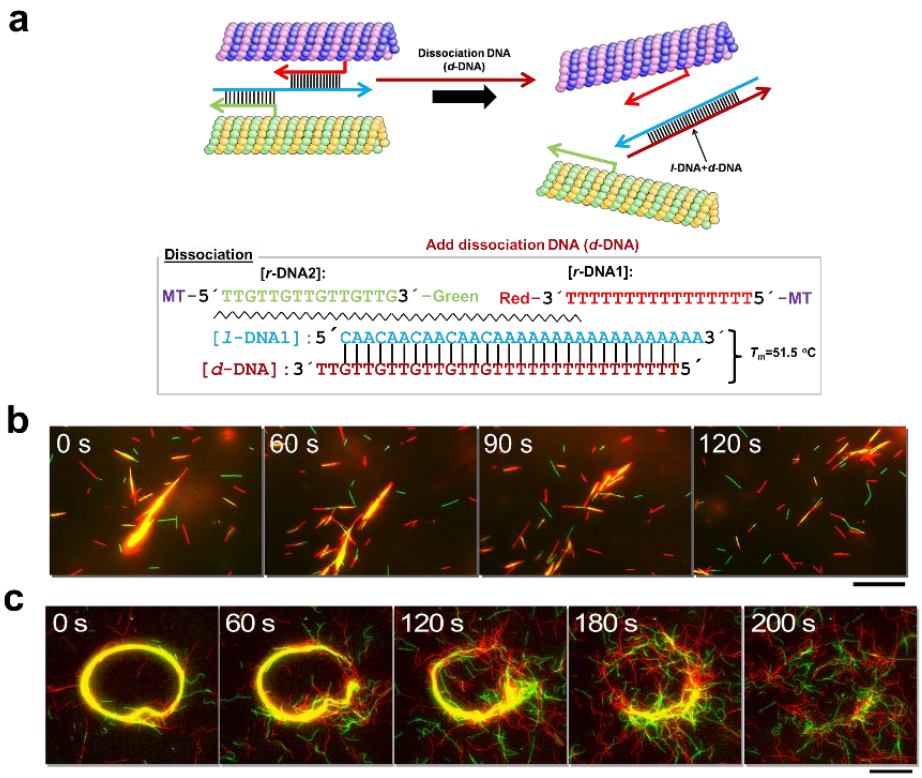

Figure 2.31 Schematic diagram of dissociation of swarming by *d*-DNA withdrawing the *l*-DNA1 through DNA strand displacement reaction favored by higher T_m than association (a). Time lapse images showing dissociation of swarm of a bundle (b) and ring (c) into individual swarm units after addition of *d*-DNA. Scale bar: 20 µm (b) (c).

Figure 2.31 shows the time lapse fluorescence images of dissociation of linear and circular swarming pattern after addition of *d*-DNA in the system. The concentration of *d*-DNA was used 0.6 µM in both case. From images, it is seen that circular pattern takes longer time than bundle pattern for dissociation. Dissociation of swarm groups depends on the number of associated swarm units and interaction among them. From the count of isolated single swarm units, as shown in **Figure 2.31b** a swarm group was estimated to be composed of ~100 individual units and for the circular pattern were estimated ~300 units (**Figure 2.31c**).

However, the dissociation for both bundle and circular swarm pattern was found to complete after 60 min of adding *d*-DNA in the system which is shown with change in association ratio with time (**Figure 2.32**).

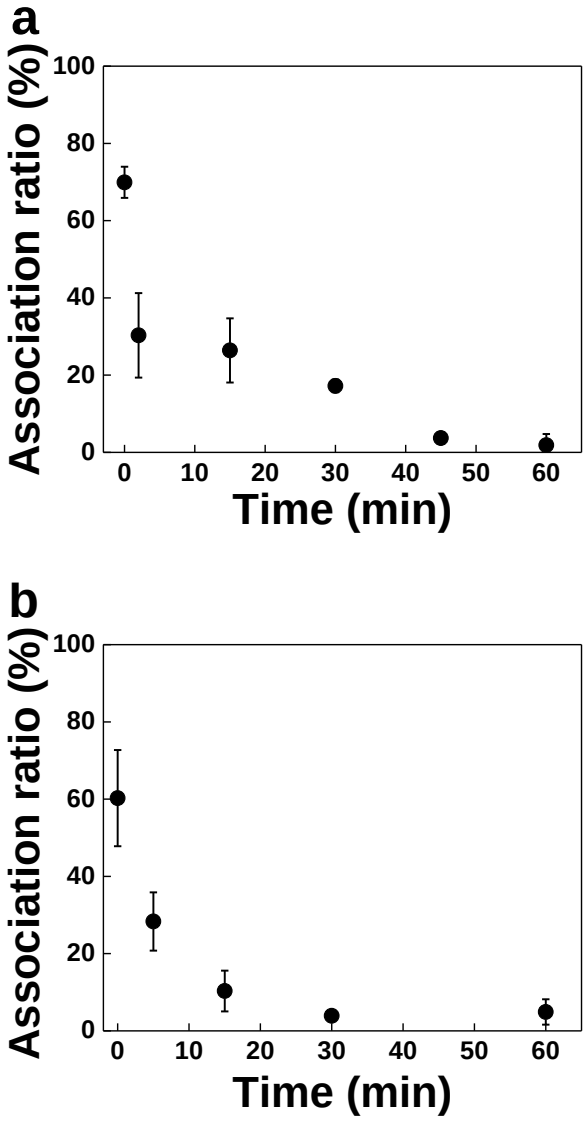

Figure 2.32 Decrease in association ratio with time in addition to *d*-DNA in the system of linear (a) and circular (b) swarming. Error bar: S. E.

The dissociation of swarm groups can be tuned for both linear and circular swarming by tuning the concentration of *d*-DNA. So, I investigated the effect of different concentration of *d*-DNA for dissociation of swarming.

2.2.5.1 Effect of concentration of *d*-DNA on the dissociation of swarm groups with translational motion

Dissociation of linear swarm group was controlled by varying the concentration of *d*-DNA from 0.05-1 µM while the concentration of *l*-DNA1 was 0.6 µM.

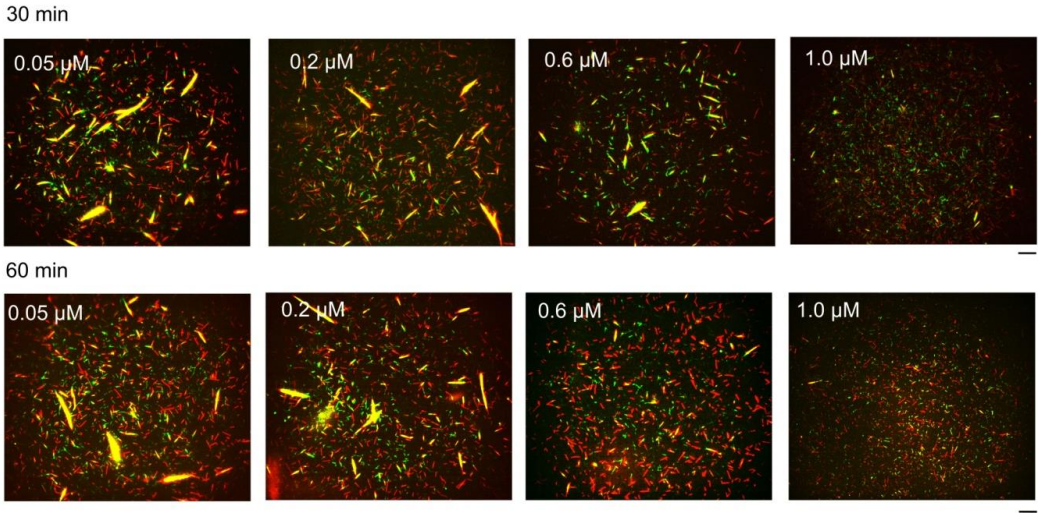

Figure 2.33 Fluorescence microscopy images showing dissociation of linear swarm groups by different concentration of *d*-DNA. The images were captured after 30 and 60 min of addition of the *d*-DNA in the system. Scale bar: 20 µm. *r*-DNA and *l*-DNA1 concentration were fixed at 500 µM and 0.6 µM respectively

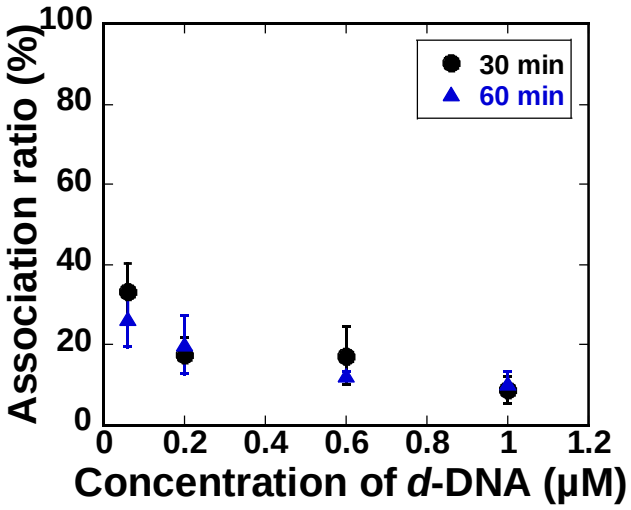

Figure 2.34 Change in association ratio of swarm units upon changing the concentration of *d*-DNA. The association ratio, estimated after 30 min and 60 min of addition of *d*-DNA, was found to decrease as the concentration of the *d*-DNA increased. Error bar: S. E.

2.2.5.2 Effect of concentration of *d*-DNA on the dissociation of swarm groups with circular motion

Control of dissociation of circular swarming mode was also successfully demonstrated by varying the concentration of *d*-DNA from 0.05-1 µM. Concentration of *r*-DNAs and *l*-DNA1 were 500 µM and 0.6 µM respectively.

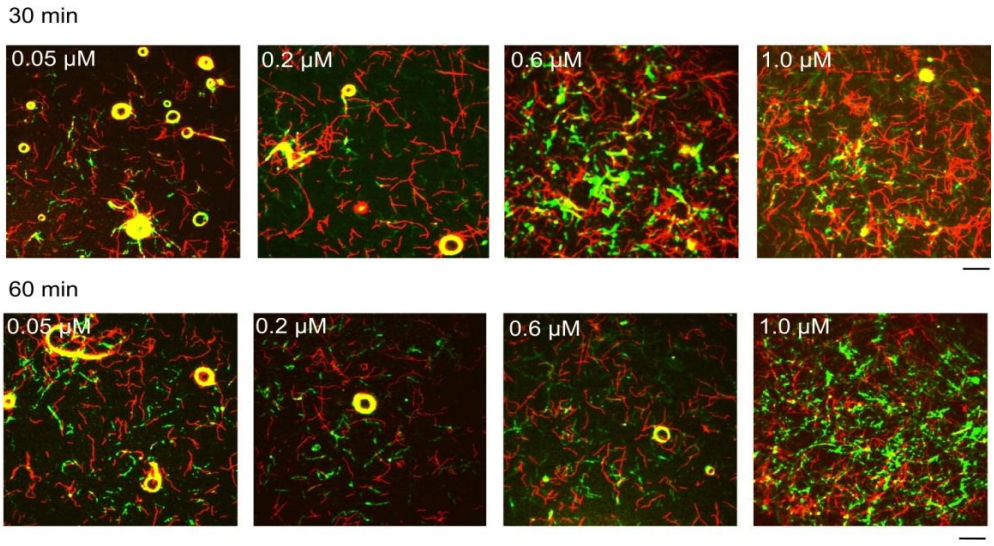

Figure 2.35 Fluorescence microscopy images showing dissociation of swarm groups with rotational motion in the presence of *d*-DNA of varying concentrations after 30 and 60 min of addition of the *d*-DNA in the system. Scale bar: 20 µm.

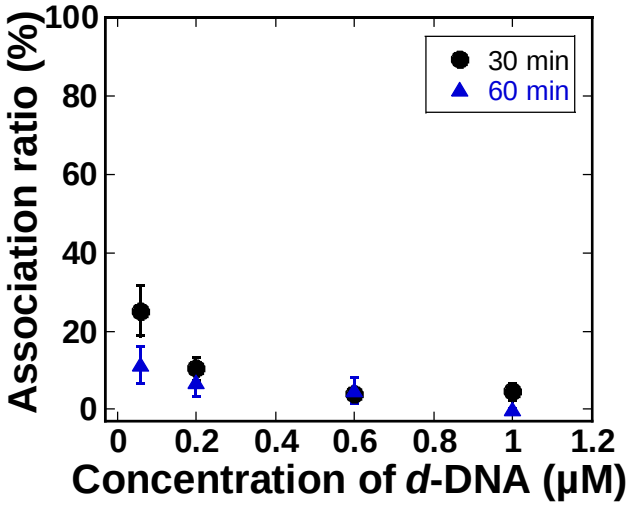

Figure 2.36 Change in association ratio, at 30 and 60 min after *d*-DNA addition, with increasing the concentration of *d*-DNA. The fluorescence microscopy images and change in association ratio reveals that dissociation process depends on the concentration of *d*-DNA. Error bar: S. E.

Thus, both bundle and circular pattern of swarming can be controlled and dissociated again into single swarm units reversibly which emerges the functional swarms in the present system. Nevertheless, control of mode of swarming from translational to rotational motion to translational again provided by such programmability of this biomolecular motor system would help us to understand different features of natural swarming.

2.3 Conclusion

In conclusion, swarming was successfully demonstrated using self-propelled biomolecular motor system. By the conjugation of functionalized MTs and DNA using click reaction, swarm units were constructed which was used to exhibit swarming in a programmed way through dynamic self-assembly. DNA interaction by input signal helps to initiate the swarming which is favored by the energy dissipative process. The extent of swarming through self-assembly can be controlled by tuning the physical properties of MTs and other parameters for both linear and circular swarming mode of motion. By introducing *d*-DNA which induces DNA strand displacement reaction in the system, reversible self-association of swarm can be successfully controlled by dissociation of swarm groups which is demonstrated for the first time. Thus, swarming of MTs programmed by DNA interaction opens us a new era to understand the concept of swarm behavior which would help to design biomolecular motor based swarm robot in near future.

2.4 Experimental Procedures

2.4.1 Purification of tubulin and kinesin

Tubulin was purified from porcine brain using a high-concentration PIPES buffer (1 M PIPES, 20 mM EGTA, and 10 mM $MgCl_2$) and 80 mM Brinkley buffer (BRB80) (80 mM PIPES, 1 mM EGTA, 2 mM $MgCl_2$) by adjusting pH to 6.8 using KOH[60]. Recombinant conventional kinesin-1 consisting of the first 573 amino acid residues of human kinesin-1 (K573) were prepared as described in previously published reports[61].

2.4.2 Preparation of azide labeled tubulin

Azide labeled tubulin was prepared using N_3-NHS-PEG-ester according to the protocol used for labeling tubulin with fluorescence dye[52] and concentration was determined by measuring absorbance at 280 nm using UV spectrophotometer (Nanodrop 2000c).

2.4.3 Design and preparation of DNA sequences

r-DNA and *l*-DNA strands were designed from T_m simulation using 'OligoAnalyzer 3.1' software with T_m between 0 ºC and 50 ºC for experimental testing.[55-57] Dibenzocyclooctyne (DBCO) and fluorescent dye labeled strands were chemically synthesized using appropriate CPG columns and a phosphoramidite (Glen Research, VA) on a ABI 3900 automatic DNA synthesizer, purified by reverse phase HPLC and fully characterized by MALDI-TOF/MS (Bruker microflex LRF). The *r*-DNA was modified at the 3' end with either 5(6)-Carboxytetramethylrhodamine (TAMRA) or 5-Carboxyfluorescein (FAM) and at the 5' end with DBCO. *l*-DNA and *d*-DNA were purchased from Eurofins Genomics LLC.

2.4.4 Preparation of swarm units

Swarm units were prepared by incubating 70.0 µM azide labeled tubulin at 37 ºC for 30 min to polymerize into azide labeled MTs. Azide tubulin and polymerization buffer (80 mM PIPES, 1 mM EGTA, 1 mM $MgCl_2$, 1 mM polymerizing agent, pH~6.8) was mixed in a 4:1 ratio respectively. Flexible swarm units were prepared using 1 mM GTP (guanidine-5´-triphosphate) and 5% DMSO (dimethyl sulfoxide) as polymerizing agent while rigid swarm units were prepared using the slowly hydrolyzable analogue of GTP, GMPCPP (guanosine-5´[(α, β)-methyleno] triphosphate) (1 mM) in premix. Click reaction was initiated by addition of dibenzocyclooctyne (DBCO) conjugated *r*-DNAs to the azide-MTs which allowed azide-alkyne cycloaddition reaction. To distinguish two different *r*-DNAs conjugated swarm units, 5(6)-Carboxytetramethylrhodamine (TAMRA) and 5' 6-Carboxyfluorescein (FAM) labeled *r*-

DNAs were used. 3.5 µL dye labeled DBCO conjugated *r*-DNA was then mixed with the prepared MTs solution and incubated for a prescribed time period at 37 ^{o}C. After completion of the click reaction, 100 µL of cushion buffer (80 mM PIPES, 1 mM $MgCl_2$, 1 mM EGTA, 60% glycerol) was used to separate the MTs by centrifugation at 54000 rpm for 1 hour at 37 ^{o}C. Pellet of MTs was washed after removing the supernatant and dissolved with 15 µL BRB80P (BRB80 with 1mM taxol).

2.4.5 Measurement of labeling ratio of *r*-DNAs to MTs (swarm units)

The modification of MTs with *r*-DNAs was estimated and confirmed by measuring the absorbance of *r*-DNA (260 nm) and MT (280 nm) respectively. The *r*-DNAs conjugated MTs were depolymerized to *r*-DNA conjugated tubulins and absorbance was measured by Nanodrop UV spectrophotometer. The absorbance peak of *r*-DNAs and tubulins were deconvoluted using Gaussian distribution function and the concentration of *r*-DNAs and tubulin was then determined from Beer-Lambert law. Finally, the labeling ratio of *r*-DNAs to MTs was calculated from the concentration of *r*-DNAs and tubulins.

2.4.6 Tuning body length of swarm units

Swarm units with different lengths were prepared by applying shear stress to MT filaments using a micro syringe. The length of GTP-MTs was tuned by varying the number of shear treatment. A Hamilton syringe (inner diameter: 2.06 mm) and a peek tube (nominal inner diameter: 0.26 mm) were used for the shearing treatment of MTs. 30 µL of MT solution in each case was passed back-and-forth (ten times) through the syringe-mounted peek tube by manual operation of the syringe[59]. Change in MT length before and after shearing treatment was manually measured using the image analysis software 'ImageJ'.

2.4.7 Preparation of flow cell and motility assay for demonstration of swarming of swarm units

Flow cell with dimensions of 9×2.5×0.45 mm^3 (L×W×H) was assembled from two cover glasses ((18×18) mm^2 and (40×50) mm^2 (MATSUNAMI)) using double-sided tape as spacer. The flow cell was filled with 5 µL casein buffer (80 mM PIPES, 1 mM EGTA, 1 mM $MgCl_2$ and ~0.5 mg mL^{-1}casein; pH 6.8). After incubation for 3 min, 300 nM of kinesin solution was introduced into casein coated flow cell and incubated for 5 min to bind the kinesins on glass surface. After washing the flow cell with 5 µL of motility buffer (~80 mM PIPES, 1 mM EGTA, 1 mM $MgCl_2$, 0.5 mg mL^{-1} casein, 1 mM DTT, 10 mM taxol; pH~6.8), 5 µL of R-swarm units was then introduced and incubated for 2 min, followed by washing with 10 µL of

motility buffer. Subsequently, 5 µL of G-swarm unit solution was introduced in the flow cell and allowed for 2 min of incubation, followed by washing with 10 µL of motility buffer. The G-swarm units were incubated with *l*-DNA for 15 min at room temperature prior to the addition into the flow cell. Finally, motility of swarm units was initiated applying 5 µL of ATP buffer (motility buffer supplemented with 0.2% methyl cellulose and 5 mM ATP). The time of ATP addition was set as 0 hour. The aforementioned experiments were performed at room temperature using the scavengers (ATP buffer supplemented with 4.5 mg mL^{-1} D-glucose, 50 U mL^{-1} glucose oxidase, 50 U mL^{-1} catalase) or inert chamber system[62] (ICS). The swarm units were monitored under fluorescence microscopy after passing nitrogen for a prescribed time period.

2.4.8 Microscopy image capture

The samples were illuminated with a 100 W mercury lamp and visualized by an epifluorescence microscope (Eclipse Ti, Nikon) using an oil-coupled Plan Apo 60×1.40 objective (Nikon) lens. UV cut-off filter blocks (TRITC: EX 540/25, DM565, BA605/55; GFP-B: EX460-500, DM505, BA510-560; Nikon) were used in the optical path of the microscope. Images were captured using a cooled-CMOS camera (NEO sCMOS, Andor) connected to a PC. To capture a field of view for more than several minutes, two ND filters (ND4, 25% transmittance for TRITC and ND1, 100% transmittance for GFP-B) were inserted into the illumination light path of the fluorescence microscope to avoid photobleaching of samples.

2.4.9 Image analysis

Length and velocity of swarm units were measured from movies of the motility assay of MTs and images captured under the fluorescence microscopy using the image analysis software (ImageJ). To determine the association ratio, pixel counting (RGY analysis) from fluorescence microscopy images was done using Adobe Photoshop software (CC 2014).

2.4.10 Estimation of association ratio (%) of swarm units

The association ratio of R- and G- swarm units were estimated from pixel measurement and using the following equation,

$$Association\,ratio\,(\%) = \frac{2 \times Yellow\,pixel}{Red\,pixel + Green\,pixel + (2 \times Yellow\,pixel)} \times 100 \quad \text{……..(1)}$$

Red, green and yellow pixels were counted by separating the pixels from the fluorescence images using RGY analysis of Adobe Photoshop. The pixels give the association ratio of swarm units by above equation. Yellow pixel was counted double as multiplied by two in equation as

it is combination of both red and green pixels coming from two swarm units (R and G- swarm units).

2.4.11 Sequences of DNAs used for demonstration of swarming

Table 2.4.1 Sequences of *r*-DNAs, *l*-DNA, and *d*-DNA used for demonstrating swarming of swarm units and dissociation of swarm groups.

DNA	Sequence (5´-3´)	5´ end	3´ end
r-DNA1	TTTTTTTTTTTTTTT	DBCO	TAMRA
r-DNA2	TTGTTGTTGTTGTTG	DBCO	FAM
l-DNA1	CAACAACAACAACAAAAAAAAAAAAAAAA	-	-
d-DNA	TTTTTTTTTTTTTTTTGTTGTTGTTGTTGTT	-	-

2.5 References

1. Whitesides, G. M.; Grzybowski, B. *Science* **2002**, *295*, 2418-2421.
2. Berg, H. C. *Annu. Rev. Biochem.* **2003**, *72*, 19-54.
3. Lawrence, P. *The Making of a Fly: The Genetics of Animal Design*, Blackwell, Oxford, **1992**.
4. Camazine, S.; Deneubourg, J.-L.; Franks, N. R.; Sneyd, J.; Theraulaz, G.; Bonabeau. E. *Self-Organization in Biological Systems*, Princeton Univ. Press, Princeton, NJ, **2003**.
5. Anderson, C.; Theraulaz, G.; Deneubourg, J. *Insectes Soc.* **2002**, *49*, 99-110.
6. Mlot, N. J.; Tovey, C. A.; Hu, D. L. *PNAS.* **2011**, *108*, 7669-7673.
7. Blum, C.; Merkle, D. Eds., *Swarm Intelligence: Introduction and Applications*, Springer, Natural Computing series, **2008**.
8. Rothemund, P.W. *Nature* **2006**, *440*, 297-302.
9. Rubenstein, M.; Cornejo, A.; Nagpal, R. *Science* **2014**, *345*, 795-799.
10. Hess, H. *Soft Matter* **2006**, *2*, 669-677.
11. Needleman, D.J.; Ojeda-Lopez, M. A.; Raviv, U.; Miller, H. P.; Willson, L.; Safinya, C. L. *Proc, Natl. Acad. Sci. USA* **2004**, *101*, 16099-16103.
12. Schaller, V.; Weber, C. A.; Semmrich, C.; Frey, E.; Bausch, A. R. *Nature* **2010**, *467*, 73-77.
13. Kakugo, A.; Shikinaka, K.; Takekawa, N.; Sugimoto, S.; Osada, Y.; Gong, J. P. *Biomacromolecules* **2005**, *6*, 845-849.
14. Bachand, M.; Bouxsein, N. F.; Cheng, S.; von Hoyningen-Huene, S. J.; Stevensc, M. J.; Bachand, G. D. *RSC Adv.* **2014**, *4*, 54641-54649.
15. Lansky, Z. *et al*, Cell **2015**, *160*, 1159-1168.
16. Nédélec, F. J.; Surrey, T.; Maggs, A. C.; Leible, S. *Nature* **1997**, *389*, 305-308.
17. Kohler, S.; Schaller, V.; Bausch A. R. *Nat. Mater.* **2011**, 10, 462-468.
18. Claessens, M. M. A. E.; Bathe, M.; Frey, E.; Bausch, A. R. *Nat. Mater.* **2006**, *5*, 748-753.
19. Schaller, V.; Weber, C.; Hammerich, B.; Frey, E.; Bausch, A. R. *Proc, Natl. Acad. Sci. USA* **2011**, *108*, 19183-88.
20. Sanchez, T.; *Nature* **2012**, *491*, 431-434.
21. Liu, H. Q. *Adv Mater* **2008**, *20*, 4476-4481.
22. Luria, I.; Crenshaw, J.; Downs, M.; Agarwal, A.; Seshadri, S. B.; Gonzales, J.; Idan, O.; Kamcev, J.; Katira, P.; Pandey, S.; Nitta, T.; Phillpota, S. R.; Hess, H. *Soft Matter* **2011**, *7*, 3108-3115.

23. Sumino, Y.; Nagai, K. H.; Shitaka, Y.; Tanaka, D.; Yoshikawa, K.; Chate H.; Oiwa, K. *Nature* ***2012***, *483*, 448-452.
24. Inoue, D.; Mahmot, B.; Kabir, A. M. R.; Farhana, T. I.; Tokuraku, K.; Sada, K.; Konagaya, A.; Kakugo, A *Nanoscale* **2015**, *7*, 18054-18061.
25. DeCamp, S. J.; Redner, G. S.; Aparna, B.; Hagan, M. F.; Dogic, Z. *Nat. Mater.* **2015**, *14*, 1110-1115.
26. Nicolau, Jr. D. V.; Lard, M.; Korten, T.; van Delft, F. C. M. J. M.; Persson, M.; Bengtsson, E.; Månsson, A.; Diez, S.; Linke, H.; Nicolau, D. V. *Proc, Natl. Acad. Sci. USA* **2016**, 113, 2591-2596.
27. Hess, H.; Clemmens, J.; Brunner, C.; Doot, R.; Luna, S.; Ernst, K. H.; Vogel, V. *Nano Lett*. **2005**, *5*, 629-633.
28. Idan, O.; Lam, A.; Kamcev, J.; John, G.; Agarwal, A.; Hess, H. *Nano Lett.* **2012**, *12*, 240-245.
29. Tamura, Y.; Kawamura, R.; Shikinaka, K.; Kakugo, A.; Osada, Y.; Gong, J. P.; Mayama. H. *Soft matter* **2011**, *7*, 5654-5659.
30. Kawamura, R.; Kakugo, A.; Shikinaka, K.; Osada, Y.; Gong, J. P. *Biomacromolecules* **2008**, *9*, 2277-2282.
31. Kawamura, R.; Kakugo, A.; Osada, Y.; Gong, J. P. *Langmuir* **2010**, *26*, 533-537.
32. Seeman, N.C. *Annu. Rev. Biochem.* **2010**, *79*, 65-87.
33. Seeman, N.C. *Cell Biol.* **1991**, *10*, 475-486.
34. Adleman, L. M. *Science* **1994**, 266, 1021-1024.
35. Goodman, R.P.; Berry, R.M.; Turberfield, A. J. *Chem. Commun.* **2004**, *12*, 1372-1373.
36. Qian, L.; Winfree, E. *Science* **2011**, *332*, 1196-1201.
37. Zhang, D. Y.; Hariadi, R. F.; Choi, H. M. T.; Winfree, E. *Nat. Commun.* **2013**, *4*:1965.
38. Goodman, R. P.*;* Heilemann, M.; Doose, S.; Erben, C. M.; Kapanidis A. N.; Turberfield, A. R. *Nat. Nanotechnol.* **2008**, 3, 93-96.
39. Robert R. F.; Ouldridge T. E.; Haley, N. E. C.; Bath, J.; Turberfield, A. R. *Nat. Commun.* **2014**, *5*:5324.
40. Hazarika, P.; Ceyhan, B.; Niemeyer, C. *Angew. Chem. Int. Ed.* **2004**, *116*, 6631-6633.
41. Lin, D. C.; Yurke, B.; Langrana, N. A. *J. Biomech. Eng.* **2004**, *126*, 104-110.
42. Dinu, C. Z.; Opitz, J.; Pompe, W.; Howard, J.; Mertig, M.; Diez, S. *Small* **2003**, *2*, 1090-1098.
43. Diez, S.; Reuther, C.; Dinu, C.; Seidel, R.; Mertig, M.; Pompe, W.; Howard, J. *Nano Lett.* **2003**, *3*, 1251-1254.

44. Hiyama, S.; Moritani, Y.; Gojo, R.; Takeuchi, S.; Sutoh, K. *Lab Chip* **2010**, 10, 2741-2748.
45. Hiyama, S.; Inoue, T.; Shima, T.; Moritani, Y.; Suda T.; Sutoh, K. *Small* **2008**, *4*, 410-415.
46. Hiyama, S.; Gojo, R.; Takeuchi, S.; Sutoh, K. *Nano Lett.* **2009**, *9*, 2407-2413.
47. Schmidt, C.; Vogel, V. *Lab Chip* **2010**, *10*, 2195-2198.
48. Steuerwald, D.; Früh, S. M.; Griss, R.; Lovchik, R. D.; Vogel, V. *Lab Chip* **2014**, *19*, 3729-3738.
49. Kagan, D.; Campuzano, S.; Balasubramanian, S.; Kuralay, F.; Flechsig, G.-U.; Wang, J. *Nano Lett.* **2011**, *11*, 2083-2087.
50. Orozco, J.; Campuzano, S.; Kagan, D.; Zhou, M.; Gao, W.; Wang, J. *Anal. Chem.* **2011**, *83*, 7962-7969.
51. Früh, S. M.; Steuerwald, D.; Simon, U.; Vogel V. *Biomacromolecules* **2012**, *13*, 3908-3911.
52. Peloquin, J.; Komarova, Y.; Borisy, G. *Nat. Methods* **2005**, *2*, 299-303.
53. Brodin, J. D.; Auyeung, E.; Mirkin, C. A. *Proc, Natl. Acad. Sci. USA* **2015**, *112*, 4564-4569.
54. Liu, J.; Postupalenko, V.; Lörcher, S.; Wu, D.; Chami, M.; Meier, W.; Palivan; C. G. *Nano Lett.* **2016**, *16*, 7128-7136.
55. Breslauer, K. J.; Frank, R.; Blöcker, H.; Marky, L. A. *Proc, Natl. Acad. Sci. USA* **1986**, *83*, 3746-3750.
56. SantaLucia, J. Jr. *Proc, Natl. Acad. Sci. USA* **1998**, *95*, 1460-1465.
57. Owczarzy, R.; Tataurov, A. V.; Wu, Y.; Manthey, J. A.; McQuisten, K. A.; Almabrazi, H. G.; Pedersen, K. F.; Lin, Y.; Garretson, J.; McEntaggart, N. O.; Sailor, C. A.; Dawson R. B.; Peek, A. S. *Nucleic acid Res* **2008**, *36*, W163-W169.
58. Mickey, B.; Howard, J. *J. Cell Biol.* **1995**, *130*, 909-917.
59. Wada, S.; Kabir, A. M. R.; Ito, M.; Inoue, D.; Sada, K.; Kakugo, A. *Soft Matter* **2015**, *11*, 1151-1157.
60. Castoldi, M.; Popov, A. V. *Protein Expr. Purif.* **2003**, *32*, 83-88.
61. Case, R. B.; Pierce, D. W.; Nora, H. B.; Cynthia, L. H. Vale, R. D. *Cell* **1997**, *90*, 959-966.
62. Kabir, A. M. R.; Inoue, D.; Kakugo, A.; Kamei, A.; Gong, J. P. *Langmuir* **2011**, *27*, 13659-13668.

CHAPTER 3

Controlling Swarming of Biomolecular Motor System through DNA Logic Gates and Photoirradiation

Abstract

In recent years biomolecular motor system have been appeared promising candidate for demonstrating swarming. However, responsiveness and sensitivity in swarming in this system like in natural swarm has not been realized yet. In this work, I have demonstrated control of swarming of microtubules (MTs) through DNA logic gate operation. Different types of logic gates such as YES, AND, OR gate operations were demonstrated which were found useful in controlling the swarming behavior by designing the input DNA signals. In addition to control of swarming, translation and circular mode of swarming were demonstrated simultaneously by employing YES logic gate through DNA molecular recognition process. The reversibly regulated swarming was also realized by applying a physical signal which was sensed by the photoresponsive DNA inserted in swarm units. Controlling of swarming by these programming strategies would help to design swarming with group features like flexibility, parallelism and responsiveness as observed in nature.

3.1 Introduction

Swarming is an attractive phenomenon in nature often exhibited by collective behavior of living organisms. Through swarming, they get many advantages such as flexibility, parallelism and robustness which are unachievable by single entity[1]. By using this advantages or group behaviors they can perform many complicated task such as path planning[2], nest constructing[3], task allocation[4] and many other complex collective behaviors using their sensitivity with the environment. To realize the group behaviors in artificial system, swarm robotics has been emerged applying of simple and small self-propelled multi-robot system. Using this system, group behaviors are trying to be demonstrated in laboratory through local sensing and responsiveness[5-14]. Designing swarm robots with group behaviors would enable to solve many sophisticated problems that are not achievable by single robot[15-19]. Besides using mechanical robots, molecular systems such as natural biomolcecular motor system is one of the suitable candidates for demonstration of swarming due to its small size and self-propelled behavior. Controlling over a large number of self-propelled units e.g. microtubule (MT) and actin, swarming was manifested modulating the interaction among them which resulted various patterns of organized structures, e.g. stream, vortex, spool, networks and bundles[20-22]. Although dynamic patterns in energy dissipative process were obtained, designing of group features from swarming is still missing in this system. Programming through input signals and sensing capabilities like mechanical robots would help to design the swarming with different group behaviors to act like as swarm robots. In this regard, such a smart and programmable processor is required that can modulate the swarming responsive to local environment. In this way DNA, not only as a natural information carrier but also as biomolecular processor gives us the opportunity to program the swarming of self-propelled system using its unique operations like logic gates, sensing properties rather than the simple self-assembly technique[23-26]. Therefore for programming the swarming of MTs in a sophisticated way I applied DNA logic gate operations which would respond to external chemical signals and also showing coexistence of different mode of patterns simultaneously by molecular recognition process[27-30]. Moreover, swarming of MTs could be also regulated in a reversible way by employing physical signal inserting photoresponsive molecule in DNA structure which added the sensing properties in the swarm[31-33]. Therefore, the study of controlling of swarm through DNA programming would help us to develop desirable functionalities like flexibility, parallelism and robustness which are prerequisite for designing artificial swarm robots using biomolecular motor system.

3.2 Results and Discussion

3.2.1 DNA based logic gate for controlling the swarming of biomolecular motor system

According to the utility of DNA as an operator for molecular computing, the swarm system discussed in the previous chapter (chapter 2) is considered as a YES logic gate, where linker DNA (*l*-DNA1) corresponds to input 1 and permits swarming of swarm units i.e; *r*-DNA1 and *r*-DNA2 conjugated MTs with translational motion as well as development of yellow color as the output 1. This operation can be expanded further using AND and OR logic gate operation to tune swarming property in a diverse way. For different logic gates, *l*-DNA sequences were designed that have the T_m greater than room temperature and serve the purpose for logic gates.

Table 3.2.1 T_m and free energy change for DNA interaction between *r*-DNAs with different *l*-DNAs for logic gate systems.

Logic gate	T_m of DNA interaction (^{0}C)	ΔG (Kcal/mol)	
YES	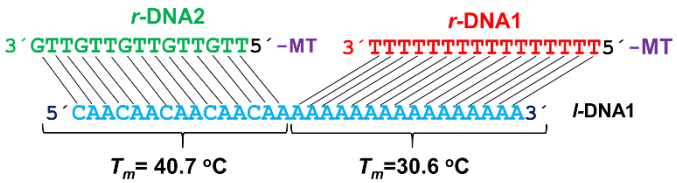	T16/A16	13
		TTG5/CAA5	15.5
AND	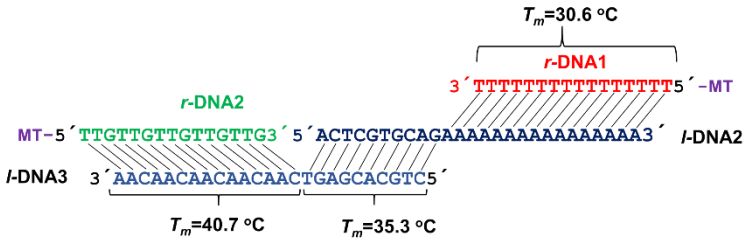	T16/A16	13
		TTG5/CAA5	15.5
		ACTCGTGCAG/ TGAGCACGTC	11
OR	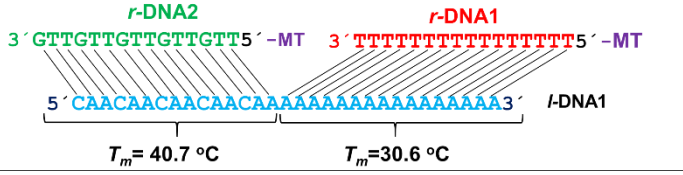	T16/A16	13
		TTG5/CAA5	15.5
	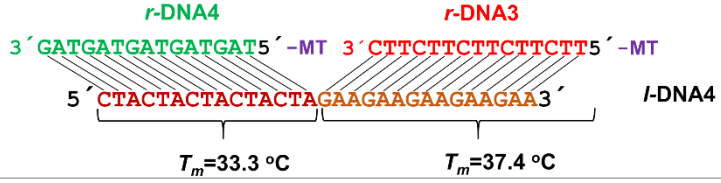	TTC5/GAA5	14.5
		TAG5/CTA5	13

T_m and ΔG were measured based on nearest neighbor interaction at the standard thermodynamic conditions: 1M NaCl at 25 ^{o}C at pH 7.

The YES, AND, OR gate operations were successfully demonstrated where swarm units were designed as gate molecules and *l*-DNAs as input signals to control swarming of self-propelled biomolecular motor system which are presented in the following sections.

3.2.1.1 Generation of YES Gate

YES gate is operated when in absence of an input signal i.e; *l*-DNA1, no output signal is obtained as swarming (0 to 0). On the other hand, when the *l*-DNA1 signal is inputted in the system, output signal is obtained as swarming (1 to 1) due to the interaction with R and G-swarm units as described in chapter 2 (**Figure 3.1**).

Gate	Truth Table		DNA interaction for output	Fluorescence signal
	In	Out		
YES	0	0	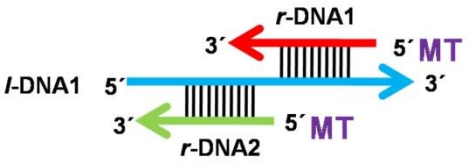	(1) Red and green
	1	1		(2) Yellow, red and green

Figure 3.1 Control of swarming through design of YES gate employing DNA input signal and consequent fluorescence output signal.

To demonstrate YES gate control of swarming, the concentration of *r*-DNA modifiers was 500.0 μM and 300 nM kinesin was used in the flow cell to drive the gate molecules i.e; swarm units. Equal density of R and G-swarm units was applied for demonstrating translational mode of swarming and concentration of *l*-DNA1 was used 0.6 μM. The output signal i.e; swarming could be observed in presence of *l*-DNA1 input signal as shown in **Figure 3.2a**. Association ratio profile with and without input signals also confirms the response of swarming by YES gate demonstration (**Figure 3.2b**).

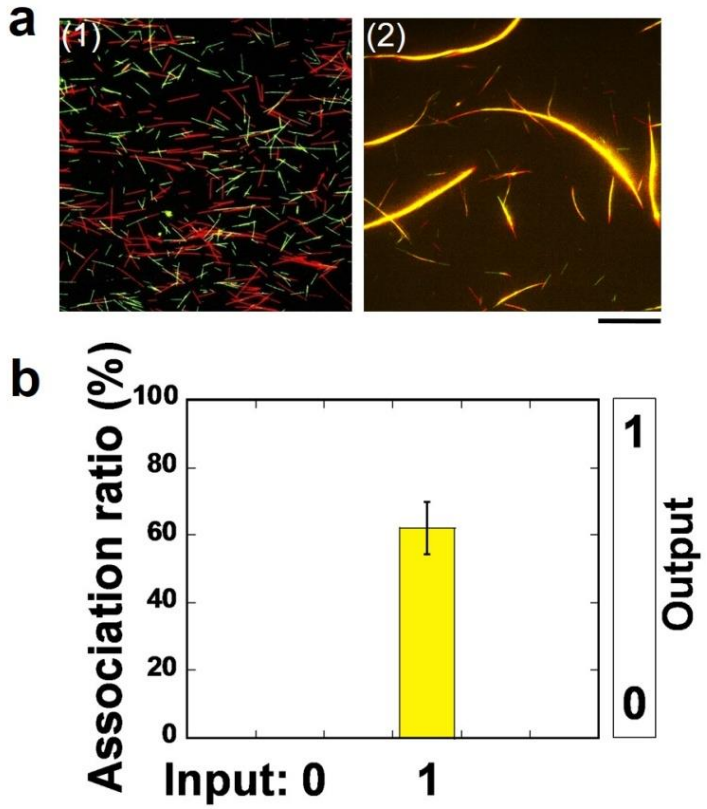

Figure 3.2 Swarming control by YES logic gate operation (a) and change in association ratio of swarming with input signals (b). Scale bar: 20 μm. Error bar: S. E.

3.2.1.2 Generation of AND Gate

AND logic gate was demonstrated by designing two different linker DNA signals as *l*-DNA2 and *l*-DNA3 which have complementary part to *r*-DNA1 and *r*-DNA2 respectively and also to each other (DNA sequences are given in section 3.4). AND gate was operated when in the absence of the input *l*-DNA signals or in the presence of any one of the *l*-DNA signals, no yellow colored output signal i.e; swarming was observed ((0, 0), (1, 0), (0, 1) in response to 0, 0, 0 respectively); when both of the signals are present output signal is obtained as yellow colored bundles (1, 1 to 1). The design of AND gate operation by input *l*-DNA signals can be understood in the following way.

Gate	Truth Table			DNA interaction for output	Fluorescence signal
AND	In_1	In_2	Out	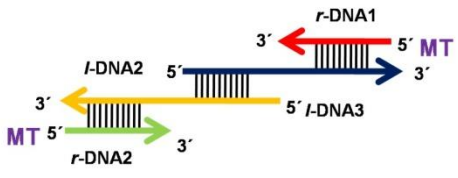	(1) Red and green
	0	0	0		
	1	0	0		(2) Red and green
	0	1	0		(3) Red and green
	1	1	1		(4) Yellow, red and green

Figure 3.3 Control of swarming through design of AND gate employing DNA input signal and consequent fluorescence output signal.

To demonstrate AND gate control of swarming, the concentration of *r*-DNA modifiers was 500.0 μM and 300 nM kinesin was used in the flow cell. Optimum density of R and G-swarm units was applied for demonstrating translational mode of swarming and concentration of *l*-DNAs (*l*-DNA2 and *l*-DNA3) were 0.6 μM. Fluorescence image shows the swarming behavior in presence of both input signals only (**Figure 3.4a**) and confirmed from their association ratio profile with and without input signals (**Figure 3.4b**).

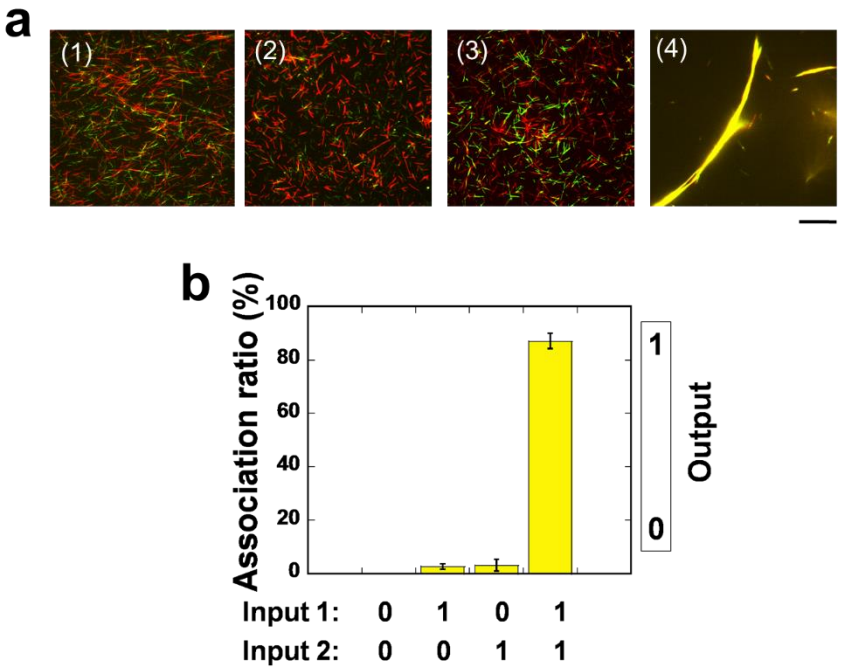

Figure 3.4 Swarming control by AND logic gate operation as input signals: output signal as swarming corresponding to input signals (1) 0, 0, (2) 1, 0, (3) 0, 1, (4) 1,1 (a) and change in association ratio of swarming with input signals (b). Scale bar: 20 μm. Error bar: S. E.

In AND GATE the association ratio for 1, 1 was found higher than the YES GATE system. This can be attributed to the higher T_m of *l*-DNA2 and *l*-DNA3 interaction with *r*-DNAs than *l*-DNA1 (**Table 3.2.1**) which favors the thermodynamics of the system.

3.2.1.3 Generation of OR Gate

For OR gate operation the computation was simplified using other two sets of *r*-DNA where *r*-DNA1 and *r*-DNA3 were labeled with red color, and *r*-DNA2 and *r*-DNA4 with green which constituted the R and G-swarm units respectively. The *l*-DNA1, that is complementary to *r*-DNA1 and *r*-DNA2, and another *l*-DNA4 which is complementary to *r*-DNA3 and *r*-DNA4 were used as the two input signals (DNA sequences are given in section 3.4). The design of OR gate operation by input *l*-DNA signals can be understood in the following way.

Gate	Truth Table			DNA interaction for output	Fluorescence signal
OR	In_1	In_2	Out	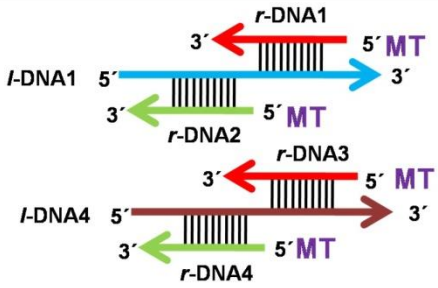	
	0	0	0		(1) Red and green
	1	0	1		(2) Yellow, red and green
	0	1	1		(3) Yellow, red and green
	1	1	1		(4) Yellow, red and green

Figure 3.5 Design of OR gate for swarming employing DNA input signal and consequent fluorescence output signal.

In the similar conditions that is applied for YES and AND gate, OR gate was operated with input signals. In absence of the input *l*-DNA signals no yellow colored output signal i.e; swarming was observed ((0, 0) response to 0). While in the presence of any one of the *l*-DNA signals swarming was observed due to the interaction of *l*-DNA1 with *r*-DNA1 and *r*-DNA2 or *l*-DNA4 with *r*-DNA3 and *r*-DNA4 respectively ((1, 0), (0, 1), response to (1, 1)). When both of the signals are present output signal is obtained as yellow colored bundles (1, 1 to 1) which fulfill the OR gate computation of self-propelled system (**Figure 3.6a**). Almost 70-90% association ratio was obtained for output 1 in all of the systems, which is much higher than the cases for output 0 (<5%) (**Figure 3.6b**).

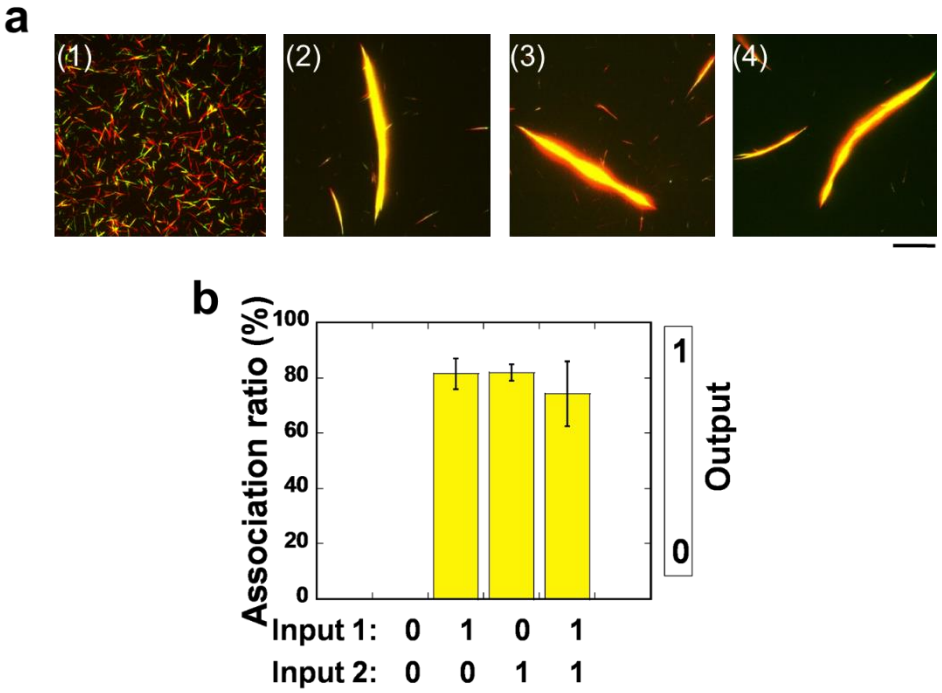

Figure 3.6 Swarming control by OR logic gate operation: output signal as swarming corresponding to input signals (1) 0, 0, (2) 1, 0, (3) 0, 1, (4) 1,1 (a) and change in association ratio of swarming with input signals (b). Scale bar: 20 µm. Error bar: S. E.

3.2.2 Orthogonal control of swarming using DNA based molecular recognition

Making use of selective hybridization property of DNA molecules, simultaneous swarming can be designed with translational and circular motion without any crosstalk. I conjugated two types of swarm units, which differed in body length and rigidity (path L_p), with two different DNA logic gates where the flexible swarm units (L_p~245 µm) were conjugated with *r*-DNA1 (red) and *r*-DNA2 (no fluorescence labeling) and the rigid swarm units (L_p ~580 µm) were conjugated with *r*-DNA5 (green) and *r*-DNA6 (green) for swarming with complimentary *l*-DNA5 with T_m 67.73 ^{0}C (detail of sequences are given in section 3.4).

To demonstrate orthogonal swarming, the logic gates were operated one by one in the flow cell. At first flexible swarm units conjugated with *r*-DNA1 and *r*-DNA2 were passed in the flow cell to form circular swarming pattern. To initiate swarming 300 nM kinesin was used and 0.6 µM *l*-DNA1 was used. After 30 minutes of passing ATP buffer when circular swarm patterns were almost formed then *r*-DNA5 and *r*-DNA6 conjugated rigid swarm units with *l*-DNA5 was passed in the flow cell after proper washing and swarming was initiated after

addition of ATP in the system. Flexible swarm units associated into swarm groups with circular motion in the presence of *l*-DNA1 and appeared in red, while the groups of rigid swarm units, visible in green, exhibited translational motion in the presence of *l*-DNA5. Formation of these two types of swarm groups was completely orthogonal. The molecular recognition was also clearly realized by operating logic gate system separately where in presence of *l*-DNA1 formed only red colored circular pattern and *l*-DNA5 formed only green colored bundle pattern. No swarming was observed in absence of any input DNA signals (**Figure 3.7**).

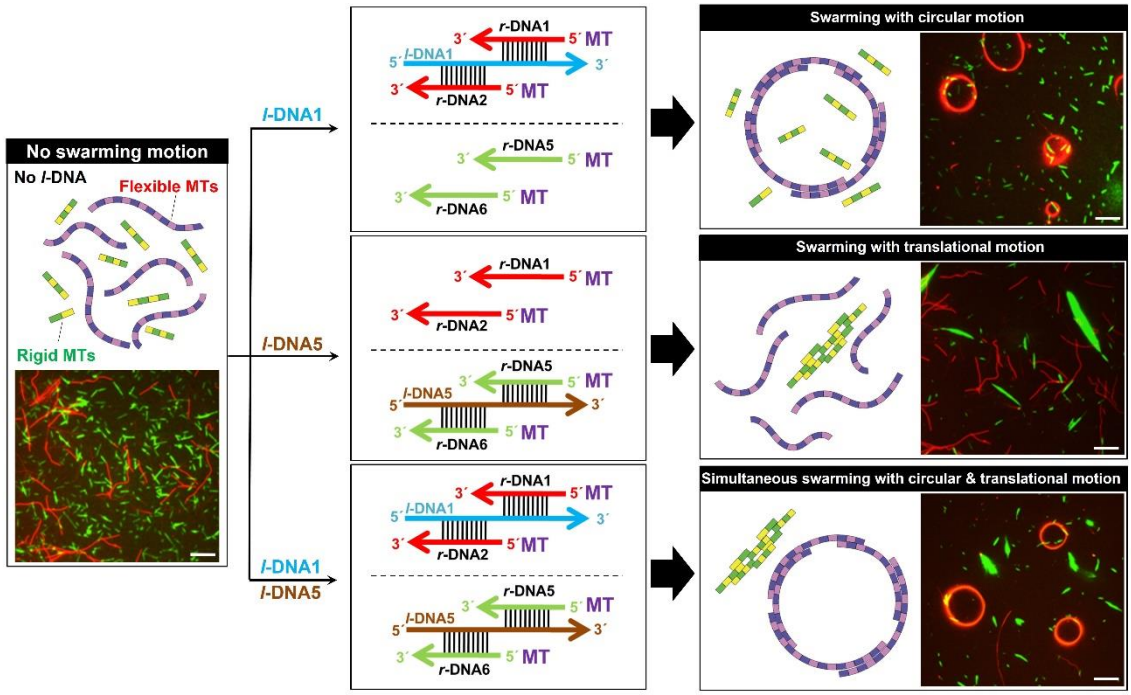

Figure 3.7 Orthogonal control of swarming of flexible and rigid swarm units. Schematic representation and fluorescence microscopy image of swarm units with different rigidity (left). The flexible swarm units (L_p~245 µm) were conjugated with *r*-DNA1 (red) and *r*-DNA2 (no fluorescence labeling), while the rigid swarm units (L_p ~580 µm) were conjugated with *r*-DNA5 (green) and *r*-DNA6 (green) (center). Upon inputting *l*-DNA1 the flexible swarm units associated into circular shaped swarm groups through hybridization of *r*-DNA1 and *r*-DNA2 and appeared in red color (right, top). Green colored swarm groups with translational motion were formed through hybridization of *r*-DNA5 and *r*-DNA6 in the presence of *l*-DNA5 (right, middle). Swarm groups with translational and circular motion were simultaneously formed without any interference in response to the introduction of both the input DNA signals (right, bottom). Scale bar: 20 µm.

In **Figure 3.7** it is seen that, although some bundles are stuck with circular patterns, most of them become free with retaining their motility on the surface which can clearly be understood from the following time lapse images in **Figure 3.8**.

Figure 3.8 Time lapse images of orthogonal behavior of different swarm pattern. Scale bar: 20 µm.

Therefore, different swarm patterns can move in parallel without hindering each other as observed from **Figure 3.8**. To investigate the effect of parallel logic operation on the swarm pattern and their motion, the number of motile bundles and rings was characterized from the following histograms.

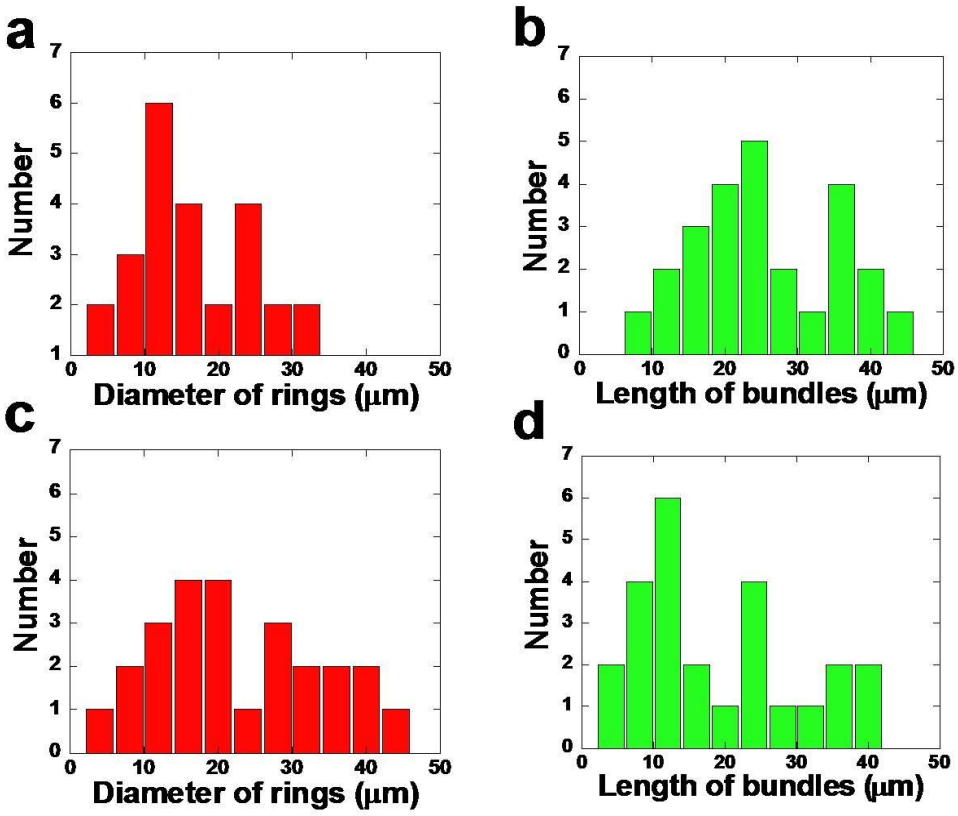

Figure 3.9 Size distribution of rings and bundles formed by two set of DNA logic gate operations in parallel due to response of DNA molecular recognition. Size distribution of rings in presence of *l*-DNA1 (a), bundles in presence of *l*-DNA5 (b) and both rings and bundles in presence of *l*-DNA1 and *l*-DNA5 respectively. Number of rings and bundles considered was 25.

From the size of circular and translational swarming pattern with distinct and parallel logic gate operation it was found that, the number or size of dynamic patterns was almost not affected in coexistence condition. The results suggest that, sorting out of swarming with different properties can be tuned orthogonally. Such parallel tasking of swarm units based on multiple logic gates would allow designing more complex systems with diverse functionality that can work using the molecular recognition process of DNA.

3.2.3 Regulation of swarming of biomolecular motor system by photoirradiation

In the previous chapter, self-assembly of swarm units and disassembly of swarming again was successfully demonstrated by using DNA strand displacement reaction but repeated regulation of reversible swarming has not been realized yet. Control of swarming reversibly in a repeated way is required which can enhance the flexibility of swarming pattern and their functionality. Controlling DNA hybridization using an external stimulus quantitatively at any given time and place could provide a mean for having switch on/off control over swarming. It could provide new insights into the sensing properties in the swarming responding to the employed signals like photoiiradiation repeatedly. Photo-control has a number of advantages such as no contamination in the system, control over excitation wavelength through the design of the photoresponsive molecule and controlling the irradiation time and local excitation. When a photo-responsive molecule is directly attached to DNA as an antenna, photo-regulation of the system regulated by that DNA molecule can in principle be achieved. A number of molecules have been found in biological process and synthesized in chemistry which can respond to the light irradiation and undergo conformational change which is precondition for many reactions to occur. Azobenzene is a typical photo-responsive molecule that isomerizes from its planar trans-form to the non-planar cis-form after ultraviolet (UV)-light irradiation (300 nm-400 nm), and from the cis-form back to the trans-form after irradiation with visible light (>400 nm). This process is completely reversible, and the azobenzene group does not decompose or induce undesirable side reactions even on repeated trans-cis isomerization. By introducing azobenzenes into DNA as a linker, the photo-regulation of the formation and dissociation of a DNA duplex[34, 35] is successfully achieved. To introduce photo control in the swarming, azobenzene was installed into the DNA processor that allowed ON/OFF switching of the hybridization between receptor DNAs through UV or visible light-induced *cis-trans* isomerization of the azobenzene moiety, resulting in melting temperature (T_m) change of DNA hybridization (**Figure 3.10**).

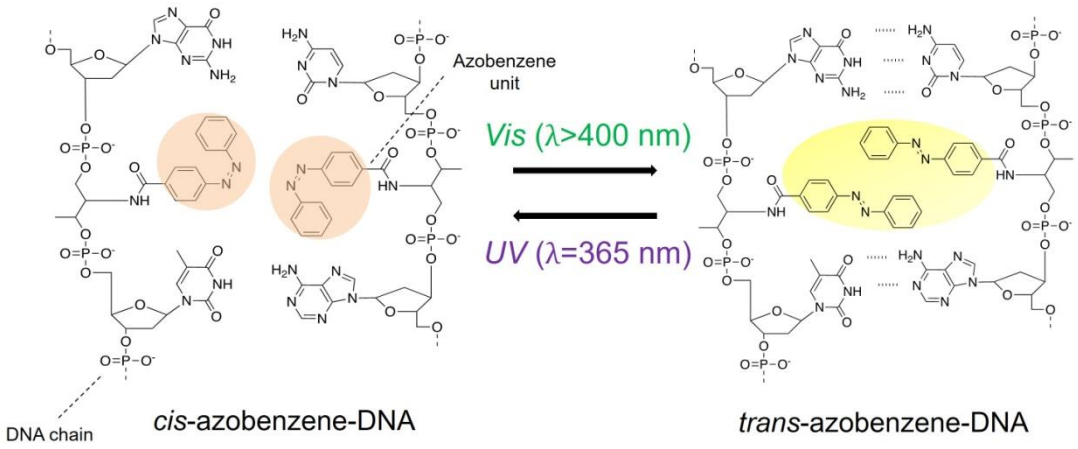

Figure 3.10 Reversible hydrogen bonding of photoresponsive DNA (*p*-DNA) by photoirradiation induced *cis-trans* isomerization of azobenzene.

Here the photoresponsive DNAs (*p*-DNA1 and *p*-DNA2, sequences are given in section 3.4) were designed so that T_m lie at <20 and 60.4 ^oC, respectively (**Figure 3.11**).

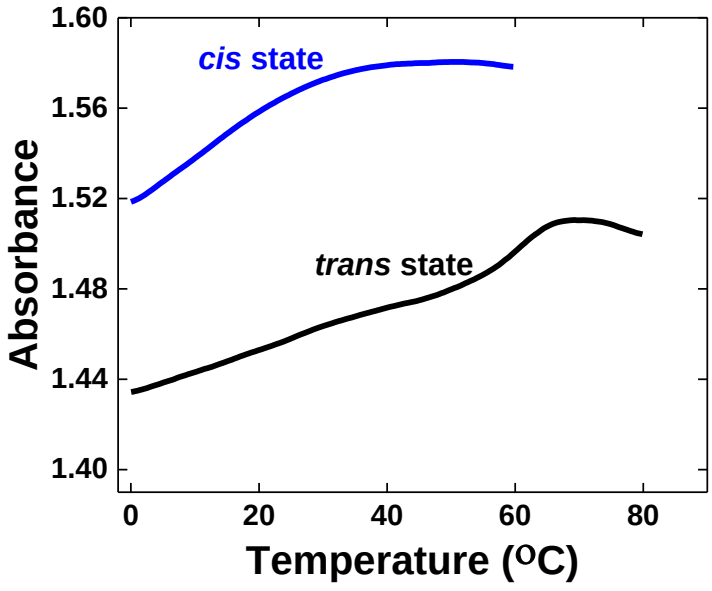

Figure 3.11 Change of melting temperature (*Tm*) for *p*-DNA duplex upon photoinduced isomerization of azobenzene. Melting temperature curves for the *p*-DNA1/ *p*-DNA2 duplex where the azobenzene was in the *trans* (black line) and *cis* form (blue line).

For *trans* form of azobenzene in the duplex the T_m was 60.4 ^oC. Upon UV irradiation (365 nm), *trans* azobenzene residue was isomerized to *cis* form. Consequently the T_m of the duplex

was lowered to <20 ^{o}C. For the *cis* and *trans* form of azobenzene the absorbance was observed at 350 and 440 nm respectively.

p-DNA conjugated swarm units were prepared by conjugating fluorescently labeled MTs with the *p*-DNAs using click reaction similarly as done for non-photoresponsive DNA conjugated MTs. Upon varying the click reaction time from 0-5 hrs the rigidity of swarm units was found to significantly decrease as shown in **Figure 3.12**.

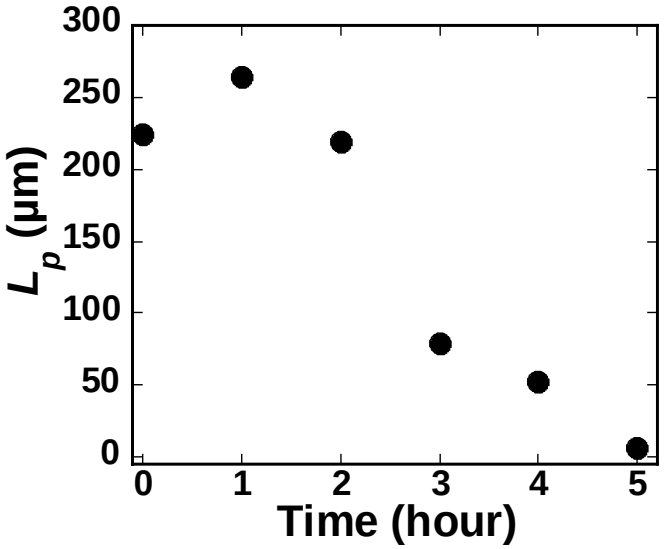

Figure 3.12 Change of L_p of swarm units with different click reaction. Initially the L_p was found to increase which then decreases gradually with time.

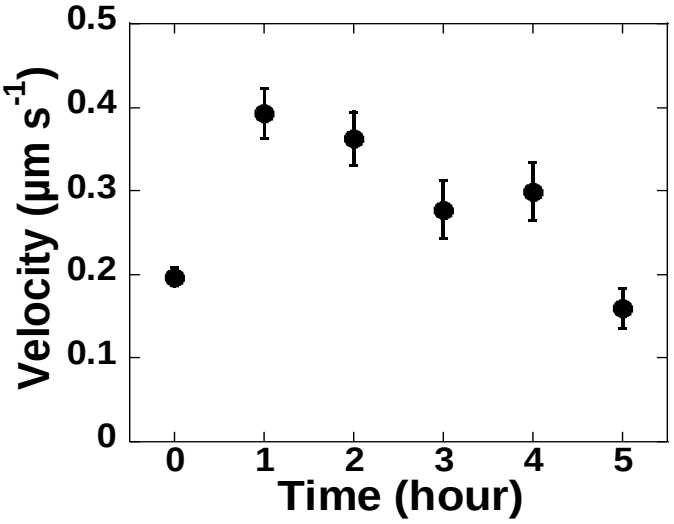

Figure 3.13 Dependence of velocity of *p*-DNA1 and *p*-DNA2 conjugated swarm units upon varying the click reaction time. Error bar: S.E.

Despite of decrease in the L_p i.e; with increasing flexibility the swarm units moved on a kinesin coated substrate without losing mobility.

Upon changing the time of click reaction the labeling ratio of *p*-DNA1 and *p*-DNA2 to MTs

was varied, which slightly affected the velocity of the swarm units, although no clear trend could be observed (**Figure 3.13**).

A schematic diagram of association and dissociation of *p*-DNA1 and *p*-DNA2 conjugated swarm units by photo-regulation by the cis-trans isomerization of azobenzene is presented in (**Figure 3.14**).

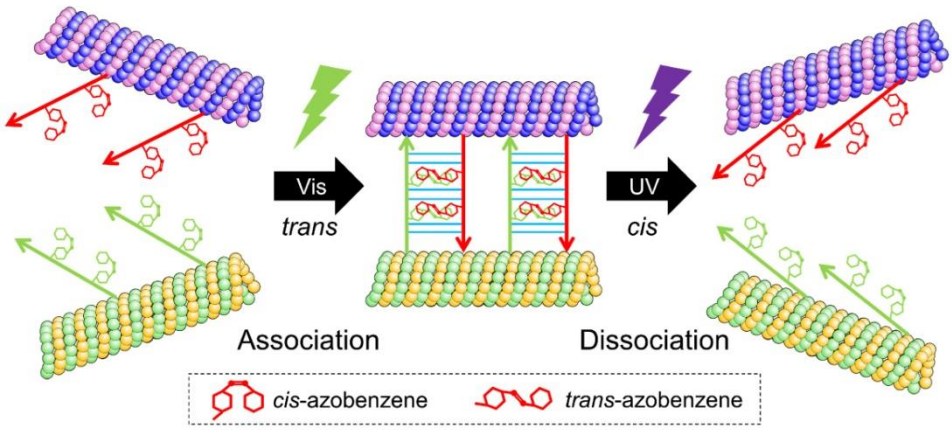

Figure 3.14 Schematic representation of selective association and dissociation of photoresponsive DNA equipped swarm units upon irradiation by visible and UV light respectively.

For demonstration of reversible swarming in a repeated way, 250 µM concentrations of *p*-DNA1 and *p*-DNA2 was used to conjugate with two different fluorescent labeled MTs to prepare photoresponsive swarm units. 800 nM kinesin was used for driving the swarm units. The preparation of flow cell was similar as used for non-photoresponsive system as described in the earlier sections. The photoresponsive swarm units was initially turned into *cis*-form by UV irradiation (λ=365 nm, intensity, I= 1.27 mW/cm^2) for 6 min following with 12 min incubation, to start with isolated movement of the swarm units after addition of ATP in the system. Swarming with translational motion was then achieved by irradiating the swarm units with visible light (λ=480 nm, I= 0.38 mW/cm^2), which triggered *cis*- to *trans*-isomerisation (**Figure 3.15a**, upper). Subsequent irradiation with UV again dissociated the swarm groups. This photo-triggered association-dissociation was repeated for three cycles (**Figure 3.15b**). Finally, by tuning the path L_p, the swarming mode was regulated from translational to circular type (**Figure 3.15b**, lower). Thus, by installing a photoresponsive molecule into DNA together with the use of a DNA based logic gate algorithm, swarming can be repeatedly regulated which enhances the flexibility of the system.

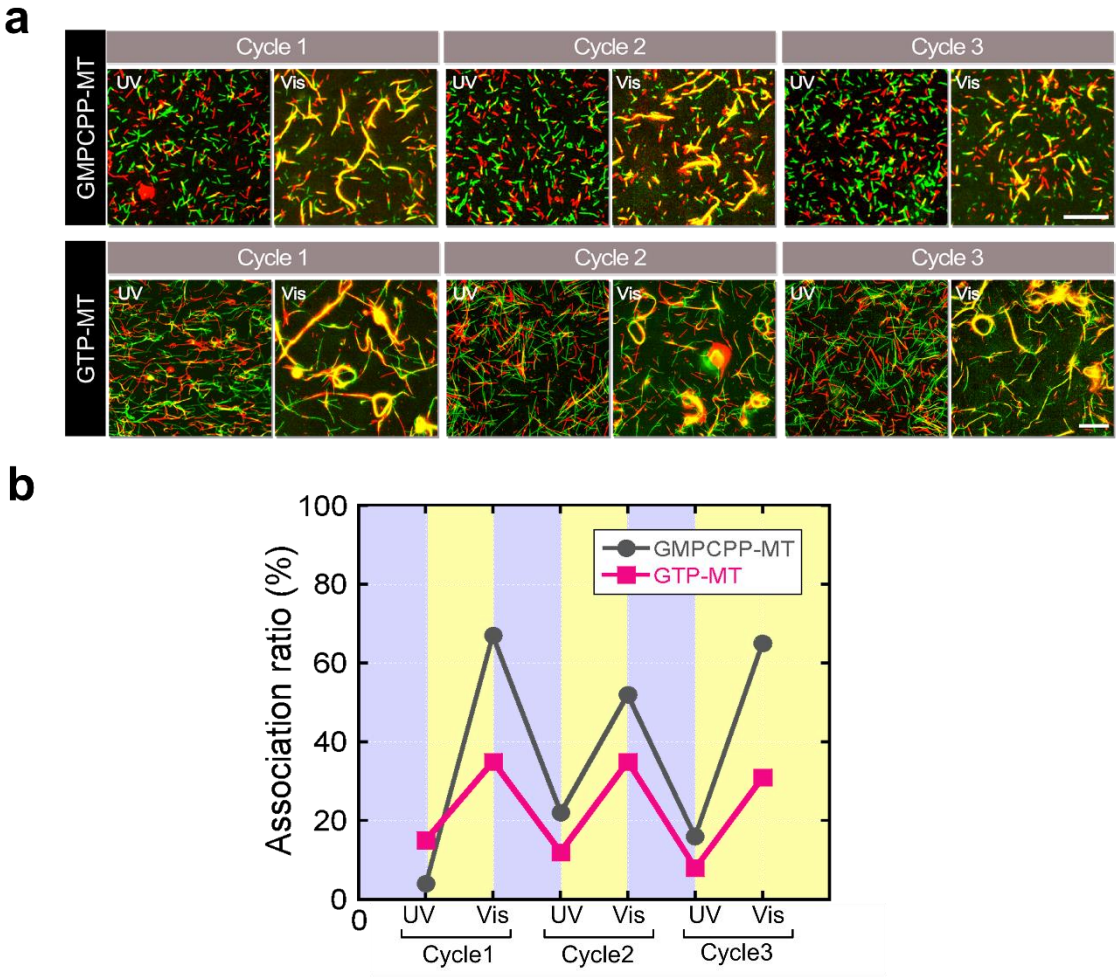

Figure 3.15 Irradiation of photoresponsive rigid swarm units (with body length= 4.2 ± 1.8 µm, L_p= 258.13 µm) by visible light (λ= 480 nm, I= 1.27 mW/cm^2), which isomerized azobenzene from *cis*- to *trans*-form, resulted in photo-triggered swarming of the swarm units into groups with translational motion (upper row). The swarm groups were then exposed to UV light (λ= 365 nm, I= 0.38 mW/cm^2) that isomerizes the azobenzene from *trans*- to *cis*-form. As a result, the swarm groups dissociated into single swarm units, and almost all of the swarm groups disappeared after 6 min of photoirradiation. This cycle was repeated three times. Visible light irradiation to flexible swarm units (body length= 11.7 ± 0.7 µm, L_p= 60.9 µm) generated swarm groups with circular motion (lower row) (a). Change in association ratio upon consecutive irradiation by visible and UV light (b). Scale bar: 20 µm.

3.3 Conclusion

In conclusion, swarming was successfully tuned by applying chemical and physical input signals. Swarming as output signal was obtained as groups of swarm units of yellow colored bundles with translational motion which was completely responsive to the input signals of simple YES, AND, OR logic gate operations. While DNA logic gates were successful in computing mathematical operations in swarming, different mode of swarming with translational and circular motion was successfully demonstrated in parallel by DNA molecular recognition process. The swarming modes with distinct physical properties of swarm units was responsive to the corresponding input DNA signals which helps to sort out the patterns, at the same time reviving their motion without any crosstalk. Finally, inserting photoresponsive DNA in the swarm units, repeated control over reversible swarming was successfully demonstrated by input physical signals like switch on-off system. Such programming of swarm of biomolecular motor system by DNA computation opens a new era of designing swarming with engineered functionalities to apply the integrated system as molecular swarm robots.

3.4 Experimental Procedures

3.4.1 Purification of tubulin and kinesin

Tubulin was purified from porcine brain using a high-concentration PIPES buffer (1 M PIPES, 20 mM EGTA, and 10 mM $MgCl_2$) and 80 mM Brinkley buffer (BRB80) (80 mM PIPES, 1 mM EGTA, 2 mM $MgCl_2$) by adjusting pH to 6.8 using KOH[36]. Recombinant conventional kinesin-1 consisting of the first 573 amino acid residues of human kinesin-1 (K573) were prepared as described in previously published reports[37].

3.4.2 Preparation of azide labeled tubulin

Azide labeled tubulin was prepared using N_3-NHS-PEG-ester according to the protocol used for labeling tubulin with fluorescence dye[38] and concentration was determined by measuring absorbance at 280 nm using UV spectrophotometer (Nanodrop 2000c).

3.4.3 Design and preparation of DNA sequences

r-DNA and *l*-DNA strands were designed from T_m simulation using 'OligoAnalyzer 3.1' software with T_m between 0 ^oC and 50 ^oC for experimental testing.[39] A further selection criterion was followed for logic gate experiments such that any undesired interactions were avoided between DNA strands. Dibenzocyclooctyne (DBCO) and fluorescent dye labeled strands were chemically synthesized using appropriate CPG columns and a phosphoramidite (Glen Research, VA) on a ABI 3900 automatic DNA synthesizer, purified by reverse phase HPLC and fully characterized by MALDI-TOF/MS (Bruker microflex LRF). The *r*-DNA was modified at the 3' end with either 5(6)-Carboxytetramethylrhodamine (TAMRA) or 5-Carboxyfluorescein (FAM) and at the 5' end with DBCO. The *p*-DNA was synthesized in laboratory according to an established protocol.[40] *l*-DNA and *d*-DNA were purchased from Eurofins Genomics LLC.

3.4.4 Measurement of melting temperature (T_m) of *p*-DNA duplex

T_m measurement of *p*-DNA1/ *p*-DNA2 duplex induced by photoirradiation was done using 2 µM concentration of each *p*-DNA, 100 mM NaCl, 10 mM Phosphate buffer (pH ~7.0). The absorbance at 260 nm was monitored with time at different temperature (Asahi spectra).

3.4.5 Preparation of swarm units

Swarm units were prepared by incubating 70.0 µM azide labeled tubulin at 37 ^oC for 30 min to polymerize into azide labeled MTs. Azide tubulin and polymerization buffer (80 mM PIPES, 1 mM EGTA, 1 mM $MgCl_2$, 1 mM polymerizing agent, pH~6.8) was mixed in a 4:1

ratio respectively. Flexible swarm units were prepared using 1 mM GTP (guanidine-5´-triphosphate) and 5% DMSO (dimethyl sulfoxide) as polymerizing agent while rigid swarm units were prepared using the slowly hydrolyzable analogue of GTP, GMPCPP (guanosine-5´[(α, β)-methyleno] triphosphate) (1 mM) in premix. Click reaction was initiated by addition of dibenzocyclooctyne (DBCO) conjugated *r*-DNAs to the azide-MTs which allowed azide-alkyne cycloaddition reaction. To distinguish two different *r*-DNAs conjugated swarm units, 5(6)-Carboxytetramethylrhodamine (TAMRA) and 5' 6-Carboxyfluorescein (FAM) labeled *r*-DNAs were used. 3.5 µL dye labeled DBCO conjugated *r*-DNA was then mixed with the prepared MTs solution and incubated for a prescribed time period at 37 ^{o}C. After completion of the click reaction, 100 µL of cushion buffer (80 mM PIPES, 1 mM $MgCl_2$, 1 mM EGTA, 60% glycerol) was used to separate the MTs by centrifugation at 54000 rpm for 1 hour at 37 ^{o}C. Pellet of MTs was washed after removing the supernatant and dissolved with 15 µL BRB80P (BRB80 with 1mM taxol). *p*-DNAs conjugated MTs were prepared following the similar procedure.

3.4.6 Preparation of flow cell and motility assay for demonstration of logic gates and photoirradiation

Flow cell with dimensions of 9×2.5×0.45 mm^3 (L×W×H) was assembled from two cover glasses ((18×18) mm^2 and (40×50) mm^2 (MATSUNAMI)) using double-sided tape as spacer. The flow cell was filled with 5 µL casein buffer (80 mM PIPES, 1 mM EGTA, 1 mM $MgCl_2$ and ~0.5 mg mL^{-1}casein; pH 6.8). After incubation for 3 min, 300 nM of kinesin solution was introduced into casein coated flow cell and incubated for 5 min to bind the kinesins on glass surface. After washing the flow cell with 5 µL of motility buffer (~80 mM PIPES, 1 mM EGTA, 1 mM $MgCl_2$, 0.5 mg mL^{-1} casein, 1 mM DTT, 10 mM taxol; pH~6.8), 5 µL of R-swarm units was then introduced and incubated for 2 min, followed by washing with 10 µL of motility buffer. Subsequently, 5 µL of G-swarm unit solution was introduced in the flow cell and allowed for 2 min of incubation, followed by washing with 10 µL of motility buffer. The G-swarm units were incubated with *l*-DNA for 15 min at room temperature prior to the addition into the flow cell. Finally, motility of swarm units was initiated applying 5 µL of ATP buffer (motility buffer supplemented with 0.2% methylcellulose and 5 mM ATP).The time of ATP addition was set as 0 hour. The aforementioned experiments were performed at room temperature using the scavengers (ATP buffer supplemented with 4.5 mg mL^{-1} D-glucose, 50 U mL^{-1} glucose oxidase, 50 U mL^{-1} catalase) or inert chamber system[41] (ICS). The swarm units were monitored under fluorescence microscopy after passing nitrogen for a

prescribed time period. Subsequently, for all logic gates and photoirradiation the similar method was followed.

3.4.7 Microscopy image capture

The samples were illuminated with a 100 W mercury lamp and visualized by an epifluorescence microscope (Eclipse Ti, Nikon) using an oil-coupled Plan Apo 60×1.40 objective (Nikon) lens. UV cut-off filter blocks (TRITC: EX 540/25, DM565, BA605/55; GFP-B: EX460-500, DM505, BA510-560; Nikon) were used in the optical path of the microscope. Images were captured using a cooled-CMOS camera (NEO sCMOS, Andor) connected to a PC. To capture a field of view for more than several minutes, two ND filters (ND4, 25% transmittance for TRITC and ND1, 100% transmittance for GFP-B) were inserted into the illumination light path of the fluorescence microscope to avoid photobleaching of samples. In order to isomerize the azobenzene unit from the *trans* form to the *cis* form in *p*-DNA swarm units, the flow cell was irradiated with light from 100 W mercury lamp passed through UV-1A filter (UV-1A: EX 365-410, DM400, BA400; Nikon).

3.4.8 Image analysis

Length and velocity of swarm units were measured from movies of the motility assay of MTs and images captured under the fluorescence microscopy using the image analysis software (ImageJ). To determine the association ratio, pixel counting (RGY analysis) from fluorescence microscopy images was done using Adobe Photoshop software (CC 2014).

3.4.9 Estimation of association ratio (%) of swarm units

The association ratio of R- and G- swarm units were estimated from pixel measurement and using the following equation,

$$Association\,ratio\,(\%) = \frac{2 \times Yellow\,pixel}{Red\,pixel + Green\,pixel + (2 \times Yellow\,pixel)} \times 100 \quad \text{.....(1)}$$

Red, green and yellow pixels were counted by separating the pixels from the fluorescence images using RGY analysis of Adobe Photoshop. The pixels give the association ratio of swarm units by above equation. Yellow pixel was counted double as multiplied by two in equation as it is combination of both red and green pixels coming from two swarm units (R and G- swarm units).

3.4.10 Sequences of DNAs used for control of swarming

Table 3.4.1 Sequences of *r*-DNAs and *l*-DNAs used in the demonstration of logic gate operations.

DNA	Sequence (5´-3´)	5´ end	3´ end
r-DNA1	TTTTTTTTTTTTTTT	DBCO	TAMRA
r-DNA2	TTGTTGTTGTTGTTG	DBCO	FAM
l-DNA1	CAACAACAACAACAAAAAAAAAAAAAAAA	-	-
l-DNA2	ACTCGTGCAGAAAAAAAAAAAAAAA	-	-
l-DNA3	CTGCACGAGTCAACAACAACAACAA	-	-
r-DNA3	TTCTTCTTCTTCTTC	DBCO	TAMRA
r-DNA4	TAGTAGTAGTAGTAG	DBCO	FAM
l-DNA4	CTACTACTACTACTAGAAGAAGAAGAAGAA	-	-

Table 3.4.2 Sequences of *r*-DNAs and *l*-DNAs used for demonstrating orthogonal control of swarming.

DNA	Sequence (5´-3´)	5´ end	3´ end
r-DNA1	TTTTTTTTTTTTTTT	DBCO	TAMRA
r-DNA2	TTGTTGTTGTTGTTG	DBCO	-
l-DNA1	CAACAACAACAACAAAAAAAAAAAAAAAA	-	-
r-DNA5	GCGGCTTGACATACCA	DBCO	FAM
r-DNA6	CACCAGCCAGTCTGTTA	DBCO	FAM
l-DNA5	TGGTATGTCAAGCCGCTAACAGACTGGCTGGTG	-	-

Table 3.4.3 Sequences of photoresponsive *p*-DNAs for demonstration of switch on/off control of swarming.

DNA	Sequence (5´-3´)	5´ end	3´ end
p-DNA1	CAAZCAAZCAAZCAAZCAAZCAAZCAAZCAA	DBCO	-
p-DNA2	TTTTTTTTTTTTTTGZTTGZTTGZTTG	DBCO	-

Z=Azobenzene

3.5 References

1. Bonabeau, E.; Dorigo, M.; Theraulaz, G. *Swarm Intelligence: From Natural to Artificial Systems*, Oxford University Press, Oxford, New York, **1999**.
2. Blum, C.; Merkle, D. Eds., *Swarm Intelligence: Introduction and Applications*, Springer, Natural Computing series, **2008**.
3. Niven, J. E. *Science* **2011**, *335*, 43-44.
4. Vittoria, A.˜ K *et al*. *J. Theor. Biol.* **2006**, *239*, 507-515.
5. Beshers, S. N.; Fewell, J. H. *Annu Rev Entomol* **2001**, *46*, 413-440
6. Thorup, K.; Alerstam, T.; Hake, M.; Kjelle´n, N. *Proc Biol Sci*. **2003**, *270*, 8-11.
7. Menzel, R.; Giurfa, M. *Trends Cogn Sci*. **2001**, *5*, 62-71.
8. Wei, H. X.; Chen, Y. D.; Tan, J. D.; Wang, T. M. *IEEE/ASME Trans Mechatron* **2011**, *16*, 745-757.
9. Seyfried, J.; Szymanski, M.; Bender, N.; Estana, R.; Thiel, M.; Wörn, H. *LNCS* **2005**, *3342*, 70-83.
10. Sahin, E. *LNCS* **2005**, *3342*, 10-20.
11. McLurkin, J.; Smith, J. *In: Distributed autonomous robotic systems 6. Japan: Springer* **2007**, 399-408.
12. Turgut, A. E.; Celikkanat, H.; Gökçe, F.; Sahin, E. *Swarm Intell.* **2008**, *2*, 97-120.
13. Arvin, F; Murray, J. C.; Shi, L.; Zhang, C.; Yue, S. *Mechatronics and Automation (ICMA), 2014 IEEE International Conference on* **2014**, 635-640.
14. Rubenstein, M.; Cornejo, A.; Nagpal, R. *Science* **2014**, *345*, 795-799.
15. Stormont, D. P. *IEEE* **2005**, 151-157.
16. Marques, L.; Nunes, U.; de Almeida A. T. *Auton Robots* **2006**, 20, 277-287.
17. Kantor, G; Singh, S.; Peterson, R.; Rus, D.; Das, A.; Kumar, V. et al. In: The 5th international conference on field and service robotics, vol. 24. Germany: *Springer* **2006**, 529-538.
18. Zafar, K.; Qazi, S. B.; Rauf, B. A. In: Computer software and applications conference, 30th annual international, vol. 2. *IEEE* **2006**, 327-332.
19. Landis, G. A. *Acta Astronautica* **2004**, *55*, 985-990.
20. Hess, H. *Soft Matter* **2006**, *2*, 669-677.
21. Hess, H.; Ross, J. L. *Chem. Soc. Rev.* **2017**, DOI: 10.1039/C7CS00030H.
22. Lam, A. T.; VanDelinder, V.; Kabir, A. M. R.; Hess, H.; Bachand, G. D.; Kakugo, A. *Soft Matter* **2016**, *12*, 988-997.

23. Zhang, F.; Nangreave, J.; Liu, Y.; Yan, H. *J. Am. Chem. Soc.* **2014**, *136*, 11198-11211.
24. Aldaye, F. A.; Palmer, A. L.; Sleiman, H. F. *Science* **2008**, *321*, 1795-1799.
25. Winfree, E.; Liu, F.; Wenzler, L. A.; Seeman, N. C. *Nature* **1998**, *394*, 539-544.
26. Zhang, D. Y.; Seelig, G. *Nature Chemistry* **2011**, *3*, 103-113.
27. Zadegan R. M.; Jepsen, M. D. E.; Hildebrandt, L. L.; Birkedal, V.; Kjems. Jorgen. *Small* **2015**, *11*, 1811-1817.
28. Xiao, Z.; Zhu, H.; Xin, A.; Li, Y.; Ling, L. *Analyst* **2015**, *140*, 7322-7326.
29. Bonnet, J.; Yin, P.; Ortiz, M. E.; Subsoontorn, P.; Endy, D. *Science* **2013**, *340*, 599-603.
30. Chen, Y. J.; Dalchau, N.; Srinivas, N.; Phillips, A.; Cardelli, L.; Soloveichik, D.; Seelig, G. *Nat. Nanotechnol.* **2013**, *8*, 755-762.
31. Kuzyk, A.; Yang, Y.; Duan, X.; Stoll, S.; Govorov, A. O.; Sugiyama, H.; Endo, M.; Liu, N. *Nat. Commun.* **2016**, *7*, 10591.
32. Yan, Y.; Chen, J. I.; Ginger, D. S. *Nano Lett.* **2012**, *12*, 2530-2536.
33. Hernández-Ainsa, S.; Ricci, M.; Hilton, L.; Aviñó, A.; Eritja, R.; Keyser, U. F. *Nano Lett.* **2016**, *16*, 4462-4466.
34. Liang, X.; Asanuma, H.; Komiyama, M. *J. Am. Chem. Soc.* **2002**, *124*, 1877-1883.
35. Asanuma, H.; Matsunaga, D.; Komiyama, M. *Nucleic Acids Symp. Ser.* **2005**, *49*, 35-36.
36. Castoldi, M.; Popov, A. V. *Protein Expr. Purif.* **2003**, *32*, 83-88.
37. Case, R. B.; Pierce, D. W.; Nora, H. B.; Cynthia, L. H. Vale, R. D. *Cell* **1997**, *90*, 959-966.
38. J. Peloquin, Y. Komarova and G. Borisy, *Nat. Methods* **2005**, *2*, 299-303.
39. https://sg.idtdna.com/calc/analyzer.
40. Asanuma, H.; Liang, X.; Nishioka, H.; Matsunaga, D.; Liu, M.; Komiyama, M. *Nat. Protoc.* **2**, 203-212 (2007).
41. Kabir, A. M. R.; Inoue, D.; Kakugo, A.; Kamei, A.; Gong, J. P. *Langmuir* **2011**, *27*, 13659-13668.

CHAPTER 4

High-Resolution Imaging of Gliding Microtubules and Protofilaments of Tubulins by HS-AFM

Abstract

In vitro gliding assay of microtubules (MTs) on kinesins has provided us with valuable biophysical and chemo-mechanical insights of this biomolecular motor system. Visualization of MTs in an *in vitro* gliding assay has been mainly dependent on optical microscopes, limited resolution of which often renders them as insufficient sources of desired information. In this work, using high speed atomic force microscopy (HS-AFM), which allows imaging with higher resolution, I monitored MTs and protofilaments (PFs) of tubulins on kinesins while gliding. Moreover, by using the HS-AFM, splitting of gliding MTs into single PFs at their leading ends was also observed. The split single PFs interacted with kinesins and exhibited translational motion, but with a slower velocity than the MTs. This investigation at the molecular level, using the HS-AFM, would provide new insights to the mechanics of MTs in dynamic systems and their interaction with motor proteins which would further help to develop molecular robots.

4.1 Introduction

Microtubule (MT)-kinesin, a cytoskeletal component, plays crucial roles in cell through its various spatial and mechanical functions[1-6]. This biomolecular motor system actively participate in cell contractility[4], development and maintenance of cell polarity[7] and also in a number of intracellular events such as intracellular transport, regulation of cell morphology and cell mechanics[8,9]. *In vitro* gliding assay, where kinesins are adhered to a substrate and MTs are propelled by the kinesins through consumption of adenosine triphosphate (ATP)[5], has been a useful method in unveiling physiological and chemo-mechanical characteristics of the biomolecular motor system[10-12]. Based on the *in vitro* gliding assay nowadays the MT-kinesin system is finding applications for nanotransport, detection, sensing, imaging, etc[13, 14]. In those works, observation of MTs in the *in vitro* gliding assay has been mainly dependent on the employment of optical microscopes, limited resolution of which often hinders detail exploration and fails to provide adequate information from the gliding assay. In this work, I performed *in vitro* gliding assay of MTs and monitored the gliding MTs and PFs of tubulins under a high speed atomic force microscope (HS-AFM). Moreover, utilizing the advantage of the HS-AFM in monitoring a specimen at the molecular level[15-17], for the first time splitting of gliding MTs into single PFs was directly observed. Upon splitting, the motile MTs were found to abruptly change their direction of movement. The split single PFs also interacted with kinesins and exhibited translational motion like the intact MTs, but with relatively lower velocity. Recently structural disintegration of MTs in the *in vitro* gliding assay has started to draw attention where, based on the investigations under fluorescence microscopy, wear or breakage of MTs into smaller parts[18] or protofilament bundles (PFBs)[19] were reported. Using the HS-AFM direct observation at the molecular level provides new insights to the structural degradation of MTs in an *in vitro* gliding assay. This work would contribute to our current understanding of the mechanics of MTs with defects in their lattice[20-23]and impact of structural change of MTs by MAPs[24], motor proteins[25, 26] or post translational modification[27] on their functionality in a dynamic system and at the same time would help promote sustainable applications of biomolecular motor systems in synthetic world[28-30]. Moreover, as a next step this understanding would also benefit us in the design of efficient molecular devices or robots for developing higher ordered system as swarming.

4.2 Results and Discussion

4.2.1 Observation of MTs and tubulin PFs on bare mica substrate

MTs and PFs of tubulins were imaged after fixing to mica substrate through electrostatic interaction (**Figure 4.1a-4.1c**). A magnified HS-AFM image shows helical lattice of MT filaments with a helix angle ~1 degree where the number of observed PFs was 16 (**Figure 4.1b**). Short and thin filaments with length of 50±20 nm (n~60, **Figure 4.1d**) and circular, curled and straight conformation were also observed (**Figure 4.1c**).

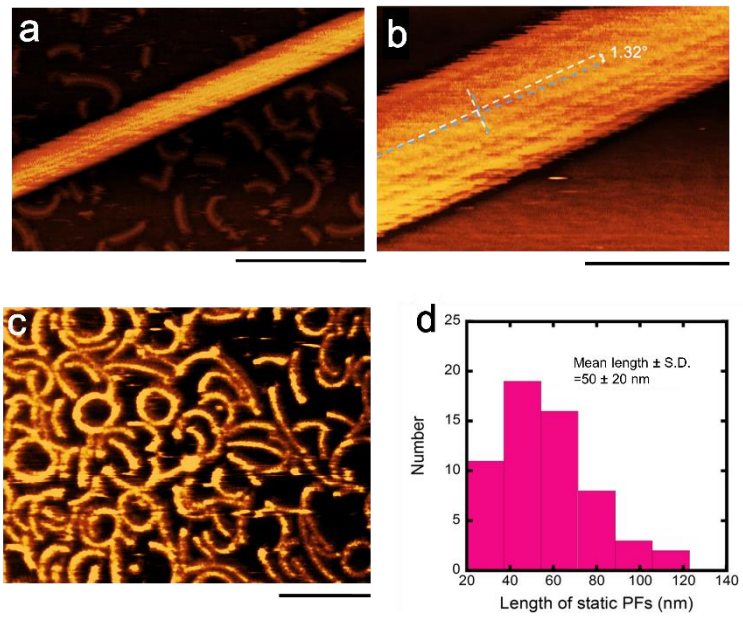

Figure 4.1 HS-AFM images of MT and PFs of tubulins. HS-AFM images of a paclitaxel stabilized MT (a, b). Scale bars: (a) 250 nm, (b) 50 nm and frame rate: 0.2 s/frame. In (b) white dotted line indicates the longitudinal axis of the MT and blue dotted line shows direction of the PFs. HS-AFM images of PFs of tubulins (c). Scale bar: 100 nm and frame rate: 0.2 s/frame. Length distribution of PFs in static condition (d).

From the topographic image and height profile, the height of a MT filament was obtained as ~25 nm (**Figure 4.2a, 4.2b**). On the other hand, for the thinner filaments the height was ~4 nm (**Figure 4.2c, 4.2d**), and these findings agree well with the literature[31]. Therefore, MTs and PFs were successfully observed using HS-AFM without any damage caused by cantilever tip force for a time period.

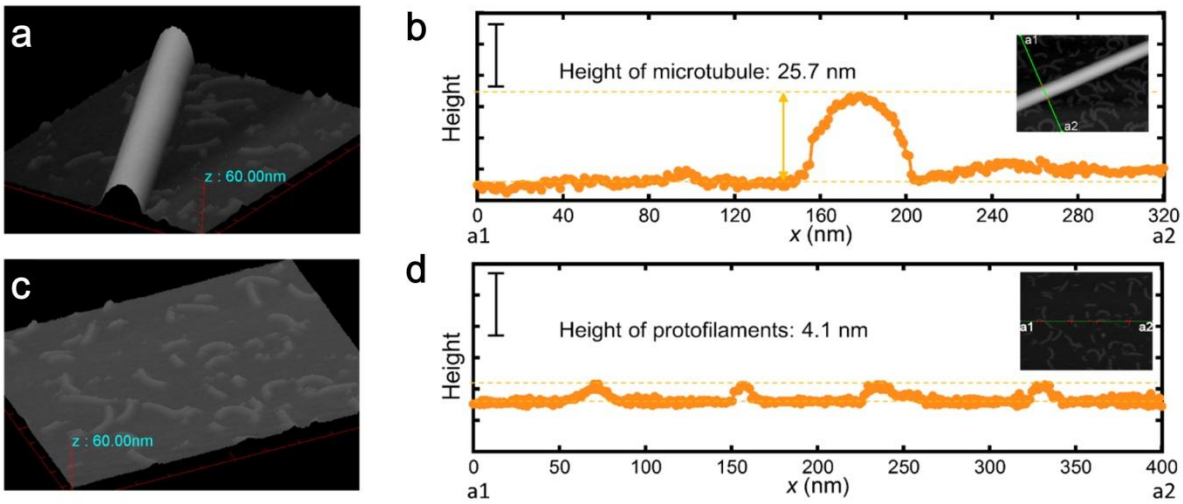

Figure 4.2 Topographic image and height profile of a MT (a, b) and PFs (c, d) obtained from HS-AFM. 3D image of a MT and PFs was obtained using HS-AFM.

4.2.2 Observation of gliding MTs and tubulin PFs on kinesin coated substrate

For observation of motility of MTs and PFs using HS-AFM, such a substrate is required that can increase the speed with smooth scan and also to avoid the non-specific adsorption of proteins on the surface. Usually, flat and soft substrate surfaces are a key to successful imaging of biological macromolecules by AFM[32]. Although usable substrate surface such as mica has been successful for still imaging of immobilized molecules, surfaces that are more suitable have recently been required and designed for dynamic imaging to accompany the progress of the scan speed of AFM. To observe the motility of MTs and PFs, I have used three types of surfaces which were found successful in imaging different proteins in action in previous work. To investigate the molecular events that occur during motility of MTs high resolution observation is required which was accompanied by developing the suitable scan speed with varying the substrate surface using HS-AFM.

4.2.2.1 Observation of gliding MTs on the nitrocellulose (NC) coated glass surface

An *in vitro* gliding assay on NC (collodion) coated mica substrate was demonstrated which is a hydrophobic surface[33] (detail information given in experimental section 4.4). The surface was covered with motor protein kinesin and MTs were attached on the kinesin coated surface. Although kinesin was not clearly observed on the substrate (**Figure 4.3a**) but the motility of MTs was successfully observed which is shown as time lapse images in **Figure 4.3b**. The velocity of MTs was found ~590 nm s^{-1} on the collodion coated mica substrate, which is very

close to the velocity of MTs on glass observed in a conventional gliding assay under fluorescence microscope[34].

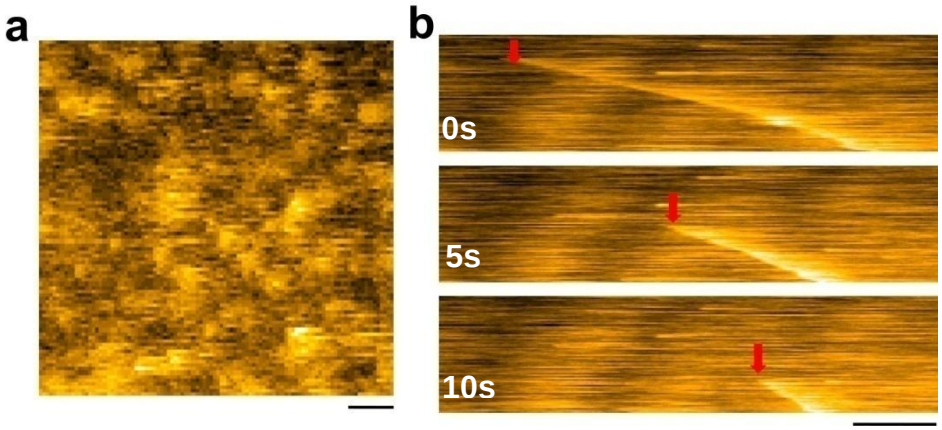

Figure 4.3 HS-AFM image of kinesins on NC coated glass surface. Scale bar: 20 nm and frame rate: 0.25s/frame (a). Time lapse images of motility of MT. Scale bar: 500 nm and frame rate: 0.66s/frame (b). The red arrow indicates the displacement of MT during motility.

Motility of MTs with their retained velocity could be clearly observed using HS-AFM which also indicates that cantilever tip force does not hamper the motility of MTs considerably. Although motility of MTs was clearly observed using HS-AFM, motility of PFs or any static PFs was not found on the surface. The roughness of the surface may hinder the clear observation of any PFs on the kinesin coated NC surface. Thus more smooth and flat surface is required to observe the motility of PFs by HS-AFM where streptavidin coated lipid surface can play an important role.

4.2.2.2 Observation of gliding MTs and PFs on kinesin coated lipid surface (lipid surface 1)

Gliding of MTs and PFs of tubulins was monitored under HS-AFM by demonstrating an *in vitro* gliding assay of MTs on kinesins fixed to a streptavidin coated lipid bilayer on mica (**Figure 4.4a**). The mica-supported biotinylated lipid bilayer was prepared as described in a previous report[35]. In brief, first unilamellar vesicles were prepared from 1,2-Dihexadecanoyl-*sn*-glycero-3-phosphocholine (DPPC), 1,2-Dipalmitoyl-3-trimethylammonium-propane (DPTAP) and 1,2-dipalmitoyl-sn-glycero-3- phosphoethanolamine-N-(cap biotinyl) (biotin-cap DPPE) (detail information given in section 4.4). The vesicles were deposited to freshly cleaved mica disks followed by the addition of streptavidin to the lipid bilayer surface. It was observed that upon application of the streptavidin solution, the streptavidin molecules started

to form small crystal islands on the biotinylated lipid bilayer (**Figure 4.4b**). After decorating the lipid bilayer with streptavidin, biotinylated kinesin solution was added onto the surface. Subsequently, taxol-stabilized MTs were applied and next by adding ATP, the motility of MTs on the kinesin coated substrate was initiated. I monitored the motility of the MTs by HS-AFM, which allowed real time imaging of the motile MTs with a high resolution. As mentioned above, the surface was divided into small islands after addition of streptavidin creating an inhomogeneous surface. As the distance between two islands was much smaller than the length of MTs, the observation of motility of MTs was continued on such surface. The motility of MTs over kinesin coated lipid bilayer substrate can be observed from the images showing their displacement with time (**Figure 4.4c**).

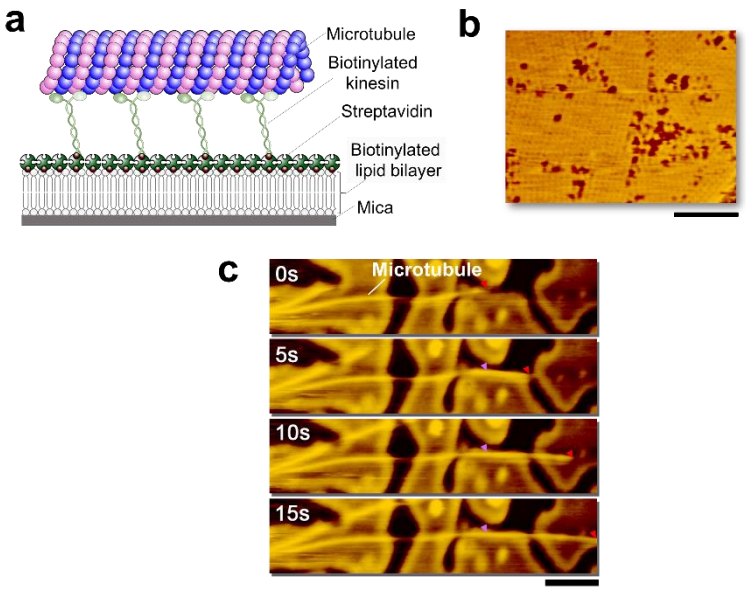

Figure 4.4 HS-AFM observation of gliding MTs. Schematic illustration of *in vitro* gliding assay of MTs on kinesins fixed to a mica supported lipid bilayer through streptavidin/biotin interaction (a). HS-AFM image of surface of the lipid membrane coated with streptavidin crystals. Scale bar: 50 nm (b). Time lapse images showing gliding motion of a MT on the kinesin coated lipid surface, Scale bar: 500 nm (c). Frame rate: 0.2 s/frame (b) and (c).

While monitoring the gliding MTs under HS-AFM, I also observed smaller and thinner filaments, as shown in **Figure 4.5a** (n~30), with length of 80±30 nm (mean ± S.D.) (**Figure 4.5b**) and height (~2.3 nm) (**Figure 4.5c**), gliding around the MTs. From the height profile the smaller and thinner filaments appear to be PFs of tubulins. The PFs might have been produced during MT polymerization but did not participate in the formation of MTs[31].

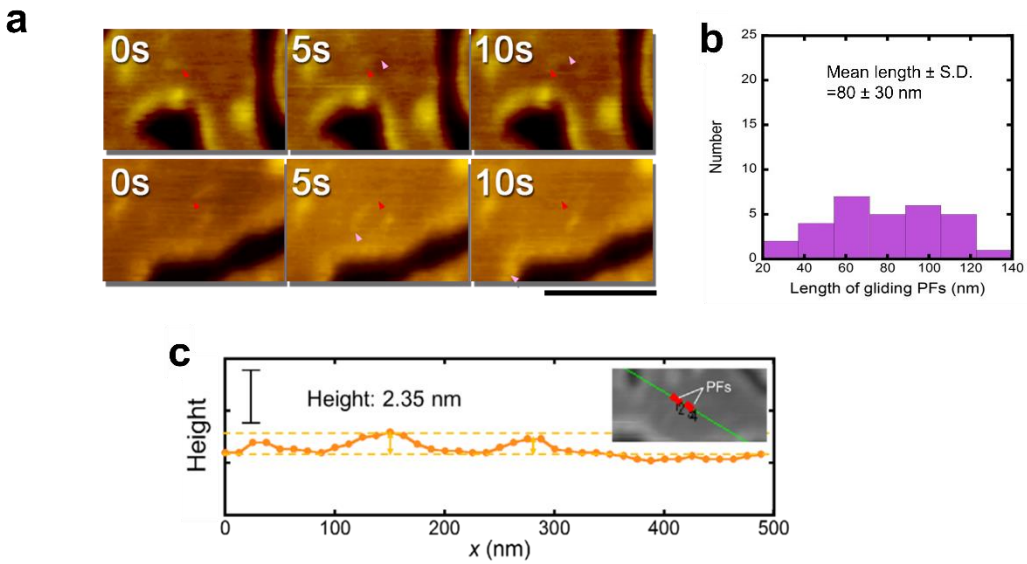

Figure 4.5 Observation of a gliding PF by using HS-AFM. Scale bar: 500 nm, frame rate: 0.2 s/frame (a). Length distribution of gliding PFs (b) and height profile of PFs (c).

While the MTs were moving with a velocity of ~100 nm s^{-1} (n=8), the PFs were moving with slower velocity (~40 nm s^{-1}) (n=18) (**Figure 4.6**).

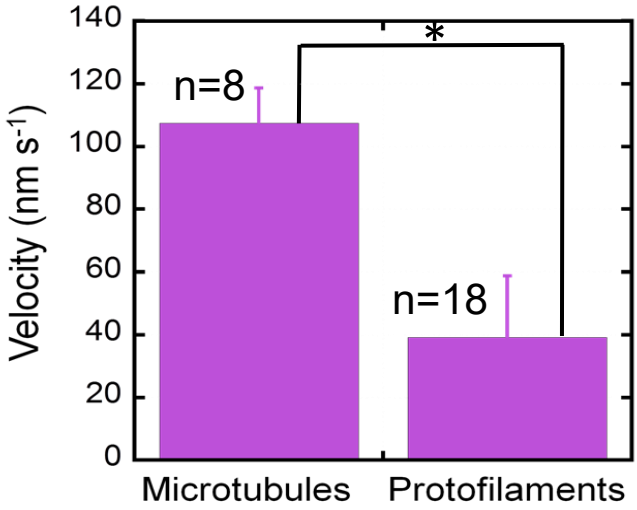

Figure 4.6 Comparison between velocity of MTs and PFs of tubulins. While gliding on a kinesin coated substrate, tubulin PFs moved with a slower velocity than the MTs. Error bar: standard deviation (S. D). Velocity differences between the two values are statistically significant. ($p<10^{-4}$).

This difference in velocity is in agreement to a previous report where a difference in velocity between MTs and protofilament bundles (PFBs) was observed under fluorescence

microscope[19]. Such difference in velocity of MTs and PFs might be related to the fluctuation of kinesins on the surface, and consequent difference in the extent of force production by the kinesins at MTs or PFs[36]. Thus, the gliding of MTs as well as PFs could be clearly observed on streptavidin coated lipid bilayer surface.

An important observation in the present experimental system is the relatively slower velocity of MTs on the lipid layer, compared to that observed in a conventional gliding assay on glass. This result suggests that the slower movement of MTs on lipid bilayer coated mica substrate might be related to the nature of substrate which can affect the specific binding of motor protein on the surface. The incomplete streptavidin crystal formation on the lipid bilayer surface may also affect the velocity of MTs (**Figure 4.4b**). To investigate the origin, the motility of MTs and PFs was observed in another lipid bilayer surface with different compositions.

4.2.2.3 Observation of gliding MTs and PFs on kinesin coated lipid surface (lipid surface 2)

Gliding of MTs and PFs was performed in an *in vitro* gliding assay on lipid coated mica substrate prepared from a lipid and composition other than used lipid surface 1. Here I prepared lipid layer on mica using vesicles prepared from 1,2-dioleoyl-*sn*-glycero-3-phosphocholine (DOPC), 1,2-dioleoyl-*sn*-glycero-3-phospho-L-serine (DOPS) and 1,2-dioleoyl-*sn*-glycero-3-phosphoethanolamine-N-(cap biotinyl) (biotin-cap DOPE)[32] (detail information given in section 4.4). On this lipid layer the velocity of MTs was~150 nm s^{-1} (n=50), which was slightly higher than that observed for the DPPC/DPTAP/biotin-cap DPPE system (lipid surface 1). It should be noted that, while preparing lipid layer using DOPC/DOPS/biotin-cap DOPE lipid system at the prescribed composition, noticeable difference was observed in the topography of streptavidin crystals compared to that for DPPC/DPTAP/biotin-cap DPPE system. While there was an incomplete and fractionate appearance of the streptavidin crystals for the DPPC/DPTAP/biotin-cap DPPE system, a much uniform layer of 2D streptavidin crystals (**Figure 4.7a, 4.7b**) was obtained for the DOPC/DOPS/biotin-cap DOPE system. On such a uniform crystal layer of streptavidin, it was also able to observe the anchored single kinesins using the HS-AFM (**Figure 4.7c**) with a density ~1200 μm^{-2} (**Figure 4.7d**). However, the density of kinesins on the lipid layer is found much lower than that on a glass surface[37].

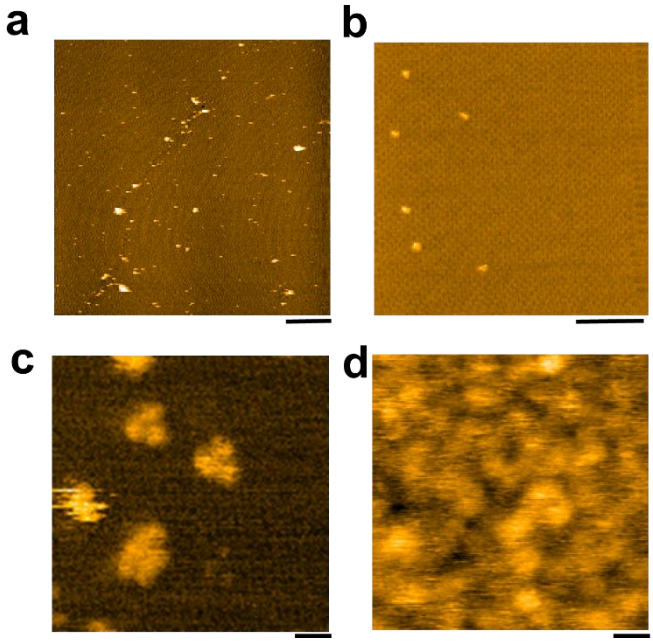

Figure 4.7 HS-AFM images of two dimensional crystals of streptavidin. (a) and (b). HS-AFM image of larger area of streptavidin 2D crystal on lipid membrane surface. Scale bar: 200 nm, frame rate: 1.0 s/frame (a) and magnified image of center part of image a. Scale bar: 40 nm (b). Motor protein kinesin on streptavidin 2D crystal surface (c) and (d). Bright spots are kinesin with head groups. Scale bar: 20 nm, frame rate: 1.0 s/frame (c) and (d).

On this lipid layer MTs was observed clearly which was also able to confirm from their height profile (23±1 nm) (**Figure 4.8a**) exhibiting motility (**Figure 4.8b**).

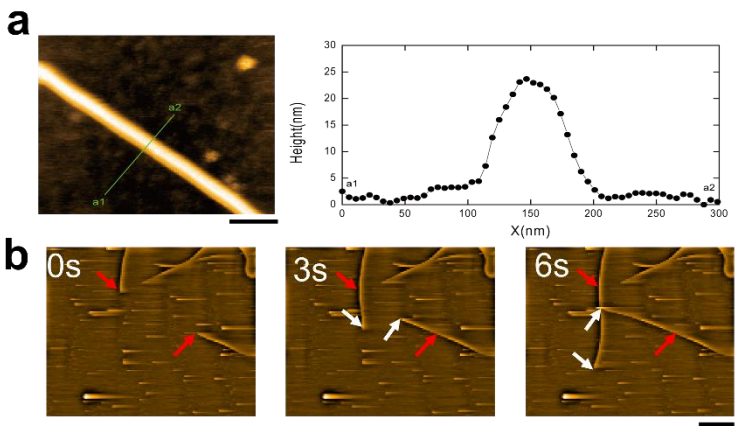

Figure 4.8 Topographic image of MT on streptavidin 2D crystal coated lipid bilayer surface fixed by kinesin (left) and its height profile (right). Scale bar: 200 nm, frame rate: 1.0 s/frame (a). Time lapse images of motility of MTs on 2D crystal coated lipid bilayer surface fixed by kinesin. Scale bar: 200 nm, frame rate: 1.0 s/frame (b). Red arrow indicates the starting point and white arrow indicates the end point of displacement of MTs with time.

Despite the formation of homogeneous streptavidin crystal layer on the DPPC/DPTAP/biotin-cap DPPE system, the velocity of MTs remained quite slow (~150 nm s^{-1}, n=50), which could be attributed to the low density of kinesin on the streptavidin/lipid surface.

Similar to the DPPC/DPTAP/biotin-cap DPPE system (lipid surface 1) difference in velocity between PFs (~60 nm s^{-1}, n=20) and MTs was also observed for the DOPC/DOPS/biotin-cap DOPE system (lipid surface 2). The PFs could be also indentified from their height profile (~2.5 nm) which agrees well with the value obtained in case of lipid surface 1 and showed motility (**Figure 4.9 a, 4.9 b**). The path length of PFs was found to be much smaller than MTs and they showed pausing events during their motility (**Figure 4.9c, 4.9d**).

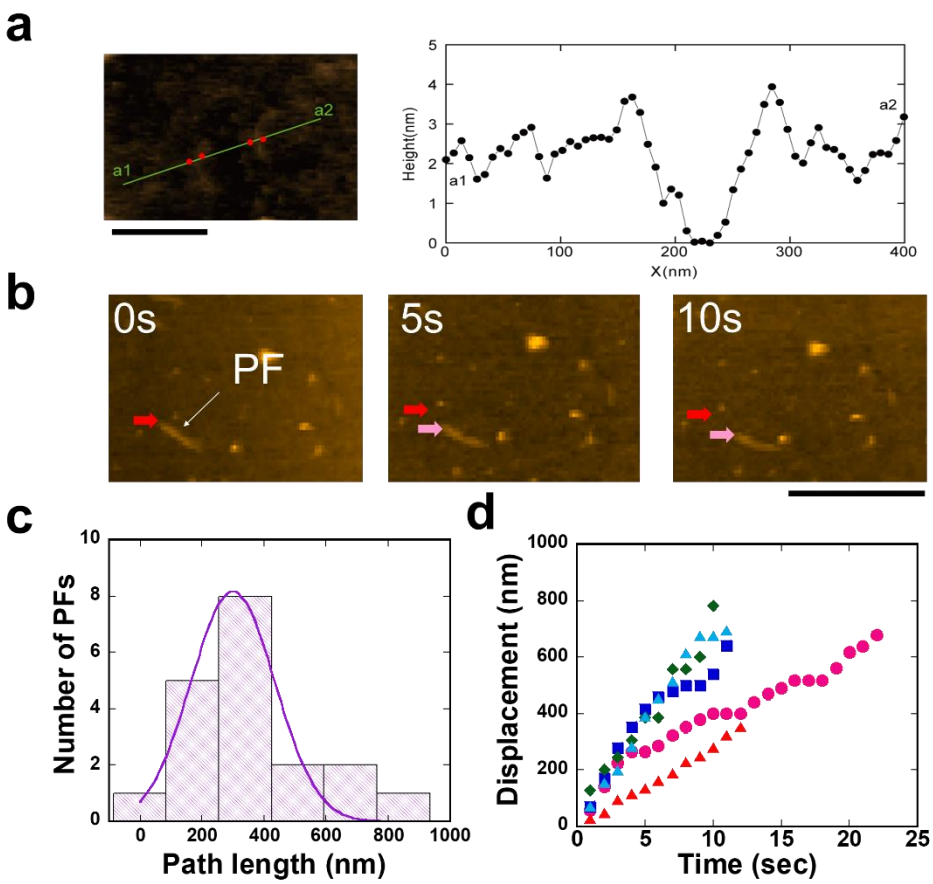

Figure 4.9 Height profile of gliding PFs obtained from HS-AFM image as shown. Scale bar: 250 nm, frame rate: 1.0 s/frame (a). Observation of a gliding PF by using HS-AFM. Scale bar: 500 nm (b). In (b) the pink/red arrows are indicating change of position of gliding short PF with time. Scale bar: 500 nm, frame rate: 1.0 s/frame. Distribution of path length of gliding PFs. Mean=300±190, R^2=0.87. n=20 (c) and typical displacement of PFs with time. n=5 (d).

It is to be mentioned that in these experiments, curled shape of single PFs during gliding on the surface was not observed. Generally, taxol-stabilized PFs are known to form curled structures as reported in a previous AFM study[31]. In fact, bundles of PFs form ring shaped structure when detaching from the MTs[19]. Usually, when a PF starts to be bent, kinesin binding surface of the PF goes inside the PF ring and inner part of the MT is exposed to the outside ring. But here if the kinesin binding side of PF is fixed on a flat kinesin coated surface, PF cannot be bent to form ring anymore and should keep straight structure (**Figure 4.10**). On the other hand, if PFs form bundle, it may produce more force to bend PFs. Therefore, single PFs are found to exhibit translational motion, unlike the PFBs which exhibit circular motion on the kinesin coated surface[19].

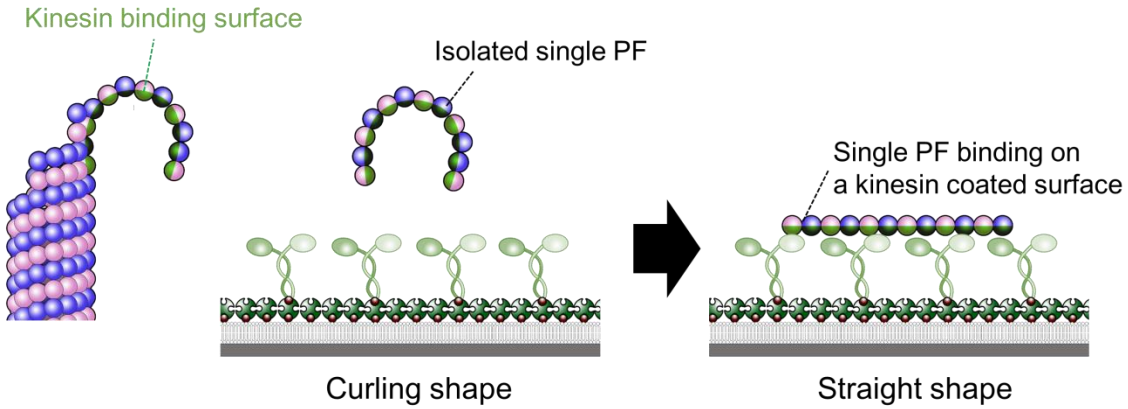

Figure 4.10 Schematic diagram showing binding of a PF of tubulins to kinesin coated surface. The PFs of tubulin showed translational motion on kinesins.

4.2.2.4 Comparison of motility of MTs and PFs on NC and lipid bilayer surfaces

Collectively the results obtained from three different surfaces confirm the effect of substrate on the velocity of MTs as shown in the following **Figure 4.11**. The velocity of MTs was found to decrease drastically on the both lipid surface (~100 nm s^{-1} and 150 nm s^{-1} respectively) compared to nitrocellulose (NC) coated mica surface (~590 nm s^{-1}). The results suggested that, the velocity was affected mainly by the surface property while mechanical process of scanning during observation under HS-AFM not to be the main factor behind the slow velocity of MTs. The streptavidin coating on the lipid bilayer surface might have influence on the velocity. Lower binding affinity of kinesins on this streptavidin crystal surface may significantly affect the velocity. Density of kinesin as estimated on streptavidin crystal surface was ~1200 μm^{-2} which was quite lower than found in the literature[37] on the glass surface as ~5000 μm^{-2}.

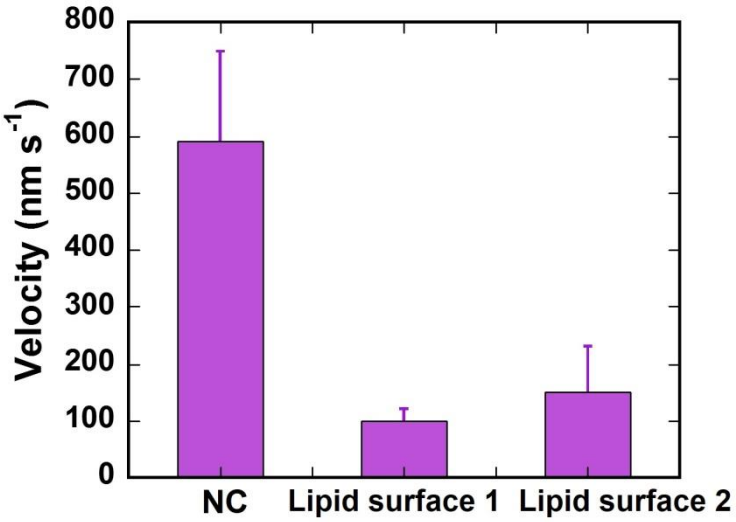

Figure 4.11 Change in velocity of MTs on different substrate. Error Bar: Standard error (S. E).

Moreover, despite of low velocity we can clearly observe the gliding PFs on both the lipid bilayer surface clearly which may attribute to the flat surface property of lipid bilayer which facilitates the high resolution images. The difference in velocity between gliding MTs and PFs was observed (lipid surface 1: MTs~100 nm s^{-1}, PFs~40 nm s^{-1} and lipid surface 2: MTs~150 nm s^{-1}, PFs~60 nm s^{-1}) which indicates that difference in velocity is caused by the fluctuation of surface bound kinesin which greatly affects the velocity of small PFs than the long MT filaments. Thus the gliding MTs and PFs were successfully observed on the streptavidin coated lipid bilayer surface which provides different information of gliding events and their inherent properties.

4.2.3 Observation of splitting of gliding MTs into single PFs

Motility of MTs on a kinesin coated substrate has been reported to be associated with molecular wear, breakage or splitting of MTs into PFBs[18, 19]. The broken and split MTs exhibited translational and circular motion respectively on the kinesin coated substrate[18, 19]. Here taking the advantage of high resolution imaging of gliding MTs by HS-AFM, the splitting of gliding MTs was directly observed into single PFs on lipid coated mica substrate. While monitoring the motile MTs by HS-AFM, it was observed that the MTs suddenly changed their moving direction after a short pause. Such abrupt change in direction of motion of the MTs was also observed under fluorescence microscope, although the reason has remained obscure. From high resolution imaging of MTs on the mica surface the leading end of many MTs was found incomplete where PFs can be clearly observed. This leading end is known as tapered end from which PFs are protruding out[38] (**Figure 4.12**).

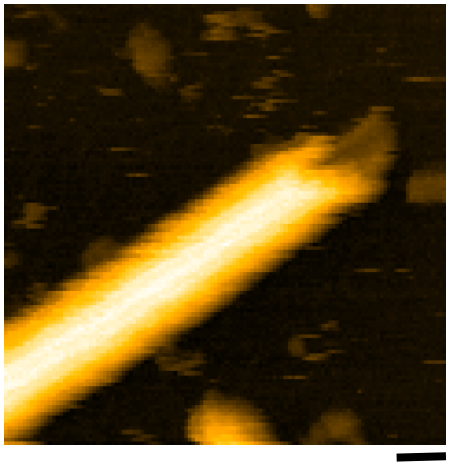

Figure 4.12 HS-AFM image of a MT with a tapered end. The bright cylindrical object is MT. At the very end of the MT, tapered end is observed showing PFs. Scale bar: 20 nm, frame rate: 1.0 s/frame.

High resolution imaging by HS-AFM revealed that after pausing, a gliding MT was split into two fragments (**Figure 4.13a**). This result suggests that, the sudden change in direction of motile MTs is related to such splitting of the MTs. Probably, When PFs at the tapered leading end of MT collides with dead kinesins or some obstacles, the PFs might be bent, and being pushed by the lagging part of the MT. Finally, the tapered PFs was broken and separated from the leading end of MTs. Consequently, MTs might change their moving direction due to the buckling force from the PF (**Figure 4.13c**). Additionally, taking into account the difference in the velocity between PFs and MTs, PFs tapered at the leading end of a MT might also cause bending of tapered-PFs due to the mismatch of the velocity and subsequently causing directional change of MTs. Thus, from the observation under HS-AFM, it was revealed that splitting of PFs from the leading end of MTs influences the motility of MTs. However, splitting of MTs into PFs can be observed on the lipid bilayer surface with some fractionate appearance of streptavidin crystals (DPPC/DPTAP/biotin-cap DPPE) (**Figure 4.13a**).We also observed such splitting on the uniform large areas of streptavidin crystals using the other lipid bilayer (DOPC/DOPS/biotin-cap DOPE) surface (**Figure 4.13b**) which indicates that incomplete or fractionate appearance of streptavidin crystals might have no considerable effect on the splitting of gliding MTs into PFs. The PF split from the motile MTs showed translational motion, which is in contrary to the circular motion exhibited by PFBs[19].

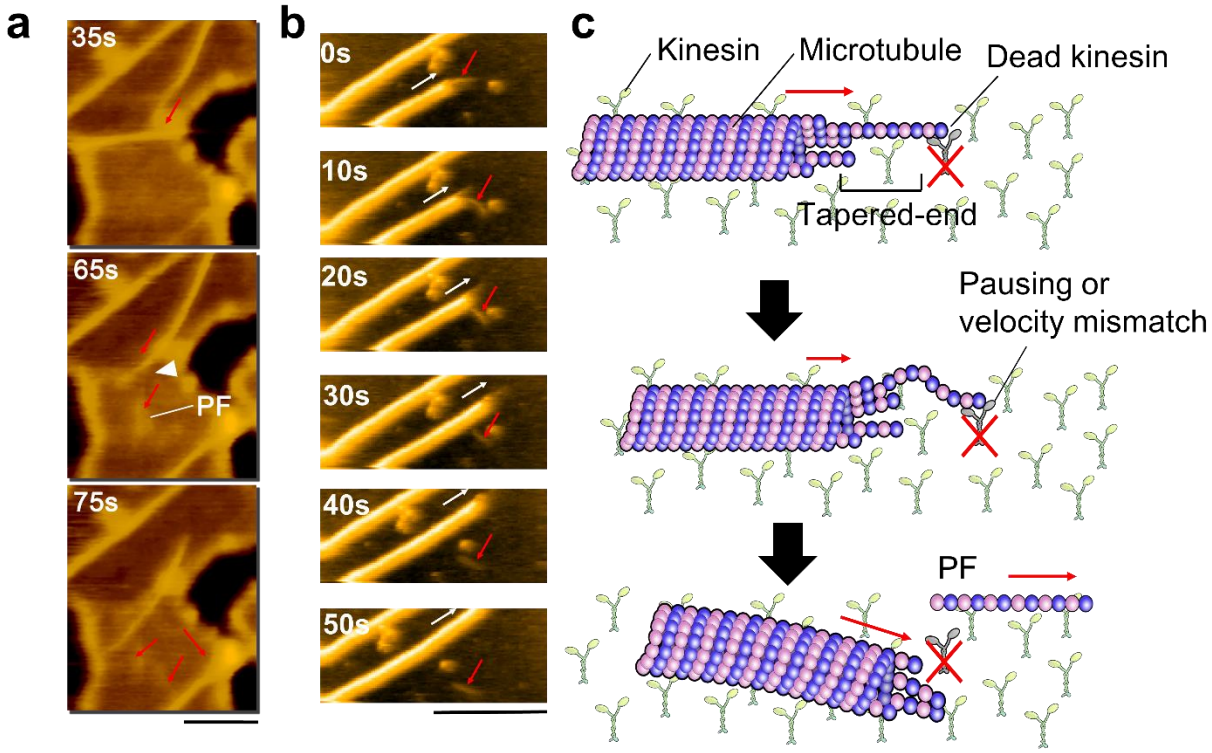

Figure 4.13 Sudden change in direction of gliding MTs with segregation of tapered PFs from the leading end. Time-lapse images showing splitting of a MT at the tapered leading end during gliding motion on lipid surface 1 (a) and on lipid surface 2 (b) Scale bar: 500 nm, frame rate: 0.2 s/frame. The red arrows show moving direction of gliding MTs and PFs separated from leading end of the MT. Schematic model showing sudden directional change of MT with segregation of a PF from the tapered leading end of the MT (c).

Therefore, splitting of single PFs is one of the significant events that may be one of the cause of damage or breakage of MTs during their gliding motion. Thus, HS-AFM images help us to unravel such events that occur at the molecular level which exceeds the limitations of conventional microscope unveiling their mechanical properties.

4.3 Conclusion

In conclusion, exploiting the advantage of high resolution imaging by HS-AFM at molecular scale, gliding motion of MTs and single PFs was successfully observed in an *in vitro* gliding assay. Moreover, splitting of the gliding MTs into single PFs has also been observed directly for the first time, which can account for the sudden directional change of the gliding MTs in the gliding assay. The investigation thus provides an answer to the long standing mystery of sudden directional change of gliding MTs in an *in vitro* gliding assay, which has been observed under epi-fluorescence microscopy. From the detail investigation of motile MTs at the molecular level using HS-AFM, detail of the relationship between structure of MTs and their motility behavior would be understandable. High resolution imaging by HS-AFM might be advantageous in the study of MT dynamics or interaction between motor proteins and MTs on their functionality in a dynamic system. The knowledge of functional property of gliding MTs would help us to find out the way to use this self-propelled system for developing efficient devices or robots in near future.

4.4 Experimental Procedures

4.4.1 Purification of tubulin and kinesin

Tubulin was purified from porcine brain using a high-concentration PIPES buffer (1 M PIPES, 20 mM EGTA, and 10 mM $MgCl_2$; pH adjusted to 6.8 using KOH). The high-concentration PIPES buffer and Brinkley Buffer 80 (BRB80) (80 mM PIPES, 1 mM EGTA, 1 mM $MgCl_2$, pH 6.8) were prepared using PIPES from Sigma, and the pH was adjusted using KOH[39]. Kinesin construct consisting of human kinesin (residues 1-465), with an N-terminal histidine tag, and a C-terminal avi-tag were prepared as described in previously published reports by partially modifying the expression and purification methods [40, 41].

4.4.2 Preparation of MTs

For preparation of MTs, 56 µM tubulin was incubated at 37 ^oC for 30 min using polymerization buffer including guanosine-5´-triphosphate (GTP) (80 mM PIPES, 1 mM EGTA, 1 mM $MgCl_2$, 1 mM GTP, pH ~6.8). Tubulin and polymerization buffer were mixed at a 4:1 volume ratio. Finally polymerized MTs were stabilized with taxol buffer (80 mM PIPES, 1 mM EGTA, 1 mM $MgCl_2$, 10 µM Paclitaxel, 5% DMSO).

4.4.3 Observation of MTs and PFs on mica surface

1 µM MT was directly deposited on the mica surface and washed with 100 µL taxol buffer including 3 µM paclitaxel to avoid the crystals of taxol during observation and observed by HS-AFM.

4.4.4 Preparation of motility assay on the nitrocellulose coated glass surface

2% nitrocellulose (NC) in isoamyl acetate (0.5 µL) was deposited on a freshly cleaved mica surface for 15 mins to completely dry. Then 200 nM kinesin-1 (2 µL) in BRB80 with 1 mM DTT (80 mM PIPES, 1 mM EGTA, 1 mM $MgCl_2$, 1mM DTT, pH 6.8) was deposited on the surface for 5 min. After that washed by excess amount of BRB80 with DTT (~100 µL) buffer. 1 mg mL^{-1} casein in BRB80 (2 µL) was deposited on the surface for 3 min. Then rinsed with taxol buffer (BRB80 with 3 µM paclitaxel) (20 µL). 1 µM of MT in taxol buffer was deposited and waited for 5 min. Finally rinsed with taxol buffer~60 µL and imaged by AFM in ~120 µL of the taxol buffer containing 2 mM ATP.

4.4.5 Preparation of streptavidin coated lipid bilayer surface

Lipid system 1: Biotinylated mica-supported lipid bilayers were prepared as described in a previous report[35]. Briefly, solution of 1,2-Dihexadecanoyl-*sn*-glycero-3-phosphocholine (DPPC) in chloroform, 1,2-Dipalmitoyl-3-trimethylammonium-propane (DPTAP) and 1,2-dipalmitoyl-sn-glycero-3- phosphoethanolamine-N-(cap biotinyl) (biotin-cap DPPE) (Avanti Polar Lipids) were mixed at a weight ratio of 0.85:0.05:0.10. The chloroform was then evaporated under a stream of nitrogen gas, and the lipids were redissolved in MilliQ H_2O at a concentration of 1 mg mL^{-1}. Solubilized lipid was diluted to ~0.05 mg mL^{-1} by MilliQ H_2O and sonicated to obtain small unilamellar vesicles. A drop of the vesicle solution (3 μL) was deposited on freshly cleaved mica disks. After ~3 h of incubation in a sealed container, in which a Kimwipe wetted with MilliQ H_2O was placed, the surface was rinsed with crystallization buffer 1 (20 mM Tris-HCl, 1 mM EDTA, 10 mM $MgCl_2$, pH~7.6). Then, a drop (3 μL) of streptavidin in crystallization buffer 1 (1 μg mL^{-1}) was deposited on the bilayer surface. After 30 min of incubation, the surface was rinsed again with crystallization buffer 1 to remove the excess streptavidin.

Lipid system 2: For the DOPC/DOPS/biotin-cap DOPE system, solution of 1,2-dioleoyl-*sn*-glycero-3-phosphocholine (DOPC) in chloroform, 1,2-dioleoyl-*sn*-glycero-3-phospho-L-serine (DOPS) and 1,2-dioleoyl-*sn*-glycero-3-phosphoethanolamine-N-(cap biotinyl) (biotin-cap DOPE) (Avanti Polar Lipids) were mixed at a weight ratio of 7:2:1. The chloroform was then evaporated under a stream of nitrogen gas, and the lipids were redissolved in MilliQ H_2O at a concentration of 1 mg mL^{-1}. Solubilized lipid was diluted to ~0.05 mg mL^{-1} by MilliQ H_2O and sonicated to obtain small unilamellar vesicles. A drop of the vesicle solution (3 μL) was deposited on freshly cleaved mica disks. After ~3 h of incubation in a sealed container, in which a Kimwipe wetted with MilliQ H_2O was placed, the surface was rinsed with crystallization buffer 2 (10 mM HEPES-NaOH, 150 mM NaCl, 2 mM $CaCl_2$, pH 7.4). Then, a drop (3 μL) of streptavidin in crystallization buffer 2 (1 mg mL^{-1}) was deposited on the bilayer surface. After 3 h of incubation, the surface was rinsed again with crystallization buffer 2 to remove the excess streptavidin. For the chemical fixation of the streptavidin crystals, a 10 mM glutaraldehyde-containing crystallization solution 2 was applied and incubated for 5 min. The reaction was quenched using 20 mM Tris buffer mixed in the crystallization buffer 2.

4.4.6 Preparation of motility assay of MTs on lipid bilayer coated mica substrate

A drop (2 μL) of biotinylated kinesin (6 μM and 200 nM for Lipid system 1 and 2 respectively) in BRB80 with 1 mM DTT (80 mM PIPES, 1 mM EGTA, 1 mM $MgCl_2$, 1mM DTT, pH 6.8) was deposited on the 2D streptavidin crystal surface. After 2~3 min incubation the surface was rinsed with 20 μL BRB80 to remove excess kinesin and then a drop of 1μM MT solution in BRB80 with 3 μM paclitaxel (80 mM PIPES, 1 mM EGTA, 1 mM $MgCl_2$, 1 mM DTT, 3μM paclitaxel/DMSO; pH 6.8) was deposited on the surface. After 3 min of incubation, the surface was rinsed with 20 μL taxol buffer and imaged by AFM in ~120 μL of the taxol buffer containing 2 mM ATP.

4.4.7 HS-AFM imaging

AFM imaging was performed using a tip scan high-speed AFM imaging system (BIXAM, olympus, Tokyo, Japan) that was improved based on a previously developed machine[42] and laboratory-made high-speed AFM imaging system[15]. Silicon nitride cantilevers (resonant frequency = 0.4-1.0 MHz in water, spring constant= 0.1 Nm^{-1}, electron-beam-deposited tip radius <15 nm; Olympus BLAC10EGS-A2). AFM images were analyzed using the AFM Scanning System Software (Olympus, Tokyo, Japan), laboratory made software, Adobe Photoshop CC and ImageJ[43].

4.5 References

1. Alberts, B.; Lewis, J.; Raff, M.; Walter, P.; Roberts, K.; Johnson, A.; Nakamura, K. Molecular Biology of the Cell 5E, Garland Science, **2010**.
2. Sharp, D. J.; Rogers, D. C.; Scholey, J. M. *Nature* **2000**, *407*, 41-47.
3. .Tay, C. Y.; Cai, P.; Setyawati, M. I.; Fang, W.; Tan, L. P.; Hong, C. H. L.; Chen, X.; Leong, D. Tai. *Nano Lett.* **2014**, *14*, 83-88.
4. Bershadsky, A. D.; Balaban, N. Q.; Geiger, B.; *Annu. Rev. Cell Dev. Biol.* **2003**, *19*, 677-695.
5. Howard, J. In *Mechanics of motor protein and the cytoskeleton*, Sinauer Associates, Inc., Sunderland, Massachusetts, **2001**.
6. Kurachi, M.; Hoshi, M.; Tashiro, H. *Cell Motil. Cytoskeleton* **1995**, *30*, 221-228.
7. Zhang, J.; Guo, W. H.; Wang, Y. L. *Proc. Natl. Acad. Sci. USA* **2014**, *18*, 16383-6388.
8. Stamenovic, D.; Mijailovich, S. M.; Tolic-Norrelykke, I. M.; Chen, J.; Wang, N. *Am J Physiol Cell Physiol* **2002**, *282*, C617-C624.
9. Wang, N.; Butler, J. P.; Ingber, D. E. *Science* **1993**, *260*, 1124-1127.
10. Howard, J.; Hudspeth, A. J.; Vale, R. D. *Nature* **1989**, *342*, 154-158.
11. Hunt, A. J.; Howard, J. *Proc. Natl. Acad. Sci. USA* **1993**, *90*, 11653-11657.
12. Jiang, M. Y.; Sheetz, M. P. *Biophys. J.* **1995**, *68*, 283-285.
13. Diez, S. & Howard, J. *Physics in Canada* **2009**, *65*, 7-12.
14. Hess, H.; Vogel, V. *Rev. Mol. Biotechnol.* **2001**, *82*, 67-85.
15. Ando, T.; Kodera, N.; Takai, E.; Maruyama, D.; Saito, K.; Toda. A. *Proc. Natl. Acad. Sci. USA* **2001**, *98*, 12468-12472.
16. Ando, T.; Kodera, N.; Takai, E.; Maruyama, D.; Takai, E.; Saito, K.; Toda. A. *Chemphyschem* **2003**, *4*, 1196-1202.
17. Ando, T.; Uchihashi, T.; Kodera, N.; Miyagi, A.; Nakakita, R.; Yamashita, H.; Sakashita, M. *Japanese journal of applied physics* **2006**, *45*, 1897-1903.
18. Dumont Emmanuel, L. P.; Do, C.; Hess, H. *Nat. Nanotechnol.* **2015**, *10*, 166-169.
19. Delinder, V. V.; Adams, P. G.; Bachand, G. D. *Sci. Rep.* **2016,** *6*, 39408.
20. Aumeier, C.; Schaedel, L.; Gaillard, J.; John, K.; Blanchoin, L.; Théry, M. *Nat. Cell Biol.* **2016**, *18*, 1054-1064.
21. Schaedel, L.; John, K.; Gaillard, J.; Nachury, M. V.; Blanchoin, L.; Théry, M. *Nat. Mater.* **2015**, *14*, 1156-1163.

22. de Forges, H.; Pilon, A.; Cantaloube, I.; Pallandre, A.; Haghiri-Gosnet, A.-M.; Perez F.; Poüs, C. *Curr. Biol.* **2016**, *26*, 3399-3406.
23. Liang, W. H.; Li, Q.; Faysal, R.; K. M.; King, S. J.; Gopinathan, A, Xu. J. *Biophys. J.* **2016**, *110*, 2229-2240.
24. Portran, D.; Zoccoler, M.; Gaillard, J.; Stoppin-Mellet, V.; Neumann, E.; Arnal, I.; Martiel, J. L.; Vantard, M. *MBoC* **2013**, *24*, 1964-1973.
25. Krebs, A.; Goldie, K. N.; Hoenger, A. *J. Mol. Biol*. **2004**, *335*, 139-153.
26. Kabir, A. M. R.; Inoue, D.; Afrin, T.; Mayama, H.; Sada, K.; Kakugo, A. *Sci. Rep.* **2015**, *5*, 17222.
27. Robison, P.; Caporizzo, M. A.; Ahmadzadeh, H.; Bogush, A. I.; Chen, C. Y.; Margulies, K. B.; Shenoy, V. B.; Prosser. B. L. *Science* **2016**, *352*, aaf0659.
28. Soong, R. K.; Bachand, G. D.; Neves, H. P.; Olkhovets, A. G.; Craighead, H. G.; Montemagno, C. D. *Science* **2000**, *290*, 1555-1558.
29. Knoblauch, M.; Peters, W. S. *Cell. Mol. Life Sci.* **2004**, *61*, 2497-2509.
30. Inoue, D.; Nitta, T.; Kabir, A. M. R.; Sada, K.; Gong, J. P.; Konagaya, A.; Kakugo, A. *Nat. Commun.* **2016**, *7*, 12557.
31. Caille, C. E.; Severin, F.; Helenius, J.; Howard, J.; Muller, D. J.; Hyman, A. A. *Curr. Biol.* **2007**, *17*:1765-1770.
32. Yamamoto, D.; Nagura, N.; Omote, S.; Taniguchi, M.; Ando, T. *Biophys. J.* **2009**, *97*, 2358-2367.
33. Nicolau , D. V.; Solana, G.; Kekic, M.; Fulga, F.; Mahanivong, C.; Wright, J.; dos Remedios, C. G. *Langmuir* **2007**, *23*, 10846-10854.
34. Kabir, A. M. R.; Inoue, D.; Kakugo, A.; Kamei, A.; Gong, J. P. *Langmuir* **2011**, *27*, 13659-13668.
35. Kodera, N.; Yamamoto, D.; Ishikawa, R.; Ando, T. *Nature* **2010**, *468*, 72-76.
36. Grover, R.; Fischer, J.; Schwarz, F. W.; Walter, W. J.; Schwille, P.; Diez, S. *Proc. Natl. Acad. Sci. USA* **2016**, *113*, E7185-E7193.
37. Dumont Emmanuel, L. P.; Belmas, H.; Hess, H. *Langmuir* **2013**, *29*, 15142-15145.
38. Kacher, C. M.; Weiss, I. M.; Stewart, R. J.; Schmidt, C. F.; Hansma, P. K.; Radmacher, M.; Fritz, M. *EurBiophys J.* **2000**, *28*, 611-620.
39. Castoldi, M.; Popov, A. V. *Protein Expr. Purif.* **2003**, *32*, 83-88.
40. Fujimoto, K.; Kitamura, M.; Yokokawa, M.; Kanno, I.; Kotera, H., Yokokawa, R. *ACS Nano* **2013**, *7*, 447-455.
41. Yokokawa, R.; Tarhan, M. C.; Kon, T.; Fujita, H. *Biotechnol. Bioeng.* **2008**, *101*, 1-8.

42. Suzuki, Y.; Sakai, N.; Yoshida, A.; Uekusa, Y.; Yagi, A.; Imaoka, Y.; Ito, S.; Karaki, K.; Takeyasu K. *Sci. Rep.* **2013**, *3*, 2131.
43. https://imagej.nih.gov/ij/docs/guide/index.html."Ferreira, T.; Rasband, W. ImageJ user guide IJ 1.46r (2012) (17/2/2017)".

CHAPTER 5

Concluding Remarks

This dissertation mainly concerns about the development of micro robots using self-propelled biomolecular motor system by programming features of DNA which would act like swarm in nature. Swarming of microtubules (MTs) was demonstrated by active self-assembly process modulated by DNA interaction and further controlled through DNA programming to introduce sensing ability in the system. Moreover, the study also includes the investigation on different features of MTs during their gliding motion using high resolution images by high speed AFM (HS-AFM) method that provides molecular level information about this self-propelled system.

In Chapter 2, swarming was demonstrated by self-propelled MTs through DNA interaction. DNA conjugated MTs or swarm units were prepared using click reaction that retained its bioactivity with same velocity in *in vitro* like MTs without any modification. Swarming takes place through input DNA signals complementary to DNAs modified to MTs by active self-assembly through formation of linear bundle shaped structures with translational motion. Size of swarm groups increased with time showing almost similar velocity as single swarm units which exhibits scalability of the system. Different shape of pattern and mode of motion of swarming was also controlled by changing the physical property of MTs where the flexible one exhibits circular mode of motion unlike the rigid one which shows translational motion. For both type of swarm units, the swarming depends on a number of relevant parameters which were varied to optimize the conditions which not only affects the initiation of swarming but also their morphology. It was found that in presence of equal density of swarm units i.e; 1:1 ratio, the length of bundles was highest with saturated concentration of *l*-DNA. The shapes of swarm groups were controlled from circular to linear bundle by shorten the length of MTs with similar rigidity. On the other hand, size of circular swarm group was also able to control changing both the rigidity and length of MTs. Dissociation of swarming to their initial single state reversibly was also successfully demonstrated by introducing DNA strand displacement reaction which was reported for the first time for controlling swarm based on biomolecular motor system. Nevertheless, their mode of motion can be also interchanged by self-assembly into circular swarm group and again dissociation of them by DNA interaction and strand displacement reaction respectively. These functions of

biomolecular motor based swarming would help to develop swarm behavior with increasing robustness.

In chapter 3, swarming was further controlled by advance use of DNA programming such as DNA logic gate operations. Logic gate programming has been first introduced in biomolecular motor system which helps to control the swarming in presence of designed sequence of input DNA signals. Different types of logic gates such as YES, AND and OR gates were demonstrated that can program the swarming following the true mathematical computation. Moreover, through logic gate operation two different patterns, linear and circular pattern with their corresponding mode of motion was able to control simultaneously through DNA molecular recognition process. The swarming modes with distinct physical properties of swarm units were responsive to the corresponding input DNA signals which help to sort out the patterns without any crosstalk. Finally, inserting photoresponsive DNA using azobenzene molecules in the swarm units, repeated control over reversible swarming was successfully demonstrated by input physical signals through cis-trans isomerization of azobenzene. Using UV and visible light irradiation repeatedly, it was possible to regulate the swarming reversibly upto three cycles which includes sensing capability in swarming. This work provides us the way to control biomolecular swarming with responsiveness and sensitivity.

In chapter 4, gliding motion of MTs was investigated using the advantage of high resolution imaging by HS-AFM at molecular scale. Gliding motion of MTs and single protofilaments (PFs) was successfully observed in an *in vitro* gliding assay. The gliding motion of PFs and its corresponding features was first observed by HS-AFM that was not reported by conventional technique. The PFs were found to move with lower velocity than the velocity of MTs with shorter path length and pausing events. While depending on the substrate used for the imaging of motile MTs, velocity was found to be decreased from the conventional substrate that was used for gliding assay due to difference in surface property. Furthermore, splitting of single PFs from gliding MTs has also been observed directly for the first time from the leading end of the MT. PFs split from the MT with some tapered part protruding PFs, which may give the answer of the cause of sudden directional change of the gliding MTs in gliding assay. From the detail investigation of motile MTs and PFs at the molecular level using HS-AFM, detail of the relationship between structure of MTs and their motility behavior would be understandable.

Finally, I would like to draw a future perspective of my entire work. Modulation of swarming of a self-propelled biomolecular motor system through DNA interaction gives us a new concept to realize swarming that takes place through active self-assembly process like in nature. Programming the self-assembly of swarm units with responsiveness and sensing ability could harness the capabilities of this dynamic system that would serve the knowledge in the view point from engineering system to develop swarm robots with different functionalities like flexibility, parallelism, robustness. Moreover, study of dynamic self-assembly process using self-propelled biomolecular system by supramolecular interaction of DNA will also be advantageous in the field of chemistry which is seeking the control over non-equilibrium system making hierarchical structures for different applications. To obtain further knowledge of this self-propelled system for their sustainable use as artificial devices or robots, study of high resolution imaging of MTs and PFs by HS-AFM would also be helpful for deep understanding of molecular events.

List of Publications

Papers (related to this dissertation)

Chapter 2 and 3

DNA-Assisted Swarm Control in a Biomolecular Motor System

Keya, J. J.; Suzuki, R.; Kabir, A. M. R.; Inoue, D.; Asanuma, H.; Sada, K.; Hess, H.; Kuzuya A.; Kakugo, A. *Nature Chemistry*, under review.

Chapter 4

High-Resolution Imaging of a Single Gliding Protofilament of Tubulins by HS-AFM

Keya, J. J.; Inoue, D.; Suzuki, Y.; Kozai, T.; Ishikuro, D.; Kodera, N.; Uchihashi, T.; Kabir, A. M. R.; Endo, M.; Sada, K.; Kakugo, A. *Scientific Reports*, **2017**, *7*, 6166.

Other Papers (not including in this dissertation)

Effect of a Water Structure Modifier on the Aqueous Electrochemistry of Supramolecular Systems: Redox-Active versus Conventional Surfactants

Keya, J. J.; Islam, M. M.; Rahman, M. M.; Mollah, M. Y. A.; Susan, M. A. B. H. *Journal of Electroanalytical Chemistry* **2014**, *712*, 161-166.

List of Conference Presentations

Conference (related to this dissertation)

1. Jakia Jannat Keya, Daisuke Inoue, Arif Md. Rashedul Kabir, Kazuki Sada, Akinori Kuzuya and Akira Kakugo, "DNA Programmed Self-Organization of Microtubules", The 64th SPSJ (Society of Polymer Science, Japan) Annual Meeting, 2015, May 27-29, Sapporo, Japan.
2. Jakia Jannat Keya, Daisuke Inoue, Arif Md. Rashedul Kabir, Kazuki Sada, Akinori Kuzuya and Akira Kakugo, "DNA Programmed Self-Assembly of Microtubules In vitro", 2015 CSE Summer School, August, 22-23, Sapporo, Japan.
3. Jakia Jannat Keya, Daisuke Inoue, Arif Md. Rashedul Kabir, Kazuki Sada, Akinori Kuzuya and Akira Kakugo, "DNA Programmed Active Self-Organization of Microtubules on Kinesin", The 53rd Biophysical Society of Japan, 2015, September, 13-15, Kanazawa University, Japan.
4. Jakia Jannat Keya, Ryuhei Suzuki, Arif Md. Rashedul Kabir, Daisuke Inoue, Kazuki Sada, Akinori Kuzuya and Akira Kakugo, "Biomolecular Motor based Micro-Robot". The 50th SPSJ (Society of Polymer Science, Japan) Hokkaido Branch Meeting, 2016, January 21, Hokkaido University, Japan.
5. Jakia Jannat Keya, Ryuhei Suzuki, Arif Md. Rashedul Kabir, Daisuke Inoue, Kazuki Sada, Akinori Kuzuya and Akira Kakugo, "Programming of Swarm Robot Based on DNA Processed Biomolecular Motor System", The 4th Frontier Chemistry Centre International Symposium, 2016, February 23-24, Hokkaido University, Japan.
6. Jakia Jannat Keya, Arif Md. Rashedul Kabir, Daisuke Inoue, ,Kazuki Sada, Akinori Kuzuya and Akira Kakugo, "DNA Assisted Control of Swarming of a Biomolecular Motor System", The First International Symposium on Advanced Soft Matter, June 13-15, 2016, Hokkaido University, Japan.
7. Jakia Jannat Keya, Arif Md. Rashedul Kabir, Daisuke Inoue, Kazuki Sada, Akinori Kuzuya and Akira Kakugo, "Construction of DNA Programmed Swarm Robots from a Biomolecular Motor System", The 67th Divisional Meeting on Colloid & Interface Chemistry, September 22-24, 2016, Hokkaido University of Education, Asahikawa Campus, Japan.
8. Jakia Jannat Keya, Arif Md. Rashedul Kabir, Daisuke Inoue, Kazuki Sada, Akinori Kuzuya and Akira Kakugo, "Regulated Swarming of Molecular Robots Prepared from a

DNA Programmed Biomolecular Motor System", The 53rd Biophysical Society of Japan, September 25-27, 2016, Tsukuba International Congress Center, Japan.

9. Jakia Jannat Keya, Arif Md. Rashedul Kabir, Daisuke Inoue, ,Kazuki Sada, Akinori Kuzuya and Akira Kakugo, "DNA Programmed Logic-Gated Control of Swarming of a Biomolecular Motor System", The 17th RIES-HOKUDAI International Symposium, December 13-14, 2016, Hokkaido, Japan.
10. Jakia Jannat Keya, Ryuhei Suzuki, Arif Md. Rashedul Kabir, Daisuke Inoue, ,Kazuki Sada, Akinori Kuzuya and Akira Kakugo, "DNA Programmed Control of Swarming Demonstrated by a Biomolecular Motor System", 11th International Gel Symposium, March 7-9, 2017, Nihon University (Tsudanuma Campus), Chiba, Japan,.

Conference (others)

(1) Jakia Jannat Keya, Md. Mominul Islam, Md. Yousuf A. Mollah, and Md. Abu Bin Hasan Susan, "Electrochemical Control of Nanocarriers for Drug Delivery System", International Workshop on Nanotechnology, December 21-23, 2012, Dhaka, Bangladesh,

(2) Jakia Jannat Keya, Md. Mominul Islam, Md. Yousuf A. Mollah, and Md. Abu Bin Hasan Susan, "Effect of a Water Structure Modifier on the Electrochemistry of a Redox-Active Surfactant Distinguishing from a Conventional One", Bangladesh Chemical Congress-2012, 7-9 December, 2012, University of Dhaka, Dhaka, Bangldesh.

(3) Jakia Jannat Keya, Md. Mominul Islam, Md. Yousuf A. Mollah, and Md. Abu Bin Hasan Susan, "Ionic Liquids as Additives for Supramolecular Interaction with Nonionic Surfactants In Aqueous Medium", The 36 Annual Conference of Bangladesh Chemical Society, 01 March, 2014, Hajee Mohammad Danesh Science & Technology, Dinajpur, Bangladesh.

Acknowledgements

I would like to complete my dissertation by acknowledging all who have helped me in various ways during my research work. The entire study presented in this dissertation was carried out under the direction of Professor Kazuki Sada during October 2014-September 2017 at Hokkaido University, Japan. I would like to express my deepest and sincere gratitude to Professor Kazuki Sada for his invaluable advices, patience, constructive discussions and earnest encouragement during the study on time to time until accomplishing this dissertation.

I am highly obliged and indebted to reverend Associate Professor Akira Kakugo (Material Chemistry Laboratory, Hokkaido University), for his guidance, understanding, and valuable advices beyond the border to allow me work in such an advanced and exciting system. I am extremely grateful to him for his continuous motivation, influential comments, wide-ranging discussion and technical supports which give me the confidence to stand in any situation.

I would like to gratefully acknowledge the cooperation and insightful suggestions from Assistant Professor Kenta Kokado and Assistant Professor Kenji Hirai of Material Chemistry Laboratory, Hokkaido University. My deepest cordial appreciation goes to Assistant Professor Arif Md. Rashedul Kabir (Material Chemistry Laboratory, Hokkaido University) not only for his guidance, effective discussions and technical help during the entire study but also for his kind support regarding my Japan life.

I owe my sincere gratitude to Associate Professor Akinori Kuzuya (Department of Chemistry and Materials Engineering, Kansai University) for the active collaboration with fruitful suggestions (Chapter 2, 3) and also to Professor Hiroyuki Asanuma (Department of Biomolecular Engineering, Nagoya University) (Chapter 3). I also gratefully acknowledge Professor Masayuki Endo (Institute for Integrated Cell-Material Sciences, Kyoto University), Assistant Professor Yuki Suzuki (Frontier Research Institute for Interdisciplinary Sciences, Tohoku University); Professor Takayuki Uchihashi, Associate Professor Noriyuki Kodera and other members of Bio-AFM Frontier Research Center (Kanazawa University) for their warm assistance with technical supports and useful advices during HS-AFM study (Chapter 4). I would also like to offer my special thanks to Dr. Daisuke Inoue for his kind cooperation and effective discussions and to Dr. Md. Sirajul Islam for his inspiration and help throughout this work.

All the current and former members of the Material Chemistry laboratory, Hokkaido University are thankfully acknowledged for their active cooperation, unceasing help and support. I would like to specially thank Dr. Tanjina Afrin, Dr. Tamanna Ishrat Farhana, Mr. Kyohei Uenishi, Ms. Shizuka Anan, Ms. Sayeda Rubaiya Nasrin, Mr. Soukurou Sunaga, Mr. Masami Naya, Mr. Ryuhei Suzuki, Mr. Ren Sasaki, Ms. Ai Saito, Mr. Seiji Nishikawa and Mr. Kentaro Kayano for their help during the period of this study. I am also thankful to all the staffs in the Graduate School of Chemical Sciences and Engineering and the Department of Chemistry, Hokkaido University for their kind assistance and supports during this study.

I would like to pay my honor to Hokkaido University (Japan) and Dhaka University (Bangladesh) under Monbukagakusho (MEXT) program and to Professor Md. Abu Bin Hasan Susan (Department of Chemistry, Dhaka University, Bangladesh), who initially motivated and guided me to be a researcher to give me the opportunity to study and enjoy the charming nature with unique cultural life in Japan. I am also grateful to Professor Mohammed Yousuf Ali Mollah (Member, University Grants Commission of Bangladesh), Associate Professor Md. Mominul Islam (Department of Chemistry, Dhaka University) and Associate Professor Mohammad Shah Miran (Department of Chemistry, Dhaka University) for their encouragement and motivation. I would also like to thank all of the former and present members of the Material Chemistry Research Laboratory (Department of Chemistry, Dhaka University) for their all sorts of supports.

Finally and most importantly, I gratefully acknowledge my father Md. Joynal Abedin, mother Kaniz Fatema and my younger siblings Jasmin Jannat Jui, Jubaida Jannat Zinia and Abdur Rahim Kaif for their endless sacrifices, love and faith on me in all circumstances and allowing me to be as ambitious as I wanted. And also, I must give my appreciation to my beloved friends Ashamoni and Shazia Sharmin Satter who are not less than my family for always giving me courage to fulfill my dreams during my study life.

Jakia Jannat Keya

Appendix

Appendix 1

Verification of analysis method

The effect of different parameters on the swarming of single rigid and flexible swarm units i.e; *r*-DNA1 and *r*-DNA2 conjugated GMPCPP and GTP microtubules (MTs) respectively was quantified by RGY analysis based on red, green and yellow pixels which has been presented in Chapter 2 and 3. To verify the analysis methodology for determining association ratio another approach for characterizing the association ratio of MTs (single MT counting) was also performed. The manual counting of single MTs is used which is more laborious approach and yields the less noisy data. In this method the association ratio at a given time *t* was determined by counting the number of single swarm units i.e; MTs manually and dividing the number at time *t* by the number present initially (*t*=0). The time-dependent association ratio *R(t)* of red and green MTs was determined as follows,

$$R(t) = \frac{N(0) - N(t)}{N(0)} \qquad \ldots\ldots\ldots\ldots\ldots\ldots\ldots\ldots\ldots\ldots\ldots\ldots\ldots\ldots (1)$$

with

$N(0)$ = Initial number of single MTs,

$N(t)$ = Number of single MTs after time *t*.

Appendix 2

Effect of different parameters on the association ratio of rigid swarm units estimated by single MT counting

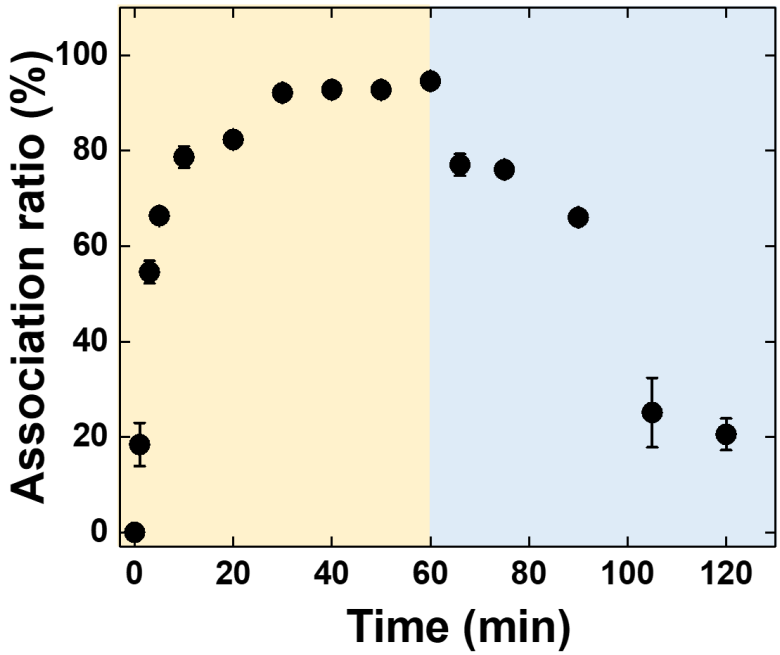

Figure S1. Change in the association ratio of *r*-DNA1 and *r*-DNA2 conjugated rigid GMPCPP-MTs (swarm units) over time after introduction of *l*-DNA1 upto 60 min and introduction of *d*-DNA after 60 min to 120 min (the trend coincides well with RGY analysis in **Figure 2.11** and **2.32a**). Error Bar: S. E.

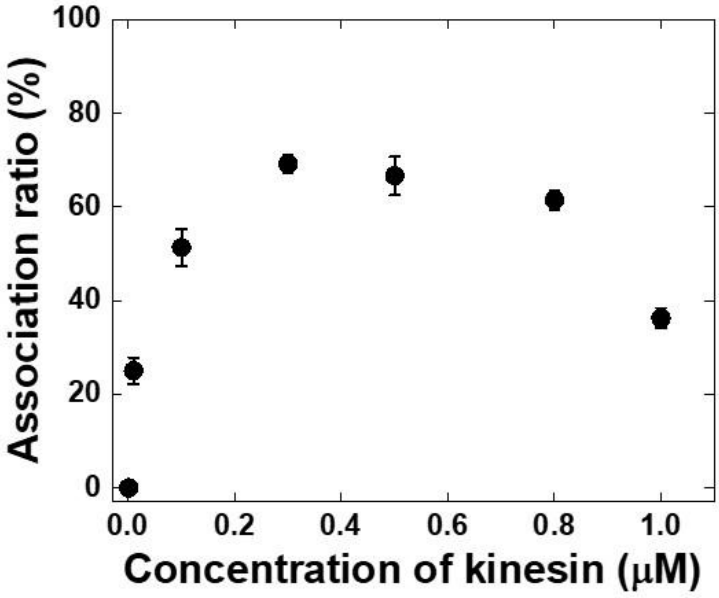

Figure S2. Change in association ratio with increasing the concentration of kinesin on the swarming of *r*-DNA1 and *r*-DNA2 conjugated rigid swarm units (GMPCPP-MTs). The trend coincides well with RGY analysis in **Figure 2.9**. Error Bar: S. E.

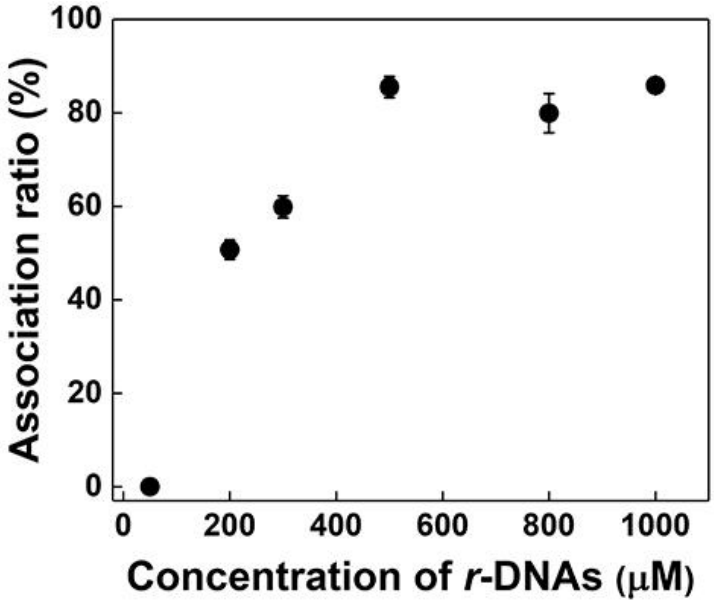

Figure S3. Change in association ratio with increasing the concentration of *r*-DNAs (*r*-DNA1 and *r*-DNA2) in the feed, used to conjugate to the rigid swarm units (GMPCPP-MTs), on the swarming of the MTs (the trend coincides well with RGY analysis in **Figure 2.14**). Error Bar: S. E.

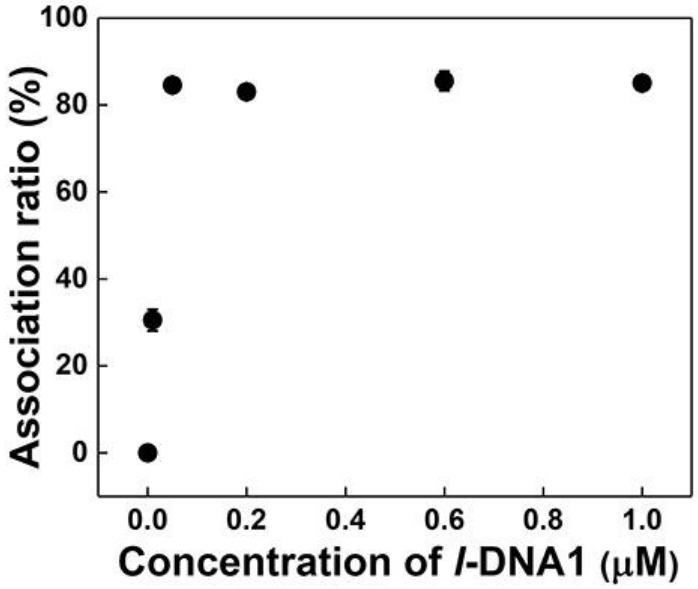

Figure S4. Change in association ratio with increasing the concentration of *l*-DNA1 on the swarming of *r*-DNA1 and *r*-DNA2 conjugated rigid swarm units (GMPCPP-MTs). The trend coincides well with RGY analysis in **Figure 2.16**. Error Bar: S. E.

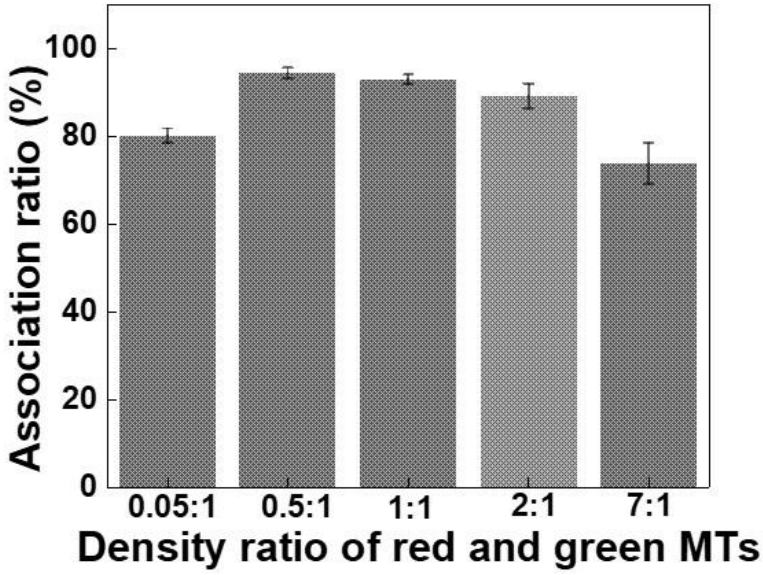

Figure S5. Change in association ratio depending on the density ratio of R- and G-swarm units (GMPCPP-MTs). At moderate density ratio (0.5:1, 1:1) the maximum swarm group formation is found to form and at lower (0.05:1) and (2:1, 7:1) higher density ratio the swarm group formation was found to decrease which can be observed from the change in association ratio. The trend is almost similar to the RGY analysis in **Figure 2.20a**. Error Bar: S. E.

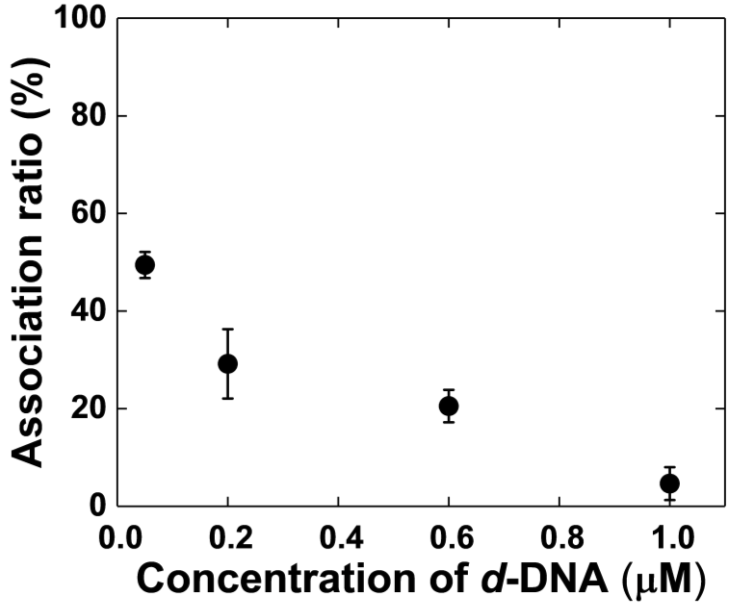

Figure S6. Change in association ratio with increasing the concentration of *d*-DNA on the dissociation of the swarms of *r*-DNA1 and *r*-DNA2 conjugated rigid swarm units (GMPCPP-MTs) into single swarm units (the trend coincides well with RGY analysis in **Figure 2.34**) after 60 min of passing *d*-DNA in the system. Error Bar: S. E.

Appendix 3

Effect of different parameters on the association ratio of flexible swarm units by single MTs counting

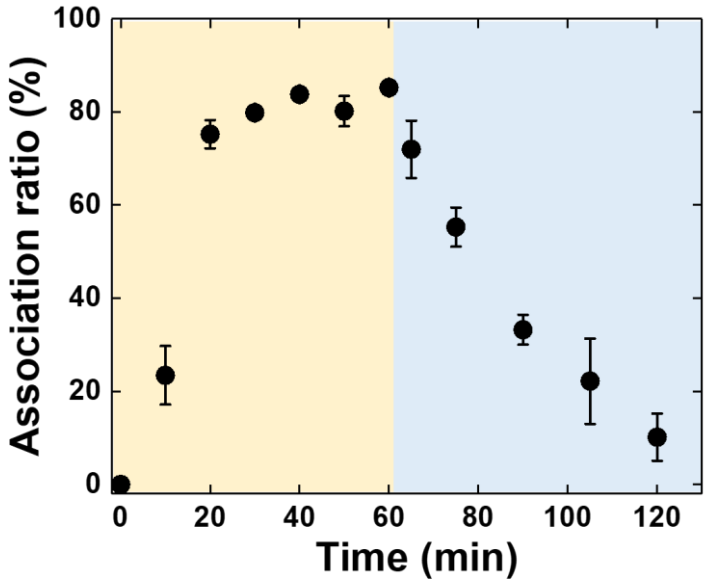

Figure S7. Change in the association ratio of *r*-DNA1 and *r*-DNA2 conjugated flexible GTP-MTs (swarm units) over time after introduction of *l*-DNA1 upto 60 min and introduction of *d*-DNA after 60 min to 120 min (the trend coincides well with RGY analysis in **Figure 2.24a** and **2.32b**). Error Bar: S. E.

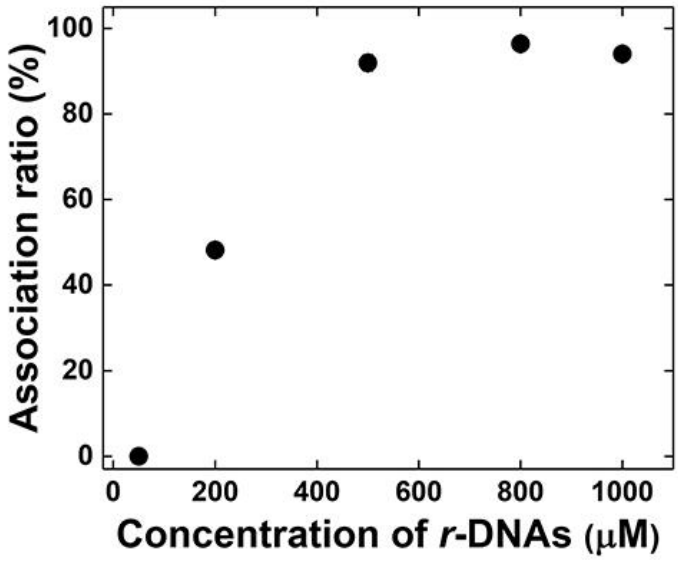

Figure S8. Change in association ratio with increasing the concentration of *r*-DNAs (*r*-DNA1 and *r*-DNA2) in the feed used to conjugate *r*-DNAs to flexible swarm units (GTP-MTs) on the swarming (the trend coincides well with RGY analysis in **Figure 2.26**). Error Bar: S. E.

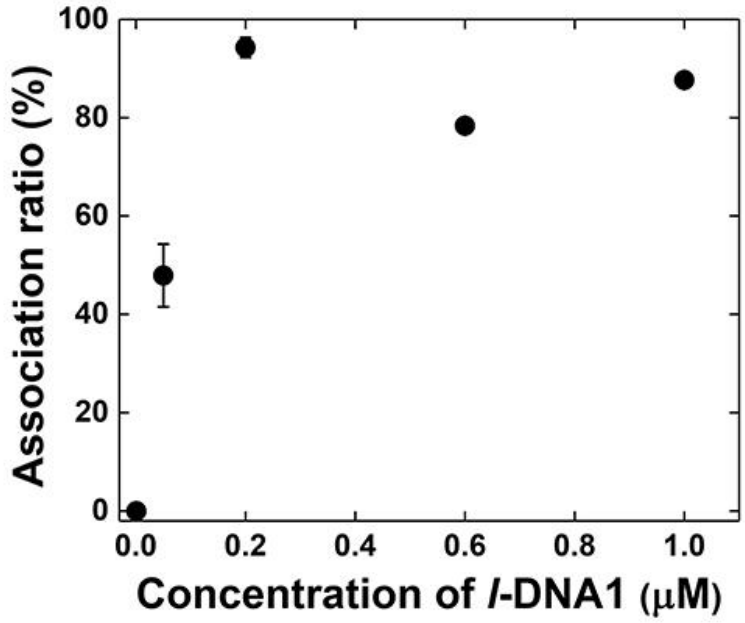

Figure S9. Change in association ratio with increasing the concentration of *l*-DNA1 on the swarming of *r*-DNA1 and *r*-DNA2 conjugated flexible swarm units (GTP-MTs) (the trend coincides well with RGY analysis in **Figure 2.38**). Error Bar: S. E.

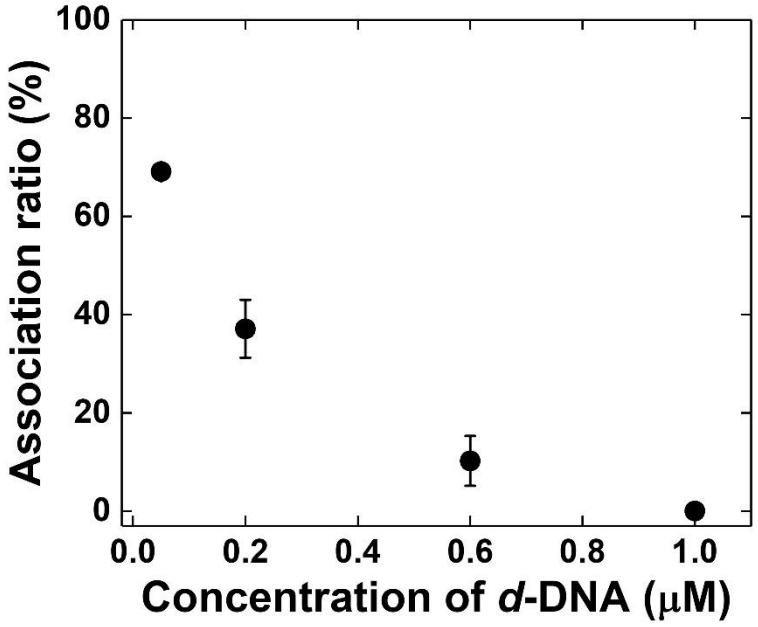

Figure S10. Change in association ratio with increasing the concentration of *d*-DNA on the dissociation of swarms of *r*-DNA1 and *r*-DNA2 conjugated flexible swarm units (GTP-MTs) into single swarm units (the trend coincides well with RGY analysis in **Figure 2.36**) after 60 min of passing *d*-DNA in the system. Error Bar: S. E.

Appendix 4

Regulation of swarming of rigid swarm units by photoirradiation estimated by single MTs counting

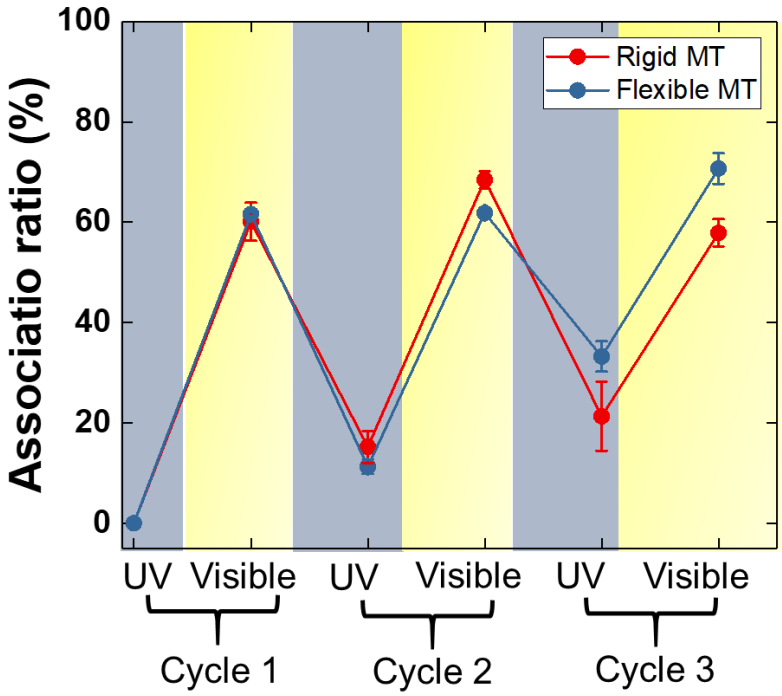

Figure S11. Switch on-off change in association ratio of photoresponsive swarm units upon consecutive irradiation by visible and UV light (the trend coincides well with RGY analysis in **Figure 3.15**). Error Bar: S. E.

Thus, single MT counting coincides well with RGY analysis which verifies the methodology for quantification of association of swarming. Although, detachment of MTs from the surface can slightly affect the association ratio but it is negligible depending on the experimental condition and overall association of MTs into swarming. Therefore, for further investigation in this system in future, the single MT counting method can be used to directly correlate the swarming with change in number of single MTs present in the system alongside with RGY analysis.

Appendix 5

Phase diagrams of evolution of swarming depending on the physical property of MTs (swarm units) and DNA interaction

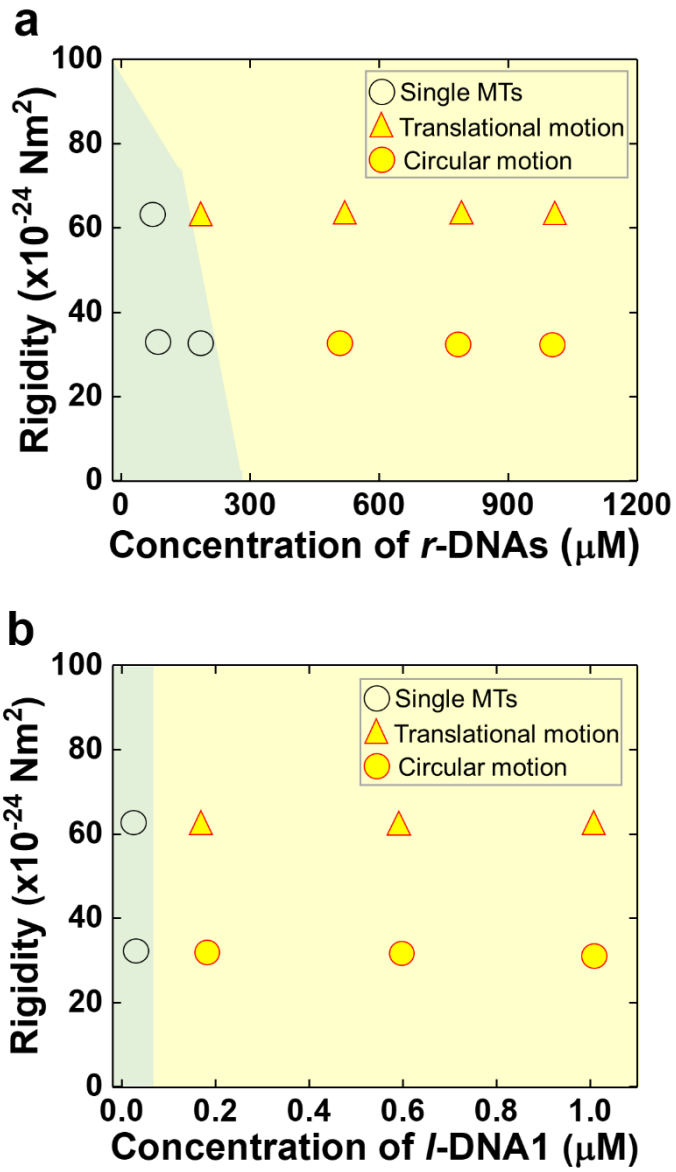

Figure S12. Phase diagrams show the evolution of different swarming modes of swarm units with the change of the rigidity of swarm units i.e; MTs and concentration of *r*-DNA and *l*-DNA1. **a,** A phase diagram showing the effect of the rigidity of MTs and concentration of *r*-DNAs on the swarming mode of the MTs. The concentration of *l*-DNA1 was fixed at 0.6 μM. **b,** A phase diagram showing the effect of the rigidity of MTs and concentration of *l*-DNA1 on the swarming mode of the MTs. Rigidity values used for GTP-MTs and GMPCPP-MTs were ~34×10^{-24} Nm^2 and 62×10^{-24} Nm^2 respectively.[1]

Reference

1. Mickey, B. & Howard, J. *J.Cell Biol.* **1995**, *130*, 909-917.